9-13-2023 3:00 PM

Modelling Prenatal Hypoxia As A Risk Factor For Schizophrenia Vulnerability In Patient-Derived Cerebral Organoids

Dana M. Gummerson, *Western University*

Supervisor: Laviolette, Steven R, *The University of Western Ontario*
A thesis submitted in partial fulfillment of the requirements for the Master of Science degree in Neuroscience
© Dana M. Gummerson 2023

Recommended Citation

Abstract

Prenatal hypoxia during fetal development is a significant environmental risk factor linked to schizophrenia (SCZ) vulnerability. However, hypoxia's impact on human brain development at the cellular level remains unclear. Our laboratory has developed human cerebral organoids using induced pluripotent stem cells (iPSCs) derived from healthy control or SCZ patient cell lines to address these questions. This creates a platform that allows for the investigation into the pathophysiology of SCZ and hypoxia in tandem. Organoids were exposed to hypoxic conditions at one month of development, mimicking the early stages of cortical growth in the human fetus. Results reveal innate differences in neuronal development markers in SCZ organoids at the transcriptomic and protein level. In response to hypoxia, SCZ organoids exhibit dysregulation of mitochondrial-associated proteins and genes required for normal metabolism and growth. Our findings highlight critical differences in the expression of vital neuronal markers in SCZ and highlight hypoxia's further impacts on neurodevelopmental pathophysiology related to SCZ risk.

Keywords

Summary for Lay Audience

Schizophrenia (SCZ) is a mental disorder illness usually characterized by delusions, hallucinations, disordered thought, and diminished emotional expression. During pregnancy, fetuses that experience a lack of oxygen, termed hypoxia, are at an increased risk of developing schizophrenia later in life. However, how low oxygen negatively impacts brain development at a cellular level is not fully understood. Moreover, how an individual's genetic risk for SCZ interacts with hypoxia has yet to be fully elucidated. To study both factors together, our laboratory grows 'mini-brains in a dish,' termed cerebral organoids, that mimic different aspects of early fetal brain development across various stages of pregnancy. These 3D sphere-like structures are grown from cells obtained from patients with SCZ or healthy individuals. At a period of growth reflecting the cusp of the first and second trimester of pregnancy, organoids were exposed to low-oxygen (hypoxic) conditions. Using various investigative techniques, we examined differences between SCZ and control organoids and the impact of hypoxia on both types of organoids. In response to hypoxia exposure, all organoids show an increased expression in proteins known to increase in response to low oxygen conditions. As expected with cell stress, we see increases in cell death due to hypoxia. Further investigation of the organoids revealed SCZ organoids show reductions in proteins and genes required for normal brain development compared to healthy controls. We also looked at proteins and genes in mitochondria, the powerhouse of the cell, as they need constant inputs of oxygen to produce energy for cells. Non-optimal functioning of mitochondria is also related to SCZ pathology as SCZ patient samples show differences in mitochondria shape and function compared to healthy individuals. RNA-Sequencing is used to determine which genes are up- and downregulated in samples. In the SCZ hypoxia-exposed organoids, there are changes in the expression of genes in mitochondria required to break down sugars into energy. Hypoxia also impacts the expression of proteins required for proper metabolism within cells in both control and SCZ organoids. This project reveals innate differences in brain development markers in SCZ and the impact of hypoxia on development via mitochondrial dysfunction and cellular stress responses.

Acknowledgments

First and foremost, I would like to thank my advisor, Dr. Steve Laviolette, for providing me this incredible experience and continued support throughout this degree. I'm so grateful for the opportunity to join your lab and take on such a new and exciting project; I learned so much about what it means to be a researcher and will take this experience forward with pride. I would also like to thank my advisory committee members, Dr. Walter Rushlow and Dr. Shawn Whitehead for all your valuable advice and suggestions throughout this process.

This project would not have come together without the endless hours of work and support from all my lab mates, especially Mar Rodriguez and Emma Proud. I am eternally grateful for all those hours spent together in cell culture praying to the science gods our organoids would grow! Mar, you took us in under your wing and were so patient and kind teaching myself and Emma the endless number of new things in the lab. Your dedication to science is inspiring and I hope to be half the researcher and teacher you've been for us. Miss you everyday and cannot wait to visit you in Spain! Emma, not only have you been an amazing support throughout this degree, but you've also become a lifelong friend. You were always willing to listen to the complaints when experiments went wrong and celebrate with me when I finally got exciting results. I'm so excited to see what the future holds us and to be right there with you. To all my other lab mates, thank you for the endless office chats about the most random topics – if I was having a bad day, I always knew I could count on you guys for a good laugh.

To my entire family, I wouldn't have gotten here without you. Mom and Dad, thank you for the late-night calls and endless support; visits home to go fishing and read by the lake kept me sane and I am so grateful to know you've always got my back. Last but certainly not least, thank you to **all** of my friends for your never-ending support and words of encouragement. I'm so grateful to have such amazing friends; love you all so much and happy to know you're in it for the long haul with me ♥

Table of Contents

List of Tables

List of Figures

List of Abbreviations

ALDOA Aldolase, fructose-bisphosphate A

ALODC Aldolase, fructose-bisphosphate C

ANOVA Analysis of variance

ATP Adenosine triphosphate

CC3 Cleaved caspase 3

CI Complex I, NADH dehydrogenase

CII Complex II, Succinate dehydrogenase

CIII Complex III, Cytochrome c reductase

CIV Complex IV, Cytochrome c oxidase

CTRL Control

CP Cortical plate

CS Citrate synthase

CTIP2 COUP-TF-Interacting Protein-2

CTRL Control

CTRL N Control normoxia

CTRL H Control hypoxia

DAPI 4',6-Diamidino-2-Phenylindole, Dihydrochloride

DE Differentially expressed

DEDD2 Death effector domain containing 2

DLPFC Dorsolateral prefrontal cortex

D-PBS Dulbecco's Phosphate-Buffered Saline

DRD1/2 Dopamine receptor D1/2

EB Embryoid body

EEG Electroencephalogram

ETC Electron transport chain

FAD Flavin adenine dinucleotide

FOS Fos Proto-Oncogene, AP-1 Transcription Factor Subunit

GABA γ-Aminobutyric acid

GEI Gene-environment interaction

GLUT1 Solute carrier family 2 member 1

GO Gene ontology

GWAS Genome-wide association studies

GW Gestational week

H Hydrogen

HDL High-density lipoprotein

H&E Hematoxylin and eosin

HK hexokinase

HIF Hypoxia-inducible factor

HSPA6 Heat shock protein family A (Hsp70) member 6

HSPA8 Heat shock protein family A (Hsp70) member 8

ICDH Isocitrate dehydrogenase

IL-6 Interleukin 6

iPSC Induced pluripotent stem cell

KEGG Kyoto Encyclopedia of Genes and Genomes

KGDHC Ketoglutarate dehydrogenase complex

LDHA Lactate dehydrogenase A

LDL Low-density lipoprotein

MAP2 Microtubule-associated protein 2

MDH Malate dehydrogenase

MEA Multielectrode array

mGluR2/3 Metabotropic receptors 2 and 3

mRNA Messenger ribonucleic acid

MT-ND1 Mitochondrially encoded NADH dehydrogenase 1

MT-ND5 Mitochondrially encoded NADH dehydrogenase 5

NAD Nicotinamide adenine dinucleotide

NDS Normal donkey serum

NMDA N-methyl-D-aspartate

NPC Neural progenitor cell

OC Obstetric complication

OXPHOS Oxidative phosphorylation

PAX6 Paired box 6

PDHC Pyruvate dehydrogenase complex

PFK2 6-phosphofructo-2-kinase/fructose-2,6-biphosphatase 3

PFKL Phosphofructokinase, liver type

PFKP phosphofructokinase, platelet

PHD Prolyl hydroxylase

PDK1 Pyruvate dehydrogenase kinase 1

PHD Prolyl hydroxylase

ROI Region of interest

SCZ Schizophrenia

SCZ N Schizophrenia normoxia

SCZ H Schizophrenia hypoxia

TLR Toll-like receptor

1 Introduction

Cerebral organoids are a complex *in vitro* system that recapitulates many aspects of a developing human brain (Lancaster and Knoblich 2014; Lancaster et al. 2013; Stachowiak et al. 2017). They are derived from either embryonic or induced pluripotent stem cells (iPSCs), taking advantage of the self-organizing potential of stem cells to develop complex structures mimicking early to mid-gestation human brain development (Lancaster and Knoblich 2014; Lancaster et al. 2013). Importantly, iPSCs derived from high-risk populations can be used to produce organoids, which creates a platform to study specific genetic and molecular components of neurodevelopmental and neuropsychiatric illnesses (Stachowiak et al. 2017; Shou et al. 2020; Kathuria et al. 2020). Various studies have shown the viability of using patient-derived schizophrenia (SCZ) cell lines to develop cerebral organoids. This *in vitro* model is a step forward from rodent models as it considers human-specific genetic landscapes and cytoarchitecture. It allows translational research from rodents to humans, which would otherwise be ethically or technically unfeasible.

Fetal brain development largely relies on appropriately timed gene expression, but poor environmental conditions during pregnancy also significantly impact neurodevelopment. One such environmental impact is oxygen deprivation, or hypoxia. With a frequency of 2–4 per 1000 live births, prenatal hypoxic insults are a primary cause of neurological impairment (Badr Zahr and Purdy 2006; Glass and Ferriero 2007). Causes of acute hypoxic insults include compression of the umbilical cord, partial detachment of the placenta from the uterine wall, respiratory infections, and low amniotic fluid levels (Giussani 2016). Exposure to hypoxic conditions during neurodevelopment is one of several environmental factors related to the risk of developing SCZ (T. D. Cannon et al. 2002; Schmitt et al. 2014). The risk of developing a psychotic condition in adulthood is twofold for infants who experienced hypoxia-ischemia (Zornberg, Buka, and Tsuang 2000). In populations exhibiting risk genes for SCZ, prenatal hypoxic insults are associated with more significant structural abnormalities in the brain, such as reduced

cortical grey matter and ventricular enlargement, and an earlier onset of psychosis (T. D. Cannon et al. 2002; Rosso et al. 2000).

Hypoxia also impacts neurodevelopment via mitochondrial function as adequate energy supplies in cells are highly reliant on oxygen availability (J. Kim et al. 2006; Tang et al. 2019; H.-S. Li et al. 2019). Widespread mitochondrial dysfunction and metabolic changes in SCZ patients are reported across the literature in adolescence and adulthood (Prabakaran et al. 2004; Roberts 2021; Maurer, Zierz, and Möller 2001; Kathuria et al. 2023). Post-mortem analyses of SCZ patients' brains show altered mitochondrial morphology, cellular respiration, and increased oxidative stress (Roberts 2021). These observations are supported by genome-wide association (GWAS) studies that found that 50% of SCZ candidate genes are regulated by hypoxia (Schmidt-Kastner et al. 2020). However, hypoxia insults alone are insufficient for the development of SCZ, as 90% of infants that experience fetal hypoxia do not develop SCZ (Maynard et al. 2001). This disconnect suggests hypoxia interacts with existing genetic risk factors to influence disease progression. This gene-environment interaction (GEI) is the basis of the two-hit hypothesis of SCZ (Maynard et al. 2001). The first hit, the expression of risk-gene mutations, "primes" the central nervous system for the second hit, subsequent exposure to maladaptive environmental conditions such as prenatal hypoxia. Collectively, these factors can work in concert to facilitate a variety of pathophysiological outcomes, including SCZ (Maynard et al. 2001; Strat, Ramoz, and Gorwood 2009).

Previous work has validated the use of human cerebral organoids as a model of prenatal hypoxic injury (M. S. Kim et al. 2021; Paşca et al. 2019; Daviaud et al. 2019), while others have developed human cerebral organoids from SCZ patient populations (Kathuria et al. 2023; 2020; Notaras, Lodhi, Dündar, et al. 2021; Notaras, Lodhi, Fang, et al. 2021; Stachowiak et al. 2017). To date, a cerebral organoid model of prenatal hypoxic injury representative of SCZ phenotypes has yet to be explored and characterized. Filling this gap in knowledge of both hypoxia and SCZ-related research is important to investigate due to the strong interaction between genetic and environmental contributions to the development of SCZ. To this end, this thesis aims to develop an *in vitro* cerebral organoid

model of prenatal hypoxia in SCZ populations to study the GEI in SCZ brain development.

1.1   Schizophrenia

SCZ is a debilitating neuropsychiatric disorder with a complex underlying pathophysiology. There is ongoing research into the mechanisms behind the development of the disorder. Decades of research points to the interaction of genetic, epigenetic, and environmental influences that collectively result in abnormal neurodevelopment and, eventually, clinical symptom presentation (Maynard et al. 2001; Hany et al. 2023; Henkel et al. 2022; Selemon and Zecevic 2015; Luvsannyam et al. 2022). SCZ prevalence varies between ethnic and racial groups, with global estimations indicating that approximately 1% of adults are diagnosed (Hany et al. 2023). There is a sex difference in the onset and rates of diagnosis: Males are slightly more likely to be diagnosed than females, with an incidence ratio of 1.4:1, although recent reviews cite no sex differences in lifetime prevalence (X. Li, Zhou, and Yi 2022). Males' age of onset peak is between 20-24 years, whereas female onset peaks slightly later at 25-29, with a subsequent peak in later adulthood around 45 years of age (Li et al. 2016).

1.1.1 *Genetics of SCZ*

There is not one singular risk factor sufficient for the development of SCZ, which makes it essential to research the disorder from a variety of biological and psychiatric points of view. At the biological level, genetics play a fundamental role in the development of SCZ, a field that is currently heavily researched to determine exact contributions. Family history of first-degree relatives is a robust risk factor for SCZ (Lu et al. 2018). In the case of monozygotic "identical" twins, both children are diagnosed with SCZ 45-60% of the time (Hany et al. 2023), and if both parents are affected, offspring are at a 40% risk of developing SCZ as well (Hany et al. 2023). However, due to the low lifetime risk in the general population, more than 95% of cases do not have a first-degree family history with SCZ (Lu et al. 2018).

Recently, the largest GWAS of over 75,000 individuals with SCZ reported common variant associated at 287 genomic loci, 106 of which were protein coding (Trubetskoy et al. 2022). Of the genes identified, many play functional roles in both excitatory and inhibitory neurons of the CNS. Gene set enrichment analysis followed by Gene Ontology (GO) analysis finds all terms were related to neuronal function, development, differentiation, synaptic transmission, and inflammation. They also determined genes related to synaptic signalling were primarily postsynaptic in nature. These genetic findings support biological and clinical reports of aberrant neuronal signalling (Luvsannyam et al. 2022). GWAS studies are based in the "common-disease common-variants" hypothesis that posits common and specific genetic variations in the genetic code is mainly associated with SCZ risk (El-Fishawy 2013; Henriksen, Nordgaard, and Jansson 2017). However, another study finds that risk of SCZ is more greatly associated with thousands of common allele mutations that individually confer small risks, but collectively explains genetic liability (Purcell et al. 2009). Of the genetic loci that have been associated with SCZ through GWAS, there is considerable overlap with other psychiatric disorders, including bipolar disorder, major depressive disorder, and autism spectrum disorder which lends to the pleiotropic quality of the genetic contributions (Luvsannyam et al. 2022; Purcell et al. 2009).

There is also strong evidence for highly penetrant, rare genetic variants (<1%) as strong contributors to SCZ risk (Henriksen, Nordgaard, and Jansson 2017), the basis of the "common-disease rare-variants" hypothesis proposed by McClellan, Susser, and King (2007). Robust associations to SCZ risk are reported in the case of 22q11.2 deletion syndrome. In this mutation, there is deletion of a 1.5 megabase portion of the 22q11.2 region which contains approximately 35 coding genes (Karayiorgou and Gogos 2004). Deleted genes include COMT that plays a role in dopamine degradation in the cortex, and PRODH which is important to glutamatergic and GABAergic neurotransmission (Qin, Chen, and Zhou 2020). Approximately 30% of patients with said deletion go on to develop SCZ (Karayiorgou, Simon, and Gogos 2010; Qin, Chen, and Zhou 2020; Karayiorgou and Gogos 2004). Other deleterious syndromes associated with SCZ risk include deletions of chromosomes 1q21.1, 3q29, and 15q13.3 (Henriksen, Nordgaard, and

Jansson 2017). Other forms of rare genetic variants include duplications on chromosomes 16p11.2 and 16p13.11 (Henriksen, Nordgaard, and Jansson 2017). Collectively, the odds ratios of these rare genetic variants range from 2 to 60 (Rees, O'Donovan, and Owen 2015).

It is now well recognized that the genetic architecture of SCZ includes influences of both common and rare risk alleles spread over a wide number of genes. Despite significant genetic heterogeneity between individuals, multiple classes of mutation have been demonstrated to converge onto similar biological pathways, including neuronal signalling, synaptic plasticity, and immune system functioning (Rees, O'Donovan, and Owen 2015; Henriksen, Nordgaard, and Jansson 2017).

1.1.2 *Gene-environment interactions of SCZ presentation*

Genetic contributions alone are insufficient for the development of SCZ, and accumulating evidence reveals various environmental factors associated with SCZ risk. Associations between *in utero* environmental stressors and SCZ development include but are not limited to gestational diabetes, preeclampsia, maternal malnutrition, maternal infection, and low birth weight (Hany et al. 2023). These associations are a key component of the two-hit hypothesis of SCZ (Bayer, Falkai, and Maier 1999). In the two-hit hypothesis, expression of risk-gene mutations "primes" the central nervous system into a vulnerable state which subsequent environmental stresses act upon. The collective influence of GEIs is thought to facilitate abnormal signalling networks and full clinical symptomology (Maynard et al. 2001; Bayer, Falkai, and Maier 1999). It is important to note that in clinical populations, rarely are two singular 'hits' are wholly responsible for the development of SCZ. Instead, multifactorial influences (i.e. combinations of hypoxia, economic status, maternal malnutrition) collectively contribute to the presentation of SCZ symptomology. It has been shown that multiple risk factors can synergistically alter brain function and in turn behaviour in animal models of SCZ (Guerrin et al. 2021). This project focuses on the two-hit hypothesis as the two contributors of risk examined are only SCZ genetic background and hypoxic exposure.

With the emergence of evidence for prenatal and perinatal risk factors as contributing factors to SCZ development, SCZ has been widely accepted as a neurodevelopmental disease (Brown 2012; Schmitt et al. 2014). The dorsolateral prefrontal cortex (DLPFC) is consistently implicated in SCZ pathology. Neuroimaging and post-mortem studies find reduced volume of cortical gray matter of the prefrontal cortex due to depleted neuronal connectivity. Additionally, SCZ patients perform poorly on tasks related to attention, working memory, and cognitive flexibility that rely highly on the prefrontal cortex, implicating these cortical areas at the biological and functional level of SCZ pathophysiology (Goldman-Rakic and Selemon 1997). During normal fetal brain development, corticogenesis is highly susceptible to environmental insults (Schmitt et al. 2014; Meyer 2001). This together leads to the neurodevelopmental hypothesis of SCZ, whereby brain development is marked by two critical developmental periods, fetal brain development and adolescence. Fetuses' as early as the first and second trimesters that experience pathological neurodevelopment prime neuronal circuits to generate psychotic symptoms in adolescence or young adulthood, often in concert with biological and psychological stress events (Nour and Howes 2015). The combination of genetic risk and environmental hits during early gestation and/or adolescence leads to SCZ development (Owen et al. 2011).

1.1.3 *Alterations to fetal corticogenesis in SCZ*

Cortical fetal development is marked by numerous milestones required for normal brain development. In a healthy developmental timeline, human corticogenesis begins between 4-5 gestational weeks (gw)(Selemon and Zecevic 2015), with the emergence of the telencephalic vesicle from the neural tube. Throughout corticogenesis, the vesicle is divided into three zones: ventricular zone (VZ), subventricular zone (SVZ), and cortical plate (CP). Lining the telencephalic vesicle are progenitor cells that undergo rapid growth and proliferation representing the VZ (Selemon and Zecevic 2015; Meyer 2001). Directly adjacent is the SVZ, where dividing progenitors spawn immature neurons that begin migrating via radial glial cells towards the outermost margin, termed the rudimentary CP. Throughout this process, key milestones include the appearance of synapses, thalamic and dopaminergic fibres developing, progenitors contining to self-renew, and the CP thickens

to 6 to 8 cells by gw 13(Selemon and Zecevic 2015; Zecevic et al. 1999). Corticogenesis continues throughout midgestational periods and ends at ~ 28 gw in the third trimester of gestation (Malik et al. 2013).

The development of a rudimentary cortex is highly reliant on the proliferation of progenitors, a process that is exceptionally vulnerable to maladaptive environmental hits. *In utero* environmental stressors linked to SCZ development are likely to disrupt normal corticogenesis, which has long-term impacts on brain development into adolescence (Stolp et al. 2012). For example, maternal infection is strongly linked to SCZ risk, and inflammatory cytokines are known regulators of the self-renewal processes of neural progenitors (Deverman and Patterson 2009). In response to infection, the overactivation of pro-inflammatory cytokines can cross the blood-brain barrier leading to fetal neuroinflammation (Elgueta et al. 2022). One such cytokine is interleukin-6 (IL-6) has been linked to increases in neural stem cell numbers that persist into adulthood and can delay the migration of immature neurons to the CP (Gumusoglu et al. 2017; Gallagher et al. 2013). The ultimate result is dysregulation of normal corticogenesis leading to abnormal brain development (Gumusoglu et al. 2017; Gallagher et al. 2013). There are cases of maternal infection where viral RNA is not detected in the fetal brain, such as the case of the influenza A virus (L. Shi, Tu, and Patterson 2005). In these cases, cytokines damage the placenta leading to growth restriction caused by a lack of oxygen (Elgueta et al. 2022). Maternal infection is only one example of an environmental stressor linked to SCZ risk and impaired neurodevelopment. As previously mentioned, various obstetric complications and malnutrition are related to SCZ risk and complications from poor environments can lead to disrupted neurodevelopment (L. Shi, Tu, and Patterson 2005; Cortés-Albornoz et al. 2021; Fitzgerald, Hor, and Drake 2020).

1.1.4 *Mitochondrial dysfunction in SCZ*

SCZ pathology implicates abnormalities in mitochondria functions and roles, including responses to oxidative stress, synaptic efficiency, and energy metabolism (Roberts 2021). Specifically, alterations to DLPFC metabolism in SCZ have been well documented (Prabakaran et al. 2004; D. Yang et al. 2022). These alterations may be related to synaptic

abnormalities reported in SCZ as neurons have a high metabolic demand to facilitate synaptic communication (Middleton et al. 2002). Mitochondria integrate environmental cues, such as low oxygen in hypoxia, to regulate homeostasis. For example, metabolites from mitochondria can trigger innate cellular responses such as cell death, changes to gene expression, inflammation, and immune modulation, to influence cell fate and function (Martínez-Reyes and Chandel 2020; Tzameli 2012). In healthy systems, mitochondria produce 95% of cellular energy supplies (Tzameli 2012). The production of energy in the form of adenosine triphosphate (ATP) is a dynamic process involving the tricarboxylic acid (TCA) cycle and protein complexes I through IV of the electron transport chain (ETC). The TCA cycle is a closed-loop metabolic system that intakes acetyl-CoA generated from glucose, fatty acids, or amino acids (Martínez-Reyes and Chandel 2020). Through a series of enzymatic reactions, the cycle generates two nicotinamide adenine dinucleotides (NAD) + hydrogen (H) and one flavin adenine dinucleotide (FAD) + 2 hydrogen (H_2). NADH and FADH2 directly interact with complexes I and II of the ETC, where oxidation of these products results in the funnelling of electrons through ETC complexes, allowing positive H+ to be transported into the inner mitochondrial membrane space. This proton gradient is required for the function and activity of complex V (ATP synthase) that shuttles protons back into the mitochondrial matrix and produces ATP (Martínez-Reyes and Chandel 2020).

In SCZ, changes to the activity of the ETC have been reported across various studies, where results are widespread and region-dependent (Roberts 2021). Decreased oxidative metabolism has been consistently documented in the frontal lobes of SCZ patients (Roberts 2021; Bubber et al. 2011). However, the biochemical basis of these changes varies between studies. Some studies have reported decreases in complex I (NADH dehydrogenase) activity and protein levels (Maurer, Zierz, and Möller 2001; Holper, Ben-Shachar, and Mann 2019). A different proteomic analysis study via LC-MS/MS also reported decreases in complexes I and III (cytochrome c reductase, Prabakaran et al. 2004). However, others report no changes to complexes I, III, or IV (cytochrome c oxidase) in the frontal cortex (Andreazza et al. 2010). A meta-analysis of mitochondrial complexes SCZ post-mortem frontal cortex revealed moderate effect sizes for reductions

in complex I, while the evidence for complex IV alterations was less robust (Holper, Ben-Shachar, and Mann 2019). While there is not yet a well-defined profile of ETC changes in SCZ across all brain regions, the research highlights evident dysregulation in bioenergetic functioning in SCZ patients' brains.

Irregularities in the function and efficiency of the mitochondrial TCA cycle are also linked to SCZ. GWAS have also demonstrated widespread downregulation of the TCA cycle, oxidative phosphorylation (OXPHOS), and glycolysis-related genes in the post-mortem SCZ prefrontal cortex (Bubber et al. 2011). Transcriptomic investigations have revealed declines in the expression of genes related to the TCA cycle in the DLPFC among individuals with SCZ (Middleton et al. 2002; Henkel et al. 2022). Specifically, the activities of key enzymes associated with the initial phase of the TCA cycle, including aconitase, ketoglutarate dehydrogenase complex (KGDHC), and succinate thiokinase (STH), were observed to be diminished in individuals with SCZ. Conversely, enzymes found in the latter phase of the cycle, such as succinate dehydrogenase (SDH) and malate dehydrogenase (MDH), displayed increased activity. Notably, the activities of pyruvate dehydrogenase complex (PDHC), citrate synthase (CS), isocitrate dehydrogenase (ICDH), and fumarase remained unaltered.

1.2 Molecular response of hypoxia

The molecular impacts of hypoxic environments are largely connected to the hypoxia-inducible factor (HIF) signalling pathway. Hypoxia-inducible factor 1 subunit α (HIF-1α) acts as the master regulator of the hypoxic response and is a crucial component of oxygen homeostasis in healthy systems. Under normal oxygen conditions (normoxia), HIF-1α is stably expressed at low levels due to a balance in expression and degradation through the ubiquitin-proteasome pathway (**Figure 1A**, Berra et al. 2001). Degradation of HIF-1α is initiated by hydroxylation of a single proline residue by prolyl hydroxylases (PHD) enzymes followed by ubiquitination that tags the protein for degradation by proteasomes (Semenza 2007; J. Kim et al. 2006). Degradation of HIF-1α only occurs in the presence of oxygen; when the oxygen levels are insufficient, the PHD enzymes cannot complete hydroxylation of HIF-1α, disrupting the degradation process (Cerychova and Pavlinkova

2018). Therefore, as oxygen levels are reduced in cells, levels of HIF-1α accumulate, and the proteins translocate to the nucleus. In the nucleus, a heterodimer composed of HIF-1α and HIF-1β binds to the hypoxia response element of the gene promoter (Orlando et al. 2020). The result is an increased production of HIF-1α mRNA, which undergoes ribosomal translation to further increase protein levels of HIF-1α (**Figure 1B**, Cerychova and Pavlinkova 2018).

Downstream targets of HIF-1α include pathways relating to metabolism, angiogenesis, cell death, differentiation, and proliferation (Slemc and Kunej 2016). Genes whose role was confirmed across multiple studies include ALDOA, ALODC, PFKL, and PFKP, all of which are implicated in metabolism pathways such as carbohydrate metabolism and glycogenesis/gluconeogenesis (Slemc and Kunej 2016). Hypoxia can influence the expression of TCA cycle enzymes, essentially inhibiting pyruvate from entering the cycle and oxidative metabolism through the ETC (Wheaton and Chandel 2011). As many of the downstream targets of HIF-1α are mitochondrial-associated, this process is strongly linked to mitochondrial dysfunction. When homeostatic processes are disrupted in mitochondria, overproduction of reactive oxygen species (ROS), a form of oxidative stress, can further affect TCA cycle activity and efficiency (**Figure 1C**).

As previously discussed, SCZ pathophysiology implicates mitochondrial dysfunction as a contributing factor to biological and clinical symptoms characteristic of the disorder. The overlapping influence of hypoxia and SCZ genetic risk, specifically on mitochondria and metabolism pathways, strongly motivates further research into the mechanisms behind this overlap.

A. Normoxia

B. Hypoxia

C.
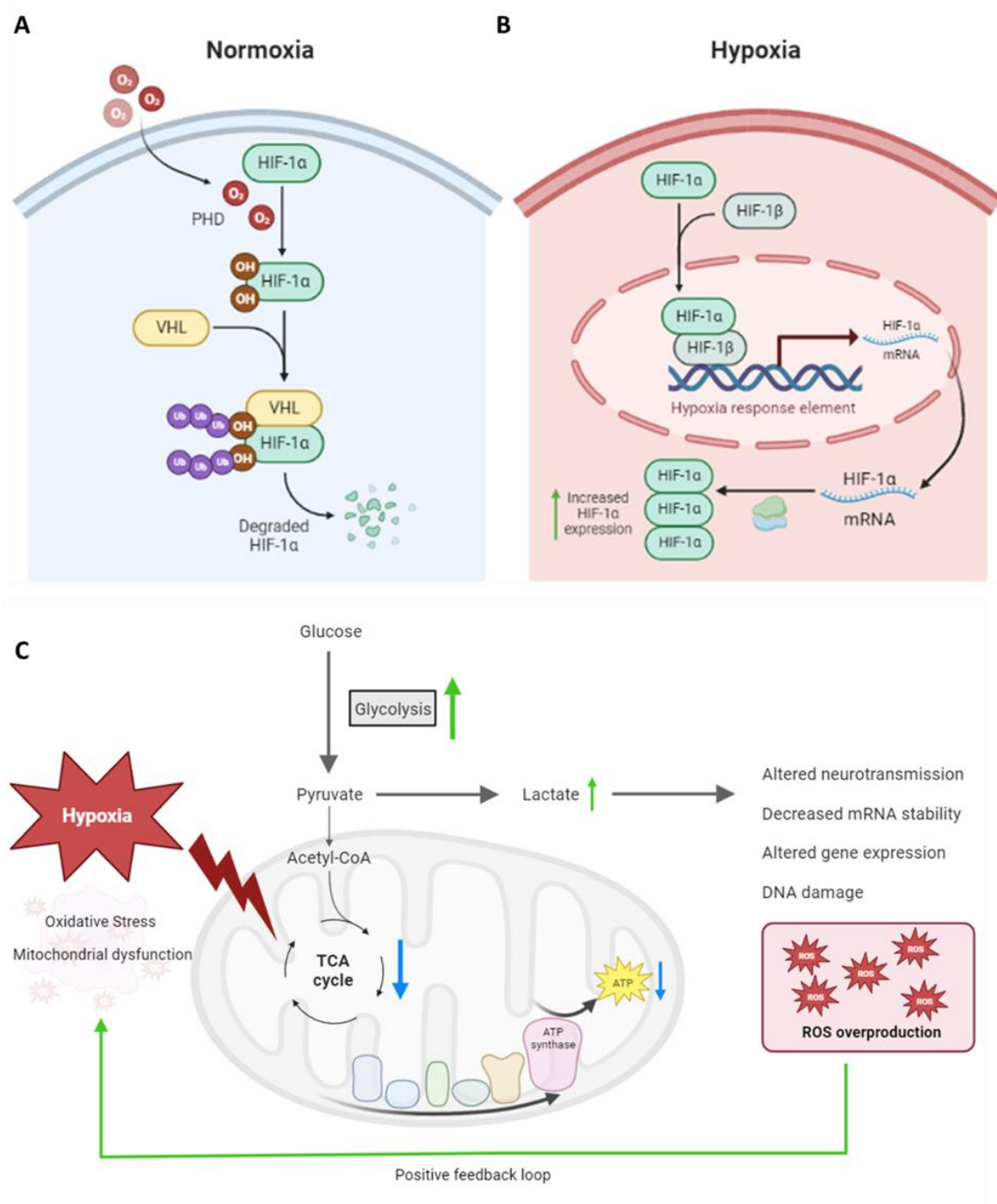
Figure 1 – Hypoxia regulates mitochondrial activity by shifting from oxidative phosphorylation to anaerobic metabolism.
(A) Degradation of HIF-1α under normal oxygen conditions. Prolyl hydroxylase (PHD) enzymes add hydroxyl groups to HIF-1α, which is then marked for proteasomal degradation via ubiquitin tags by von hippel lindau (VHL) protein.
(B) Under hypoxic conditions, HIF-1α is not degraded and instead is translocated to the nucleus with HIF-1β. The heterodimer binds to hypoxia response elements of various genes. HIF-1α mRNA undergoes ribosomal translation leading to increased protein levels of HIF-1α **(C)** During hypoxia, oxidative stress and mitochondrial dysfunction result from the inhibition of pyruvate from entering the TCA cycle and inefficient electron transport through the electron transport chain; the result is lower ATP production and utilization. Energy utilization shifts to anaerobic metabolism by increasing glycolysis activity and lactic acid formation. As lactate levels increase, pH changes lead to altered neurotransmission, changes to mRNA stability and gene expression, and DNA damage. Cellular hypoxic responses work on a positive feedback loop as increased production of reactive oxygen species (ROS) due to reductions in mitochondrial homeostasis, leading to more stress on the system. Figure generated using BioRender.com.

1.2.1 *Links between hypoxia and SCZ*

Prenatal hypoxic insults caused by obstetric complications (OCs) such as preeclampsia, asphyxia, and placental abruption are well-documented epidemiologic risk factors for SCZ (Schmitt et al. 2014). Fetal hypoxia leading to low birth weight and subsequent development of SCZ has been documented (Fineberg et al. 2013). Offspring of individuals with such complications face an elevated risk of SCZ, ranging from 1.5 to 3 times higher (M. Cannon, Jones, and Murray 2002). Additionally, patients that experienced multiple OCs leading to fetal hypoxia are also associated with the development of an earlier onset of symptoms (Rosso et al. 2000). The neurological impacts of prenatal hypoxia are widespread and include neuronal death, damage to white matter and decreased myelination, and reduced dendritic growth (Réthelyi, Benkovits, and Bitter 2013). Dysregulation of neuronal development is greatest when the impact occurs at midgestational periods (Schmitt et al. 2014). In SCZ specifically, the hippocampus and cortical gray matter are susceptible to hypoxic insults. Fetal hypoxia has been linked to increased ventricular size, reduced cortical gray matter, and reduced hippocampal volume (T. D. Cannon et al. 2002; Meisenzahl et al. 2010; Schmitt et al. 2014). Dysregulation of synaptic pruning processes during adolescence, resulting in excessive loss of synaptic connections, is a hallmark of SCZ pathology. Fetal brains predisposed with genetic risk factors for SCZ paired with hypoxia resulting in loss of neuronal synaptic connections may lead to exacerbation of clinical symptoms later in life (Schmitt et al. 2014; Réthelyi, Benkovits, and Bitter 2013).

Schmidt-Kastner et al. (2020) explored this GEI between SCZ genetic risk using GWAS-derived SCZ genes and ischemia-hypoxia gene sets to determine the overlap between gene sets. They report that 55% of GWAS SCZ genes are subject to regulation by genes invoked during hypoxic responses. Another study developed and validated 12 hypoxia-related signature genes to be used as biomarkers to distinguish nonpsychiatric controls (CTRL) from SCZ patients (Z. Li et al. 2023). Of these 12 genes, vascular endothelial growth factor (VEGFA) was highly related to SCZ in protein-protein interaction network analysis. VEGFA is a critical neurotrophic factor involved in neurogenesis, brain plasticity, and angiogenesis (Lizano et al. 2018). In SCZ, altered VEGFA expression at the transcriptomic and genomic level in the prefrontal cortex of post-mortem SCZ samples has been found (Fulzele and Pillai 2009; Lee and Huang 2016).

1.3   Cerebral organoid model

Examining GEI in a clinical setting is very difficult to assess (Uher 2009), thus, many researchers have turned to neurodevelopmental animal models of SCZ and other psychiatric disorders. These are valuable resources to improve knowledge on the neurobiological bases of mental illness (Białoń and Wąsik 2022). However, SCZ is an extremely complex and heterogenous disorder that is difficult to recapitulate fully at a molecular level due to species-specific differences in cytoarchitecture and genetic landscape. The ability to study *in vitro* specifics of neurodevelopmental illness can be remedied using the cerebral organoid model.

This three-dimensional culture system was developed in 2013 by Lancaster et al. and was initially used to mimic microcephaly phenotypes (Lancaster et al. 2013). Cerebral organoids comprise tissue that recapitulates early corticogenesis stages of human fetal brains. They are derived from embryonic stem cells or iPSCs, where various growth factors and nutrient-rich media push differentiation toward neural fates. Throughout their growth, cerebral organoids recapitulate the layering observed in fetal brains: a lower VZ, intermediate SVZ, and rudimentary CP. While individual labs have differences in organoid generation methodology, the general pipeline is as follows. iPSCs cultures are dissociated to single-cell suspensions and aggregated into embryoid bodies (EBs).

Applying neural induction media to EBs leads to the formation of a neuroectoderm that contains neural stem cells. To mimic *in vivo* extracellular matrix qualities, developing EBs are embedded into Matrigel®, which contains four major basement membrane proteins that promote cell growth. Variations of differentiation media are continually applied, and by day 10, organoids contain neuroepithelia that surround fluid-filled cavities similar to human ventricles.

By day 40, several cortical-like regions become evident upon cryosectioning and immunostaining with markers specific to the developing human cortex. Mirroring *in vivo* fetal brain development, paired box 6+ (PAX6) apical progenitors are confined to a VZ-like area, clearly distinct from class III β-tubulin+ (TUJ1) neurons. Additionally, a CP-like region emerges, housing COUP-TF-Interacting Protein-2 (CTIP2)+ and TUJ1+ neurons. Through RNA-Sequencing (RNA-Seq) analysis, it becomes apparent that the cerebral organoids and the fetal brain exhibit comparable expression levels of genes linked to synaptic transmission and neurogenesis (C. Luo et al. 2016). The similarity in gene expression and molecular layering observed in the organoids reconfirms this as a powerful model system for studying fundamental aspects of brain development. Long-term culturing of organoids also leads to maturation of neural tissue; at 6-months old cerebral organoids expresses markers indicative of oligodendrocyte formation and excitatory and inhibitory neurons (Matsui et al. 2018). Cerebral organoids create a platform that recapitulates both early and later periods of embryonic human brain development.

In the years since, the cerebral organoid model has been expanded to various neurodevelopmental disorders, including SCZ, bipolar disorder, major depressive disorder, and autism spectrum disorder (Dixon and Muotri 2023). Other applications have included research into brain tumorigenesis, infectious disease, drug effects and toxicology studies (Shou et al. 2020). Using induced pluripotent stem cells from SCZ patients allows for the modelling of the genetic component of the disorder and gives insight into how environmental stressors such as hypoxia influence subsequent cortical development at a molecular level.

1.3.1 *Organoid models of SCZ*

Numerous studies have validated the use of SCZ patient-derived iPSCs to develop brain organoids (Sawada et al. 2020; Stachowiak et al. 2017; Srikanth et al. 2018; Qian et al. 2020; Notaras, Lodhi, Dündar, et al. 2021; Kathuria et al. 2020; Nascimento et al. 2022; Notaras, Lodhi, Fang, et al. 2021; Notaras et al. 2022). Commonalities arise between these studies regarding progenitor differentiation and changes to distributions of proteins and altered layering uncharacteristic of healthy development. Neural progenitor cell (NPC) proliferation in the VZ-like region of SCZ organoids is decreased, which contrasts the accelerated differentiation of NPCs into immature and mature neuron identities (Sawada et al. 2020; Stachowiak et al. 2017; Srikanth et al. 2018). Additionally, post-mitotic neurons that usually reside in the CP in standard organoids are displaced throughout the SVZ and VZ (Stachowiak et al. 2017). At mature stages, mature neurons expressing cortical-layer specific transcription factors and proteins do not arrange into distinct and characteristic layers in SCZ organoids compared to CTRLs. Additionally, SCZ organoids have shown decreased differentiation of glutamatergic neurons followed by an increased differentiation of γ-Aminobutyric acid (GABA)ergic neurons (Qian et al. 2020). Transcriptomic analysis of SCZ organoids across multiple studies shows differential expression of genes involved in neurodevelopment, synaptogenesis, and immune responses. Kathuria et al. (2020) completed total RNA-Seq on 6-month-old SCZ organoids, and the top GO: Biological Processes terms include "nervous system development", "neurogenesis", and "generation of neurons". Single-cell RNA-Seq of SCZ organoid transcriptomes classified ~75% of cells as neural progenitors, proliferating cells, or cortical-type cells.; CTRL organoids contained a higher percentage (~93%) of neuronal-specific cells (Notaras et al. 2022).

Functional characterization of the electrical activity and mitochondrial dysfunction implicated in SCZ pathology is also reflected in the SCZ organoid model. For example, mitochondrial dysfunction was measured using a live-cell metabolic stress experiment in 9-month-old organoids; reductions in basal O_2 consumption, ATP production, proton leaks, and nonmitochondrial oxygen consumption were observed in SCZ compared to CTRLs (Kathuria et al. 2020). These results are supported by transcriptomic profiles of

the same organoids where gene set enrichment analysis found terms such as "mitochondrial translation", "oxidative phosphorylation", and "glycolysis" (Kathuria et al. 2023). These results further verify that SCZ organoid models represent metabolic differences observed in SCZ clinical populations. Another critical aspect of organoid development is mature neurons' functional connectivity and activity. This activity can be effectively measured through various electrophysiological techniques, with microelectrode arrays (MEA) systems becoming increasingly popular (Zourray et al. 2022). Brain activity measured via electroencephalogram (EEG) recordings in SCZ patients consistently reports aberrant neuronal activity (Perrottelli et al. 2021). Additionally, positive and negative symptoms of SCZ have been associated with irregular EEG activity (Perrottelli et al. 2021; Mitra et al. 2017; Martínez et al. 2015). Human iPSC-derived neurons from SCZ patients showed altered sodium channel function and increased GABAergic neurotransmission and correlated various electrophysiological measures to patients' cognitive and clinical symptoms of SCZ (Zourray et al. 2022). These results may reflect disruptions to synaptic excitatory-inhibitory balance, a hallmark of SCZ pathology. A functional assay of SCZ-iPSC-derived organoids using an MEA system found similar baseline electrical activity to CTRLs, but a diminished response to electrical stimulation and depolarized state induced by potassium chloride application (Kathuria et al. 2020).

1.3.2 *Organoid models of hypoxia/ischemia*

Due to the high prevalence of fetal hypoxic insults during various stages of pregnancy and birth and minimal research into which specific cell types and brain regions are implicated in the molecular responses, researchers have turned to cerebral organoid models of hypoxia/ischemia. The first group to develop and characterize hypoxic insults in cerebral organoids was Paşca et al. (2019). Using a needle-type fibre optic oxygen microsensor, they found that organoids exposed to low oxygen tension for 48 hours led to a drop in partial oxygen pressure from 85 mmHg to ~25 mmHg at the organoid surface, levels that are below the critical oxygen tension of the brain (Paşca et al. 2019). This method of hypoxia induction also leads to the expected increase in HIF-1α protein expression without inducing massive cell death and cytoarchitectural collapse (Paşca et

al. 2019). Another group tested similar hypoxia induction protocols with slightly higher oxygen levels of 3% O_2 exposure for 24 hours and similarly reported stabilization of HIF-1α (Daviaud et al. 2019).

In terms of transcriptomic responses to hypoxia in the organoid model, Pasca et al. (2019) completed RNA-Seq after 24- and 48 hours of low O_2 exposure and after 72 hours of recovery at 21% O_2. They report 1,500+ differentially expressed (DE) genes between 24- and 48-hour hypoxic exposed organoids to unexposed organoids and no transcriptomic differences in organoids in the 72-hour recovery group. Transcriptomic changes in response to transient hypoxia are most prominent immediately following the insult, and a period of recovery appears to return the expression to its original state.

Cerebral organoids exposed to hypoxia express distinct vulnerability based on cell type. For example, neural stem cells in the lowermost VZ of organoids do not suffer significant losses in. In contrast, outer radial glial cells and intermediate progenitors expressed response to hypoxia in the SVZ exhibit immediate and prolonged apoptosis (Paşca et al. 2019; Daviaud et al. 2019; M. S. Kim et al. 2021). These results reflect perinatal hypoxia models in rats that detect loss of various progenitor cell types in the SVZ of the dorsolateral cortex of P6 rats (Levison et al. 2001). Long-term resilience in neural stem cell (NSC) populations is found in animal and organoid hypoxia models. In a neonatal mouse model of hypoxia, they reported reductions in progenitors and immature neurons, but NSC populations remained stable (Kwak et al. 2015). Additionally, another group reported resilience of NSC populations in the proliferative VZ of neonatal mice hippocampus post-hypoxic injury (Shin et al. 2020).

Hypoxia at its' core is defined as insufficient oxygen; however, in clinical settings, pure hypoxia is unusual and instead is often paired with a drop in cerebral blood flow (ischemia). In this case, the energy crisis resulting from low oxygen and toxic metabolites usually removed in normal circulation builds up, further exacerbates physiological stress (Dirnagl, Iadecola, and Moskowitz 1999). While the existing organoid models of hypoxic injury are reflective of molecular alterations observed in various animal models, one of the major limitations is a lack of vascularization and blood flow within the cerebral

organoid *in vitro* model. Groups have worked towards a vascularized human brain organoid model to remedy this. Thus far, various publications have successfully co-cultured human brain organoids with vascular cells to produce vascular-like structures that still lack blood flow (Matsui et al. 2021). Blood circulation has also been achieved by transplanting vascularized organoids into immunodeficient mice, where the organoids become perfused with the blood circuitry of the mice (Pham et al. 2018; Cakir et al. 2019; Y. Shi et al. 2020; Mansour et al. 2018). Using vascularized organoids is out of this project's scope but provides an interesting new platform to investigate hypoxia and ischemic models further using cerebral organoids.

1.4   Literature Gap

The specific gap in the research literature this project hopes to fill is the absence of a cerebral organoid model of prenatal hypoxia representative of SCZ genotypes. While previous studies have validated the use of cerebral organoids as a model of prenatal hypoxic injury and have developed organoids from SCZ patient populations, the combination of these two areas to create a model of prenatal hypoxia in SCZ populations has yet to be explored and characterized. Developing a cerebral organoid model that incorporates both prenatal hypoxia and SCZ genotypes allows for the specific investigation of the impacts of the GEI between hypoxia and SCZ genetic-influenced brain development in a human-based model. This model could help elucidate the specific molecular pathways and cellular processes affected by prenatal hypoxia in individuals with SCZ-associated genetic predispositions. Understanding the interplay between hypoxia and genetic factors in SCZ brain development could provide valuable insights into the underlying mechanisms of the disorder. Therefore, exploring this research gap is essential for advancing our understanding of the complex etiology of SCZ.

1.5   Research Objectives and Hypotheses

The primary goal of this project is to examine how the SCZ genetics and environmental influence of hypoxia influence brain development via cerebral organoids. To this end, the goal is comprised of three main aims:

Aim 1. Characterize the cerebral organoid model and method of hypoxic exposure in both SCZ and healthy CTRL organoids via the expression of expected neuronal development markers and hallmarks of hypoxia cellular responses.

Aim 2. Establish the impacts of SCZ genetics and hypoxia exposure on mitochondrial-specific proteins and genes associated with metabolism and reactive oxygen species responses using western blot and RNA-Seq.

Aim 3. Determine the transcriptomic changes resulting from SCZ genetics and hypoxia exposure alone and in tandem to elucidate GEI between SCZ genetics and hypoxia

We hypothesized that hypoxia-exposed human iPSC-derived cerebral brain organoids from SCZ populations will exhibit altered neuronal differentiation and development, changes to mitochondrial related genes and proteins, and differential expression of genes implicated in hypoxia pathways and neuronal development.

2　　Methods

2.1　　Induced pluripotent stem cell culturing

Induced pluripotent stem cells (iPSCs) were acquired through the NIMH Genetics
Repository collection (Rutgers Infinity Biologix). Patient demographic information is
provided in **Table 1**. Feeder-free iPSC cell lines were maintained in mTeSR™1 (Stem
Cell Technologies, CAT#85850) on Matrigel-coated 6-well plates according to Stem Cell
Technologies Maintenance of Human Pluripotent Stem Cell Technical Manual (Stem Cell
hPSC Manual)(STEMCELL Technologies Inc. 2019).

Table 1 – Induced pluripotent stem cell subject demographic information

Alias	NIMH Sample ID	Sex	Race	Age (Years)	Diagnosis
CF1	MH0185865	F	White	24	CTRL
CF2	MH0185916	F	White	25	CTRL
CF3	MH0185905	F	White	33	CTRL
CM1	MH0185913	M	White	26	CTRL
CM2	MH0185983	M	White	29	CTRL
CM3	MH0185984	M	White	29	CTRL
SM1	MH0185897	M	White	27	SCZ
SM3	MH0185975	M	White	28	SCZ
SM2	MH0185900	M	White	31	SCZ
SF1	MH0185954	F	More than one	34	SCZ
SF2	MH0185964	F	Asian	43	SCZ
SF3	MH0185958	F	White	56	SCZ

Briefly, Matrigel (Corning® Matrigel® hESC-Qualified Matrix, CAT# 354277) was
dissolved in DMEM/F-12 with 15 mM HEPES (Stem Cell Technologies, CAT#36254)

according to the dilution factor provided in the Matrigel Certificate of Analysis. When handling Matrigel, all tips and tubes were kept cold to prevent gelling. Immediately after diluting, 1 mL/well of the diluted matrix was added to a standard 6-well culture plate. Plates were gently swirled so the solution coated the entire bottom surface, then plated were incubated at 37°C for 1 hour. After incubation, excess Matrigel solution was removed via aspiration, and 2 mL/well of mTeSR™1 (Stem Cell Technologies, CAT#85850) medium was added. Plates were stored in an incubator until ready for use.

iPSCs were thawed and plated into Matrigel-coated cultureware according to section 7.3 of Stem Cell hPSC Technical Manual (STEMCELL Technologies Inc. 2019). In brief, vials of cells were defrosted in the vapour phase of a nitrogen tank for 1 hour before plating. Vials were then fully thawed, dissolved in 5 mL of mTeSR™1, and gently mixed. Cells were centrifuged at 300 x g for 3 minutes, then the medium was aspirated, leaving the pellet intact. The cell pellet was resuspended in 1 mL of mTeSR™1 medium and plated into a single well of Matrigel-coated 6-well plate. Plates were rocked to evenly distribute the cells and placed inside a hypoxic chamber at 5% O_2, 5% CO_2 incubator at 37 °C. To promote and maintain pluripotency, RHO/ROCK pathway inhibitor Y-27632 (Stem Cell Technologies, CAT#72302) was added to iPSCs on the first day of culture at a final dilution of 1:1000 per well.

Passaging of iPSCs was completed according to section 5.2 of Stem Cell hPSC Technical Manual (STEMCELL Technologies Inc. 2019). iPSCs were passaged when confluency met ~60-70%. A daily feeding schedule was used, where wells below 50% confluency were fed 2 mL/well of new mTeSR™1 medium until passaging was required.

Prior to passaging, an upright microscope was used to identify regions of differentiation which were removed by scraping with a pipette tip. Media was removed via aspiration, and 1 mL of Gentle Cell Dissociation Reagent (Stem Cell Technologies, CAT#100-1077) was added per well. The dissociation reagent was incubated at room temperature for ~ 2-3 minutes, or until colony edges appeared bright, then aspirated and 1 mL of mTeSR™1 media was added to the well. Colonies were gently scraped using a cell scraper, transferred to a conical tube, and large colonies were broken up by carefully pipetting up

and down 2-5 times until cell aggregates were 50 – 200 μm in size. Cells were plated into a Matrigel-coated 6-well plate at dilutions based on the confluency of each well according to **Table 2**. Plates were returned to the incubator and not disturbed for 24 hours to allow colonies to adhere to the Matrigel.

Table 2 – Suggested Split Ratios for iPSC Passaging

iPSC Confluency	Split Ratio
>50%	Not passaged
60-70%	1:4
70-80%	1:6
80% +	1:8

iPSC cells were maintained in culture for 18 days before the organoid differentiation process began. Two days prior to differentiation, iPSCs underwent a pre-treatment of growth factors that have been shown to increase the expression of genes associated with cortical tissues (M. Watanabe et al. 2019) at the following concentrations: BMP4 = 0.1 ng/mL, TGFβ-1 = 0.1 ng/mL, TGFβ-3 = 1.0 ng/mL, ACTIVIN A = 15 ng/mL (all purchased from Stem Cell Technologies).

2.2   Cerebral organoid generation

Cerebral organoids were generated using the STEMdiff™ Cerebral Organoid Kit (Stem Cell Technologies, CAT #08570, #08571). **Figure 2A** represents a visual schematic of the differentiation protocol. Preparation of all the media required for differentiation is listed in Appendix 5.1.2.

EB FORMATION - DAY 0 - 4: iPSCs were checked for areas of differentiation and removed if found. Cells were rinsed with 1 mL with Dulbecco's Phosphate-Buffered Saline (D-PBS, without Ca^{++} and Mg^{++}), then dissociated using Gentle Cell Dissociation Reagent incubated at 37°C for ~5 minutes and a cell scraper. Cells were transferred to a conical tube, and aggregates were broken up via pipetting until a single-cell suspension was achieved. To the cells, 1 mL of EB Seeding Medium was added, then samples were centrifuged at 300 x g for 3 minutes, aspirated supernatant and resuspended pellet in 2 mL EB Seeding Medium. Cells were counted using Trypan Blue and a hemocytometer. Cell

counts were used to calculate dilution factors required to plate 9,000 cells/well of a 96-well plate; cells were diluted with EB Seeding Medium to achieve the required concentration. Using a multichannel pipette, 100 μL of the cell suspension was added to each well of a 96-well round-bottom ultra-low attachment plate (Corning®, CAT#7007). Plates were incubated in a 5% CO_2 incubator at 37ºC and not disturbed for 24 hours. Small EBs, approximately 100 – 200 μM, formed. Media was added on days 2 and 4, where 100 μL of new EB Formation Medium was added per well using a multichannel pipette. The differentiation process was continued if rounded EBs with smooth edges formed.

INDUCTION - DAY 5: Ultra-low attachment plates were made by coating standard 24-well plates with 0.5 mL of Anti-Adherence Rinsing Solution (Stem Cell Technologies, CAT#07010) to each well, incubated for 5 minutes at room temp, then rinsed with 1 mL sterile PBS. 0.5 mL of Induction Medium was added to each well of the 24-well plate. EBs were transferred into the 24 well plates, where 1-2 EBs added to each well. To transfer EB's, wide-bore 200 μL pipette tips were used to remove EBs from the 96-well plate. Once the EB was in the tip, it was ejected into the 24-well plate, ejecting as little EB Formation Medium as possible. Plates were incubated at 37ºC for 48 hours.

EXPANSION - DAY 7-9: Using a wide-bore 200 μL pipette tip, EBs were drawn up from the 24-well plate and transferred into a well of an Organoid Embedding Sheet (Stem Cell Technologies, CAT#08579). Excess media around the EB was removed, then using a cold 200 μL pipette tip, 15 uL of Matrigel (Corning® hESC-Qualified Matrix, CAT# 354277) was added on top of each EB. The Matrigel droplets were polymerized via incubation at 37ºC for 30 minutes. To 6-well ultra-low adherent plates (Stem Cell Technologies, CAT#8071), 3 mL/well of Expansion Medium was added. To transfer the EBs off the embedding sheet after polymerization, a 1 mL pipettor was used to draw up Expansion Medium and wash EBs off the sheet directly into the well, repeating until all EBs were in the well. Plates were incubated at 37ºC for 3 days. Neuroepithelia development was determined by 'budding' of the EB surface occurring.

ORGANOID MATURATION - DAY 10+: On day 10, media was carefully removed using a 2 mL serological pipette and replaced with 3 mL/well of Maturation Medium. Plates were also transferred to an orbital shaker in a 37ºC incubator set to a shaking speed of 65 rpm. Full media changes were completed every 3 days. Cultureware was tilted and medium removed using a serological pipette. Maturation Medium was added at 3 mL/well until organoids were ~70 days old, then volume increased to 3.5 mL or 4 mL/well if the media was yellow by day 3 media change. Starting at Day 40, Cultrex Reduced Growth Factor Basement Membrane Extract, Type 2, Select (R&D Systems, CAT# 3536-005-02) was added to the Maturation Media at a 1:200 dilution to promote cerebral differentiation and growth of the organoids.

2.3   Exposure of cerebral organoids to low oxygen

On Day 29-30 of differentiation, organoids previously maintained in 21% O_2 and 5% CO_2 were transferred to a C-chamber hypoxia sub-chamber (Biospherix, CAT#C-174) on an orbital shaker set to 65 rpm. Oxygen levels were set to 3% O_2 at least 24 hours prior to moving the organoids; O_2 levels were controlled by a ProOx 110 Compact Oxygen Controller (Biospherix) and a mixed CO_2/N_2 compressed gas source. After 24-hour exposure, D30 organoids were immediately collected for analysis. Remaining organoids were transferred back to normoxic conditions (21% O_2 and 5% CO_2) and maintained in maturation medium until analysis when organoids were fully mature, day 170 post-differentiation (**Figure 2B**).
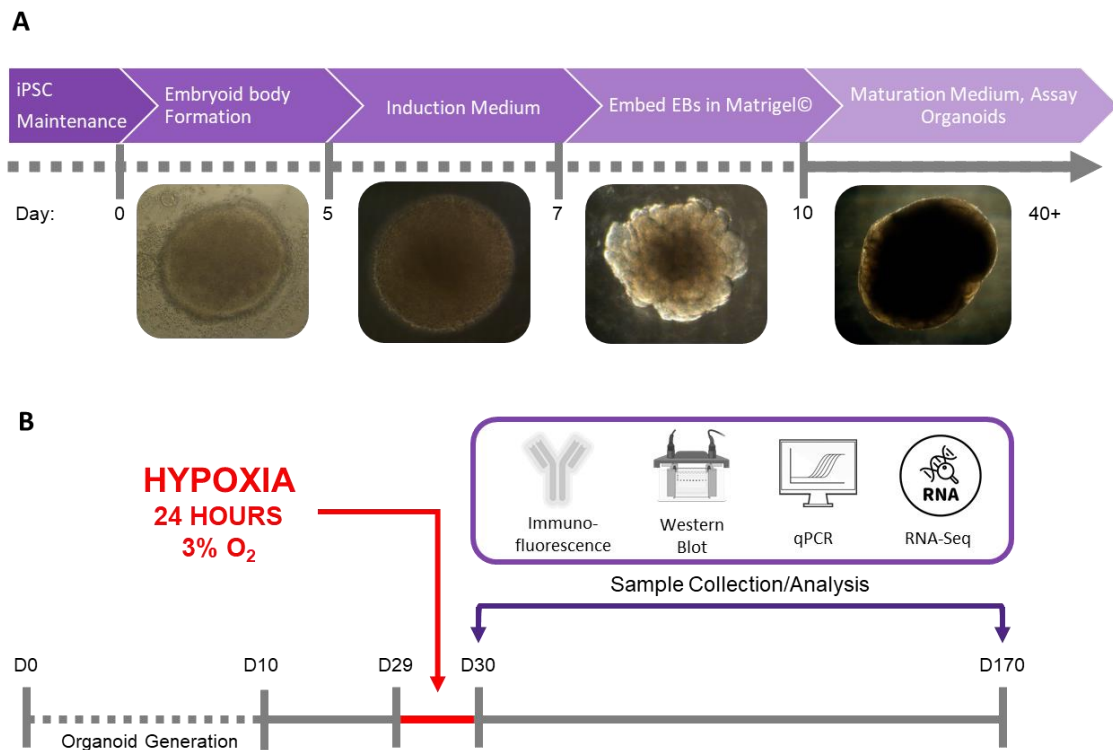
Figure 2 - Organoid generation timeline and experimental design.
(A) Schematic illustrating the major stages in organoid generation from CTRL and SCZ iPSC cells. **(B)** At day 29-30 of *in vitro* differentiation, organoids are exposed for 24 hours at 3% O_2 in a gas-controlled culture chamber and then maintained at 21% O_2 for the remainder of culturing. Normoxic organoids are maintained at 21% O_2 throughout. Samples were collected for analysis immediately post-hypoxia (D30) and once organoids were fully matured (D170) for the following experimental analysis: immunofluorescence, western blot, and quantitative PCR. RNA-Sequencing samples were only collected at D30.

2.4   Immunofluorescence

2.4.1 *Cryopreservation and Sectioning*

For cryoprotection, organoids were washed in 5 mL of sterile D-PBS (without Ca^{++} and Mg^{++}) for 5 minutes, then transferred to into 2.5 mL of 4% paraformaldehyde (PFA) for 16-18 hours and stored at 4°C. Organoids underwent 3× washes of 5 mL D-PBS-T for 10 minutes each to remove PFA. Washed organoids were transferred into 3 mL of 30% sucrose and equilibrated for 2-3 days at 4°C. Fixed and preserved organoids were embedded in disposable embedding molds (Peel-A-Way®, CAT#18646A-1) a 7.5% gelatin solution (Appendix 5.1.1). Once in the molds, organoids and surrounding gelatin were snap-frozen in a dry-ice ethanol bath for 5 minutes, samples stored at -80°C.

For immunofluorescence and hematoxylin and eosin (H&E) staining, using a cryostat (CryoStar NX50, Thermo Scientific) set to -18°C, organoids were cut into 20 μm thick sections. Sections were directly collected onto Superfrost® Plus Micro Slide (VWR, CAT#48311-703) coated with 1:10 Poly-L-lysine (Sigma Aldrich, CAT#P4707) and stored in microscope slide boxes at 4°C.

2.4.2 *Immunohistochemistry*

In PBS-T (phosphate-buffered saline with Tween 20) warmed to 37°C, organoid cryosections were washed for 10 minutes to remove excess gelatin. Sections were circled with a hydrophobic barrier PAP pen (Invitrogen, CAT#R3777). Blocking was done with a 5% normal donkey serum (NDS) in PBS-T for 1 hour at room temperature with slides in humidified chambers. Blocking was removed via pipette, then sections were incubated overnight at 4°C in primary antibodies of interest diluted in 5% NDS in PBS-T. Primary antibody species and dilutions are listed in **Table 3**. For each combination of primary antibodies host species, a no primary antibody control was run. Tissues were incubated with the antibody diluent alone and no primary antibody, followed by incubation with secondary antibodies and detection reagents. This ensures that staining is produced from the detection of the antigen by the primary antibody and not by the detection system or the specimen.

$3\times$ washes of 10 minutes in PBS-T were used to wash off the primary antibodies, then cryosections were incubated with species-appropriate fluorophore-conjugated secondary antibodies (donkey anti– rabbit, rat, mouse or sheep Alexa Fluor™ 488, 568, 647, Thermo Scientific) in 5% NDS in PBS-T for 2 hours at room temperature. After secondary incubation, $3\times$ washes of 10 minutes in PBS-T was done. Once slides were dry, nuclei were stained with 4',6-Diamidino-2-Phenylindole, Dihydrochloride (DAPI, Thermo Scientific, CAT#D1306) for 5 minutes. Coverslips with a thickness #1 and either 18x18 cm or 20x50 cm (Fisher Scientific, CAT#12-542A) were applied to slides and edges sealed with clear nail polish to prevent air bubbles from forming.

Table 3 - Primary Antibodies for Immunofluorescence

Target	Host Species	CAT#	Company	Dilution
HIF-1α	Rabbit	ab179483	Abcam	1:100
MAP2	Mouse	MAB3418	Sigma-Aldrich	1:100
Cleaved Caspase 3	Rabbit	9661	Cell Signaling Technology	1:200
Ki67	Rabbit	ab15580	Abcam	1:500
mGluR2/3	Rabbit	06-676	Sigma-Aldrich	1:50
Synaptophysin	Rabbit	ab32127	Abcam	1:100
CTIP2	Rat	ab18465	Abcam	1:300
β-actin	Mouse	A2228	Sigma-Aldrich	1:100
NMDAR2A	Rabbit	ab1555P	Sigma-Aldrich	1:50
NeuN	Mouse	94403	Cell Signaling Technology	1:300
Doublecortin	Mouse	sc-271390	Santa Cruz Biotechnology	1:50
5HT1A Receptor	Rabbit	ab85615	Abcam	1:100

2.4.3 *Confocal Microscopy*

Images were acquired using a Leica SP8 LIGHTNING confocal microscope or a Leica STELLARIS 5 upright confocal microscope at 40X or 63X magnification, depending on the sample size and time point. Images were taken in 2048 x 2048 format, line averaging of 2, scan speed of 400. Two to four regions of interest (ROI) per organoid were scanned. Z-stacks spanning 1.5 µM to 3 µM containing 5 images each were acquired for each ROI.

2.4.4 *Immunofluorescence Quantification and Statistical Analysis*

A blind analysis technique was used throughout the immunofluorescent quantification process to eliminate experimenter bias. Image files were assigned a random alias by an uninterested third party. Decryption of the alias was only completed after all image data was acquired and was ready for statistical analysis.

Images were processed and analyzed in ImageJ Fiji (version 2.1.0) (Schindelin et al. 2012). Leica image files (lif.) were imported and viewed with the hyperstack function and composite colour mode. Z-stacks were projected into a single plane using the "Z-projection" function, using the projection type "Average Intensity". Fluorescent channels were split into separate files for further analysis. Images were converted to 8-bit, followed by thresholding. The thresholding method for each target of interest was chosen based on which method best represented the original fluorescent staining patterns. Images were then made binary and despeckled. If there was remaining background signal, the "remove outliers" function was applied, where the radius and threshold were adjusted only to

include signal and exclude background noise. Watershed separation was applied to separate clumped cells into individual entities. ROI selection was completed with the DAPI staining corresponding to the target of interest's image; this was to ensure the entire 'ventricular-like' region was included in analysis and any background was excluded. The ROI was applied to the original watershed image, and the following measurements of the ROI were recorded in Excel: Area, mean gray value, integrated density, and raw integrated density. Particle counts within each ROI were recorded using the "Analyse Particles" function; the size (μm^2) and circularity discrimination cut-offs were adjusted for each marker to include only objects represented in the original fluorescent stain. To account for differences in 'ventricular-like region' sizes between ROIs and samples, particle counts were normalized to area (number of particles/area(mm^2)). For certain targets, the signal distribution was widespread, with particles of various sizes across a single sample. In this case, watershed and particle counts were inaccurate. Instead, an 'integrated density (IntDen)' measure was used to compare expression levels between groups, where IntDen = (sum of pixel values in selection) * (area of one pixel).

A two-way ANOVA was used to determine differences in target expression levels between disease state (CTRL vs SCZ) and hypoxia treatment effect within groups. Outliers were determined and removed after a Grubb's test. Significant level (α) was set, a priori, at 0.05. If the results of the ANOVA were found to be significant, *post hoc* Fisher's LSD analyses were performed. A value of $p < 0.05$ was considered to indicate statistical significance. Unless otherwise indicated, data are presented as means +/- SEM. All analyses were performed using GraphPad Prism (version 9.5.1 for Windows 10).

2.5   Hematoxylin and eosin (H&E) stain

Whole organoids embedded in gelatin-filled molds were cut into 20 μm thick sections using a cryostat. Sections were directly collected onto Superfrost® Plus Micro Slide (VWR, CAT#48311-703) coated with 1:10 Poly-L-lysine (Sigma Aldrich, CAT#) and stored in microscope slide boxes at 4°C. Samples were sent to the Molecular Pathology Core Facility (Robarts Research, Western University) for hematoxylin and eosin (H&E) staining. Slides were imaged using a brightfield microscope Nikon H600L microscope

equipped with a DS-Qi2-Nikon camera and the NIS-Elements software with the following settings: auto white balanced setting applied using slide background, 10X magnification, exposure: 2.5 ms, 2048 x 2048 formatting. To capture the entire sample, tiling of entire organoid was completed with 20% overlap between frames and stitched via "blending" operation.

2.6   Western Blot

2.6.1 *Protein Extraction*

Organoids were collected into 1.5 mL microcentrifuge tubes and flash-frozen on dry ice (1 to 2 organoids per tube); samples were stored at -80°. During protein extraction, samples were kept on ice between all steps. RIPA Lysis buffer contained: 50mM Tris pH 7.4, 150mM NaCl, 1% NP-40, 0.5% sodium deoxycholate, 10% glycerol, and 0.1% SDS, diluted in water, with 1:100 protease and phosphatase inhibitor (HALT 100× inhibitor cocktail, ThermoFisher, CAT#78440). 200µL of lysis buffer was added to each microcentrifuge tube, and samples were homogenized in 10-second increments using an electric homogenizer. Samples were rotated at 4°C for 1 hour, then centrifuged at 15,000 rpm for 15 minutes at 4°C. Supernatant was transferred to a new microcentrifuge tube, and 10 µL was set aside for protein quantification. The remaining sample solution was mixed with an equal volume of 2× Laemmli sample buffer. Half the sample volume was heated at 95°C for 5 min before storage at −20°C. The remaining samples were not denatured to use in OXPHOS staining later and stored at −20°C.

Protein quantification was completed using the Pierce™ BCA Protein Assay Kit (ThermoFisher, CAT#23225). BSA standards ranging from 0.1 µg/µL to 2.0 µg/µL and samples of interest were loaded into a clear flat-bottom 96-well plate. 200 µL of a 1:50 mixture of Reagent B: Reagent A was added to each well, and the plate was incubated at 37°C for 30 minutes prior to scanning with a microplate reader, wavelength 562 nm. Protein concentration of samples was calculated via the standard curve equation ($R^2 >$ 0.99).

2.6.2 *Gel Electrophoresis and Electroblotting*

2 µL of a reference ladder (FroggaBio BLUelf Prestained Protein Ladder, CAT#PM008-0500) was loaded into the first well. Either 10 or 15 µg of stored protein diluted to 30 µL with 2× Laemmli sample buffer was loaded into 10% denaturing SDS-PAGE gels. Electrophoresis was completed using a Bio-Rad Mini-PROTEAN Tetra cell Western blotting apparatus with 10X Tris/glycine/SDS buffer (Bio-Rad) at 125 V for approximately 1 hour 20 minutes. Proteins were transferred onto nitrocellulose (carbonic anhydrase IX) or methanol-activated PVDF membranes (OXPHOS) using the Trans-Blot Turbo Transfer System (Bio-Rad) at 2.5 A for 10-20 minutes. Membranes were then blocked with either 1% (OXPHOS) or 5% (carbonic anhydrase IX) non-fat dry milk in Tris-buffered saline with Tween 20 (0.05% TBS-T) for 1 h with rocking at room temperature.

2.6.3 *Antibody Incubation*

Primary antibody host species, dilutions and sources were as follows: α-tubulin (rabbit, 1:500, Proteintech #11224-1-AP), α-tubulin (mouse, 1:500, Santa Cruz Biotechnology #sc-8035), carbonic anhydrase IX (rabbit, 1:500, Novus Biologicals #NB100-417), total OXPHOS antibody cocktail (5 mouse mAbs, 1:250, Abcam # ab110413). Membranes were incubated in primary antibody of interest overnight at 4°C on a rocking platform. Prior to secondary antibody incubation, membranes 3× washes of 10 minutes in TBS-T. Species-appropriate fluorophore-conjugated secondary antibodies (LI-COR IRDye 680RD and IRDye 800CW; Thermo Scientific) were both used at a 1:10,000 dilution. Secondaries were incubated for 2 hours at room temperature on a rocking platform.

2.6.4 *Protein Quantification and Statistical Analysis*

Membranes were scanned using a LI-COR Odyssey Infrared Imaging System, and densitometry measurements were obtained using Image Studio analysis software. Each sample's target protein band was normalized to the intensity of the respective α-tubulin band. For statistical analyses, two-tailed unpaired t-tests were used to determine the effect of hypoxia on protein expression in CTRL or SCZ organoids. Normality was tested using

a D'Agostino & Pearson test. If the n-size was too small, a Shapiro-Wilk normality test was used instead. A two-tailed Mann-Whitney U test was used if normality was not reached. A value of $p < 0.05$ was considered to indicate statistical significance. Due to the physical limitation of western blot gels, each blot contained samples from the normoxic and hypoxia condition from one disease state (i.e. SCZ normoxia and hypoxia in one blot, CTRL normoxia and hypoxia in another). Due to this limitation, we could not perform two-way ANOVAs as was done for other techniques used throughout this project. Data are presented as means +/- SEM. All analyses were performed using GraphPad Prism (version 9.5.1 for Windows 10).

2.7 Real-time quantitative PCR (qPCR)

2.7.1 *RNA Isolation and cDNA Conversion*

Total RNA was extracted from normoxia and hypoxia-exposed organoids at developmental time points D30 and D170. Samples were homogenized for ~10 seconds in 1 mL TRIzol™ Reagent (Thermo Fisher Scientific, CAT#15596026) using a VWR® 200 homogenizer with a 5mm x 75 mm Flat-Bottom Generator Probe (Avantor, CAT# 10032-326). Samples were incubated on ice in TRIzol™ Reagent for 5 minutes. 200 µL of chloroform (Thermo Fisher Scientific) was added to each sample, and tubes were inverted continuously for 3 minutes. Samples were centrifuged at 12,500 rpm at 4°C for 15 minutes. Without disturbing the lower TRIzol layer, 400-450 µL of supernatant was transferred to a new Eppendorf. RNA was precipitated using an equal volume of isopropanol, and samples were stored at -20°C overnight. RNA underwent $2\times$ rounds of washes with 70% ethanol in DEPC-Treated water (Invitrogen, CAT#AM9906). Final purified RNA was diluted in 20 µL of DEPC-H_2O. RNA concentration and purity was assessed using a NanoDrop™ One micro-UV/vis spectrophotometer (Thermo Fisher Scientific). Any sample with a 260/280 ratio below 1.70 was excluded from the cDNA synthesis step. Template cDNA was prepared by reverse transcription using a High-Capacity cDNA Reverse Transcription Kit (Applied Biosystems, CAT#4368814). $1 - 2$ µg of RNA was loaded per sample and reactions were carried out using a C1000 thermocycler (Bio-Rad) using the following parameters: Denaturation: 25°C for

25 minutes, Annealing: 37°C for 120 minutes, Extension: 85°C for 5 minutes. Samples were diluted to 1:40 in DEPC-H$_2$O and stored at -20°C.

2.7.2 *qPCR Analysis and Statistics*

Quantitative PCR was carried out using the SensiFast SYBR No-ROX Kit (FroggaBio, #BIO-98050) and the CFX Opus 384 real-time PCR detection system (Bio-Rad). For each primer (**Table 4**), melt curves were used to verify the specificity and melting temperature of the amplicon. RT-qPCR reactions were run in technical triplicate, and values used in analysis was the mean of three replicates per sample. Samples in triplicates that were further than 0.5 C$_t$ from the other reads were excluded from analysis. Results were analyzed using the $2^{-\Delta\Delta CT}$ method. Gene expression was normalized to the expression level of two endogenous reference genes, glyceraldehyde 3-phosphate dehydrogenase (GAPDH) and β-actin (ACTB).

Two-way ANOVAs were used to determine differences in gene expression between disease state (CTRL vs SCZ) and hypoxia treatment effect within groups. Outliers were determined and removed after a Grubb's test. Significant level (α) was set, a priori, at 0.05. Normality was tested using a D'Agostino & Pearson test. If the n-size was too small, a Shapiro-Wilk normality test was used instead. If the results of the ANOVA were found to be significant, *post hoc* Fisher's LSD analyses were performed. A value of $p < 0.05$ was considered to indicate statistical significance. Unless otherwise indicated, data are presented as means +/- SEM. All analyses were performed using GraphPad Prism (version 9.5.1 for Windows 10).

Table 4 – Oligonucleotides for qPCR

Gene	Primer Sequence		Reference
	Forward (5')	Reverse (5')	
ACTB*	AAATCTGGCACCACACCTTC	AGAGGCGTACAGGGATAGCA	Wang et al. (2018)
GAPDH	CGCTCTCTGCTCCTCCTGTT	CCATGGTGTCTGAGCGATGT	Rydbirk et al. (2016)
HIF-1a	TATGAGCCAGAAGAACTTTTAGGC	CACCTCTTTTGGCAAGCATCCTG	Iwasa et al. (2021)
PDK1	CTGTGATACGGATCAGAAACCG	TCCACCAAACAATAAAGAGTGCT	Pasca et al. (2019)
PAX6	TGGGCAGGTATTACGAGACTG	ACTCCCGCTTATACTGGGCTA	Harvard PrimerBank ID: 189083679c1
SOX1	TATCTTCTGCTCCGGCTGTT	GGGTCTTCCCTTCCTCCTC	Lancaster et al. (2013)
CTIP2*	GGTGCCTGCTATGACAAGG	GGCTCGGACACTTTCCTGAG	Harvard PrimerBank ID: 12597634c1
TUJ1*	CTCAGGGGCCTTTGGACATC	CAGGCAGTCGCAGTTTTCAC	Ao et al. (2020)
DRD1	GACCTTGTCTGTACTCATCTCCT	GTCACAGTTGTCTATGGTCTCAG	Harvard PrimerBank ID: 88758587c3
DRD2	CAATACGCGCTACAGCTCCAAG	GGCAATGATGCACTCGTTCTGG	Origene, CAT#HP200736
GRM2	CCGCATTGCACGCATCTTC	GGCCCGAGATAAGTGCCAG	Harvard PrimerBank ID: 194248050c2
GRM3	AGCAATCACTGGAGTTTGTCAG	GCAATGAGAAGTGGGATGTTTTC	Harvard PrimerBank ID: 46358416c2
VEGFA	AGGGCAGAATCATCACGAAGT	AGGGTCTCGATTGGATGGCA	Harvard PrimerBank ID: 284172466c1
HSP1A/B	AGCTGGAGCAGGTGTGTAAC	CAGCAATCTTGGAAAGGCCC	Wallace et al. (2017)
MT-ND1	CCACCTCTAGCCTAGCCGTTTA	GGGTCATGATGGCAGGAGTAAT	Wallace et al. (2017)
MT-ND5	CAGCAGCCATTCAAGCAATGC	GGTGGAGACCTAATTGGGCTGATTAG	Wallace et al. (2017)
FOS	CCGGGGATAGCCTCTCTTACT	CCAGGTCCGTGCAGAAGTC	Li et al. (2020)

*Also known as: ACTB = β-actin, CTIP2 = BCL11B, TUJ1 = TUBB3

2.8   RNA-Sequencing

2.8.1 *Sample Preparation*

Organoids were collected into 1.5 mL microcentrifuge tubes and flash-frozen on dry ice
(1 organoid per tube); samples were stored at -80°. Organoids aged D30, immediately
post-hypoxic insult, were sent for analysis. Total RNA extraction was completed by
Genome Quebec, followed by a quality control check. Samples were assessed on a
Bioanalyzer (Aligent) to determine RNA quality via RNA Integrity Number (RIN);
samples with a RIN value greater than 6.5 were included in further analysis. Stranded
mRNA libraries were prepped and underwent a second round of quality control checks.

Libraries were sequenced using the NovaSeq6000 PE100 Sequencing system (Illumina), acquired ~50 million paired-end, 100 bp reads for each sample.

2.8.2 *Bioinformatics and Data Analysis*

Paired-end reads were obtained from Genome Quebec. All reads were aligned and annotated with the latest ENSEMBL Homo Sapien GRCH38.p13 reference genome using STAR version 2.7.10a with recommended settings. Raw counts were generated using the Rsubread sub package featureCounts. Lowly expressed genes were filtered out using a counts per million (CPM) cut-off of 0.4 in at least 2 or more samples. Normalization and differential expression (DE) were analyzed using the edgeR R package (Chen et al., 2016). Briefly, counts were normalized for library size and composition using the trimmed means of M-values (TMM) method. Normalized counts were then fit to a genewise negative binomial generalized linear model, and a quasi-likelihood F test used for DE analysis. To account for multiple testing, p-values were adjusted using Benjamini & Hochberg False Discovery Rate (FDR) correction. An FDR cut-off of < 0.05 and a log (base 2) fold change cut-off of +/- 2 were used to determine significance. The gprofiler2 (Kolberg et al., 2020) R interface for the web toolset g:Profiler was used to convert ENSEMBL gene IDs to gene symbols, and to perform functional enrichment analysis (over-representation analysis) on the DE genes from contrasts of interest. A g:SCS adjusted p-value threshold of < 0.01 was used to determine significance for the functional enrichment analysis. DE genes were submitted to various online databases for functional enrichment analysis: ShinyGO ver. 0.77 (Ge, Jung, and Yao 2020), Kyoto Encyclopedia of Genes and Genomes (KEGG) (Kanehisa et al. 2021), MalaCards (Rappaport et al. 2013), Reactome (Gillespie et al. 2022), GeneCards (Stelzer, Rosen, et al. 2016), and the Human Protein Atlas (HPA) (Uhlén et al. 2015). To visualize KEGG pathways represented in the functional enrichment analysis, we used PathView (W. Luo and Brouwer 2013) built into the ShinyGO online resource.

2.9   Reporting of n sizes

A range of the n sizes of experimental groups are reported in the figure captions for each technique throughout this document. In all techniques, one 'n' represents a singular

organoid taken for analysis. In some experiments and techniques, two organoids from the same cell line were analyzed; in this case each organoid was treated as an independent 'n' and sample. The decision to analyze individual organoids rather than cell line comes from the variability in levels and rates of differentiation between organoids even within the same cell line. Previous groups have reported n sizes in organoids studies in a similar manner (Daviaud et al. 2019; Notaras, Lodhi, Dündar, et al. 2021; Kathuria et al. 2020; M. S. Kim et al. 2021).

3 Results

3.1 Establishment of hypoxia exposure in SCZ human cerebral organoids

To study the GEI of hypoxic insults and SCZ genetics impact on fetal brain development, we developed human cerebral organoids from six CTRL and six SCZ iPSC cell lines using the STEMdiff Cerebral Organoid Kit (StemCell Technologies). To mimic transient prenatal hypoxia in our SCZ cerebral organoid model, we adapted well-established and previously used methods of hypoxic insults in CTRL cell lines (Daviaud et al. 2019; Paşca et al. 2019; M. S. Kim et al. 2021). Daviaud et al. (2019) examined a long-term exposure (3% O_2 for 14 days), which resulted in massive cell death, the collapse of cytoarchitecture, and poor differentiation of organoids. They also tested a shortened 24-hour hypoxic exposure paradigm to mimic the milder effects of non-lethal prenatal hypoxia, which allowed organoids to maintain structural integrity and lower cell death rates (Daviaud et al. 2019).

Another aspect of modelling hypoxia that varies widely across previous studies is the day of hypoxic injury. Multiple groups have demonstrated organoids in culture between 25 and 40 days recapitulate human fetal cortex development occurring at midgestational periods, ranging from gw 14.5-18.5 (Daviaud et al. 2019), and organoids at D100 recapitulate ~gw 24-38 or the third trimester (Paşca et al. 2015; Yoon et al. 2019). In fetal brain development, the first and second trimesters of gestation are hallmarked by key differentiation events, including neural progenitor cells and cortical neuron proliferation, axonal growth, and synaptogenesis (Selemon and Zecevic 2015; Räsänen et al. 2022). As we were interested in the impacts of hypoxia and SCZ genetics on these critical developmental processes, hypoxia exposure was induced on D29 whereby CTRL and SCZ organoids were subjected to 3% O_2 for 24 hours in a gas-controlled chamber and then returned to normoxic conditions (21% O_2, 5% CO_2) until analysis.

In response to hypoxia exposure, we expected to see immediate increases in amounts of HIF-1α, a key regulator of the hypoxia response that stabilizes in low oxygen conditions (Semenza 2007; H.-S. Li et al. 2019). As expected, in the quantification of

immunofluorescence (IF) staining, a two-way ANOVA revealed a significant main effect of treatment (Interaction: $F_{(1,43)} = 0.2692$, $p = 0.6066$, Disease: $F_{(1,43)} = 0.3766$, $p = 0.3766$, Treatment: $F_{(1,43)} = 14.81$, $p = 0.0004$, **Figure 3A**). IF staining also shows the expected nuclear localization of the protein HIF-1α (**Figure 3A**). Previous hypoxia organoid models have demonstrated increased cell death via innate apoptosis pathways in the outermost SVZ and CP layers of ventricular-like regions of organoids (Daviaud et al. 2019). Our results reflect the existing literature as we observe increases in apoptosis marker cleaved caspase 3 (CC3) in response to hypoxia exposure. Two-way ANOVA analysis shows a main effect of treatment (Interaction: $F_{(1,41)} = 0.0674$, $p = 0.7965$, Disease: $F_{(1,41)} = 0.0781$, $p = 0.7813$, Treatment: $F_{(1,41)} = 9.674$, $p = 0.0034$, **Figure 3B**). Representative IF images also show the localization of CC3 primarily concentrated in the SVZ/CP layers in SCZ and CTRL organoids (**Figure 3D**).

In the first month of development, organoids rapidly developed neuroepithelium, and D30 structural H&E staining reveals the development of ventricular-like structures (**Figure 4**). Within these ventricular regions, both CTRL and SCZ organoids express similar amounts of cellular proliferation marker Ki67 (**Figure 5E**). Reflective of proliferation patterns observed in human fetal brain growth (Selemon and Zecevic 2015), proliferation is primarily concentrated in the lowermost VZ of the organoids (**Figure 5G, H**), with a small fraction of Ki67+ cells appearing in outer layers. CTRL and SCZ organoids also expressed other expected neuronal markers reflective of successful differentiation, such as **s**ynaptic vesicle release protein synaptophysin, glutamate metabotropic receptors 2 and 3 (mGluR2/3), deep layer subcortical projection neuron marker CTIP2, and serotonin receptor 5-HT1AR (**Figure 5F**). Two-way ANOVAs revealed no significant main effects of disease, treatment, or interaction between factors for any of these neuronal markers in IF staining (**Figure 5A-D**, Synaptophysin: (Interaction: $F_{(1,44)} = 2.379$, $p = 0.1320$, Disease: $F_{(1,44)} = 2.2529$, $p = 0.1189$, Treatment: $F_{(1,44)} = 0.6907$, $p = 0.4104$); mGluR2/3: (Interaction: $F_{(1,43)} = 1.729$, $p = 0.6797$, Disease: $F_{(1,43)} = 0.9485$, $p = 0.3355$, Treatment: $F_{(1,43)} = 0.7805$, $p = 0.3819$); CTIP2: (Interaction: $F_{(1,44)} = 0.7480$, $p = 0.3918$, Disease: $F_{(1,44)} = 0.1224$, $p = 0.7281$, Treatment: $F_{(1,44)} = 1.476$, $p = 0.2309$); 5-HT1A: (Interaction: $F_{(1,40)} = 2.602$, $p = 0.1146$, Disease: $F_{(1,40)} = 1.299$, $p = 0.2612$, Treatment: $F_{(1,40)} = 0.0357$,

$p = 0.8510$); Ki67: (Interaction: $F_{(1,40)} = 0.0025$, $p = 0.9605$, Disease: $F_{(1,40)} = 0.3993$, $p = 0.5307$, Treatment: $F_{(1,40)} = 0.9566$, $p = 0.3334$).

A D30 HIF1α

B D30 Cleaved Caspase 3

C Normoxia Hypoxia

D Normoxia Hypoxia

Figure 3 - Hypoxia activated expected hypoxia response pathways and led to increased cell death.
In immunofluorescence analysis, **(A)** hypoxia exposure leads to increased expression of hypoxia-inducible factor 1 subunit α (HIF-1α), the primary regulator of hypoxia response pathways. **(B)** Quantification of apoptosis marker cleaved caspase 3 (CC3) shows increases in cell death in response to hypoxia. IF images for HIF-1α **(C)** and cleaved caspase 3 **(D)** for each experimental group. Images were acquired with a Leica SP8 confocal microscope at 40X magnification and processed and quantified using ImageJ Fiji. Scale bars in represent 20 µM (A, B) or 50 µM (C, D). Protein expression was normalized to ventricular size in mm^2. Statistical analysis 2-way ANOVAs, main effects reported in legends. n =11-13, *p<0.05, **p<0.01, ***p<0.01.
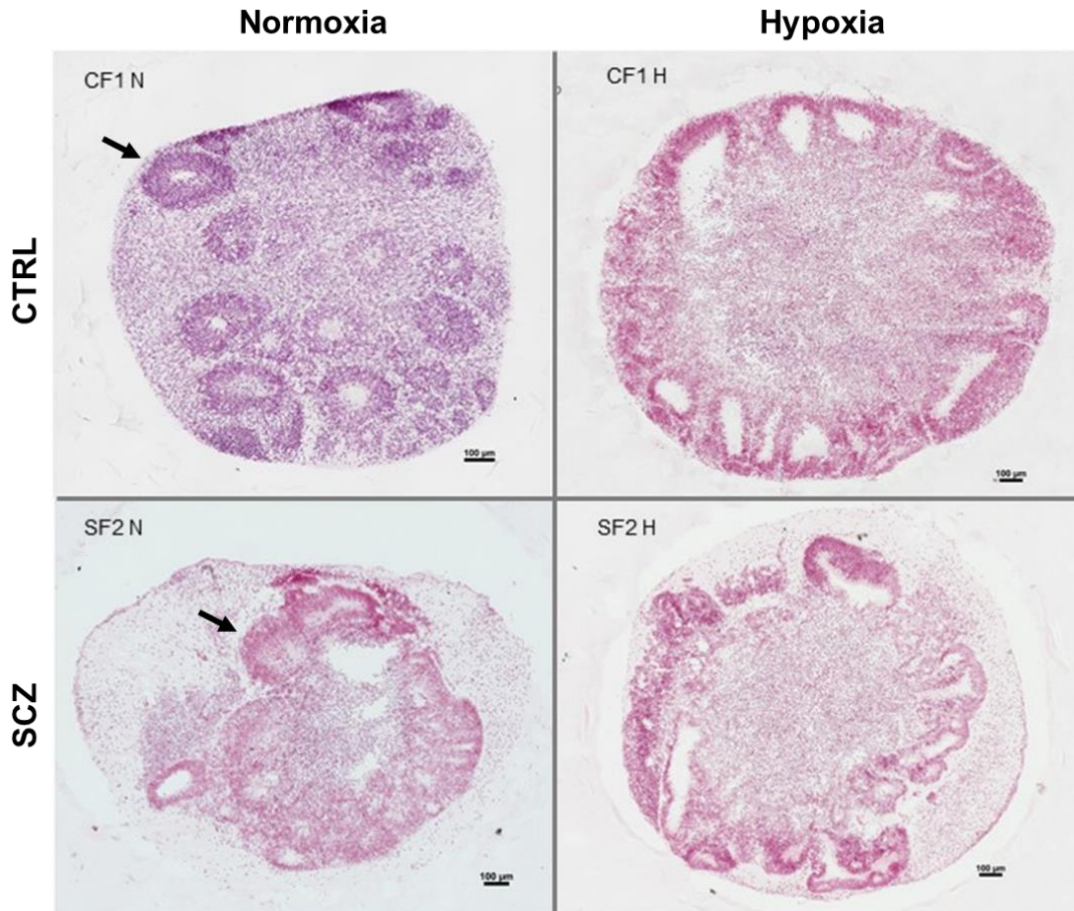
Figure 4 - Structural cortical differentiation stain of D30 organoids.
A-D Hematoxylin and eosin staining of **(A)** CTRL; normoxia, **(B)** CTRL; hypoxia, **(C)** SCZ; normoxia, **(D)** SCZ; hypoxia D30 cerebral organoids. Arrows depict neuronal tissue surrounding 'ventricular-like' regions, highlighting cortical differentiation within the organoids.
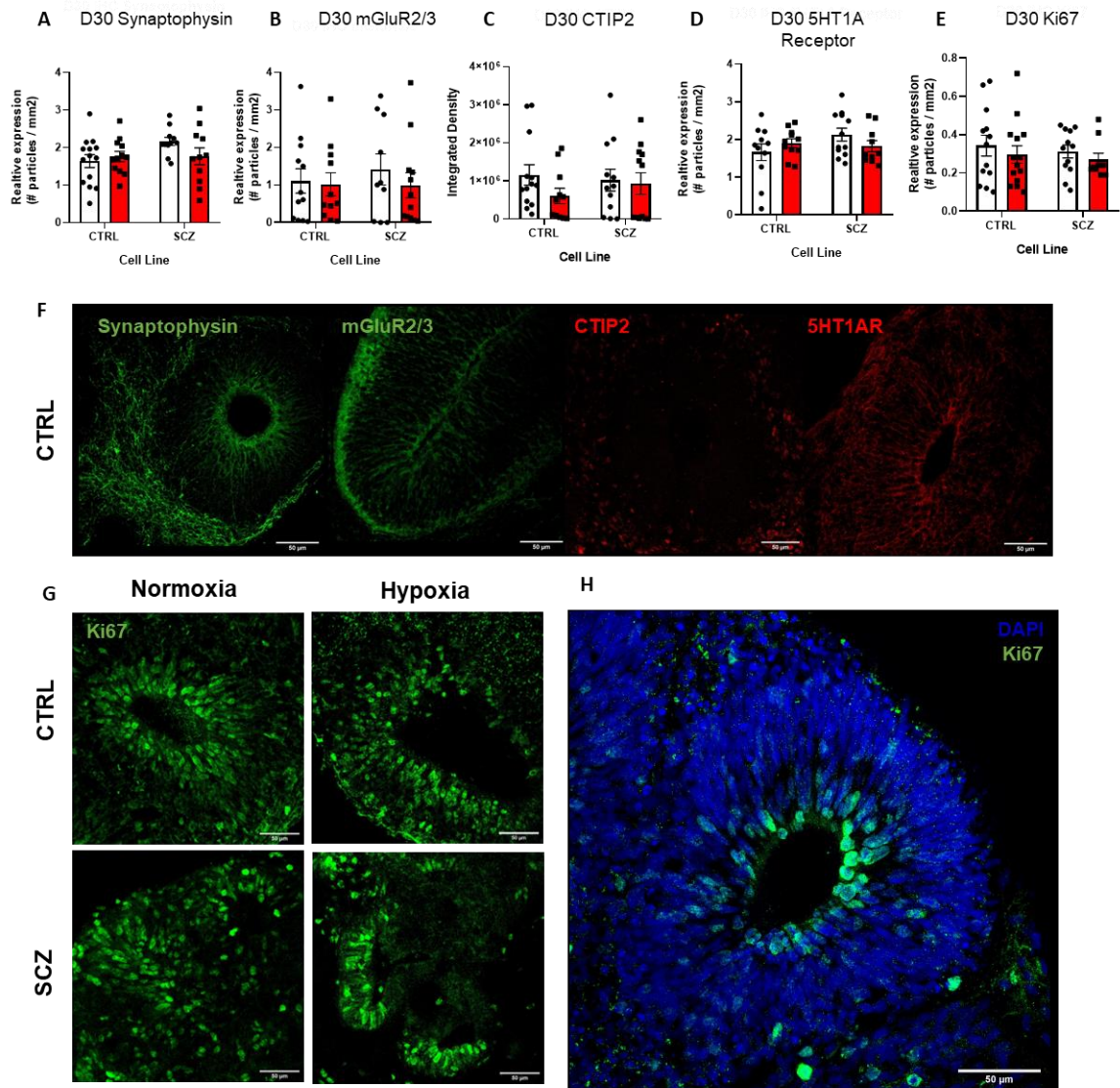
Figure 5 - CTRL and SCZ organoids express expected neuronal-associated proteins and receptors. Immunofluorescence quantification shows no change in expression of **(A) s**ynaptic vesicle release protein, synaptophysin, **(B)** metabotropic glutamate receptors 2 and 2 (mGluR2/3), **(C)** mature neuronal marker CTIP2, **(D)** serotonin receptor 5HT1A or **(E)** proliferation marker Ki67 **(F)** Representative immunofluorescent images of quantified proteins; images show day 30 CTRL normoxia organoids. **(G)** Representative images of Ki67+ cells across all experimental groups. **(H)** Overlay of Ki67 (green) and nuclear stain DAPI (4′,6-diamidino-2-phenylindole) in blue. Multiple 'ventricular-like' regions are present in each organoid slice. Images were acquired with a Leica SP8 confocal microscope at 40X magnification and processed and quantified using ImageJ Fiji. Scale bars represent 50 µM. Protein expression was normalized to ventricular size in mm^2. Statistical analyses were done using 2-way ANOVAs. n =10-14 * $p<0.05$, ** $p<0.01$.

3.2 SCZ organoids have innate differences in neural progenitor and cytoskeletal development.

At both immature (D30) and mature (D170) stages of differentiation, qPCR reveals consistent and long-term reductions in neuronal differentiation markers' mRNA levels in SCZ organoids. PAX6 is a pleiotropic transcription factor critical to the development of the central nervous system during fetal growth (Yogarajah et al. 2016); PAX6+ cells are markers of radial glial cells. At D30, two-way ANOVA analysis reveals a main effect of disease (Interaction: $F_{(1,27)} = 0.1627$, $p = 0.6899$, Disease: $F_{(1,27)} = 5.262$, $p = 0.0298$, Treatment: $F_{(1,27)} = 1.449$, $p = 0.2391$ **Figure 6A**). At D170, two-way ANOVA of PAX6 expression shows a significant main effect of disease (Interaction: $F_{(1,22)} = 0.0202$, $p = 0.8883$, Disease: $F_{(1,22)} = 9.027$, $p = 0.0065$, Treatment: $F_{(1,22)} = 1.880$, $p = 0.1842$, **Figure 6B**).

SRY-Box Transcription Factor 1 (SOX1) is an essential transcription factor that promotes neuronal cell fate determination and differentiation and is primarily expressed in the VZ of cerebral organoids (Lancaster et al. 2013). Two-way ANOVAs of SOX1 expression at D30 have significant main effects of treatment and disease (Interaction: $F_{(1,27)} = 0.3847$, $p = 0.5403$, Disease: $F_{(1,27)} = 6.229$, $p = 0.0184$, Treatment: $F_{(1,27)} = 3.932$, $p = 0.0576$, **Figure 6A**). Once organoids are mature, two-way ANOVA significant main effects are only found for disease (Interaction: $F_{(1,22)} = 0.0615$, $p = 0.8064$, Disease: $F_{(1,22)} = 4.843$, $p = 0.0239$, Treatment: $F_{(1,22)} = 1.365$, $p = 0.2252$, **Figure 6C**).

Genes reflective of mature neuronal development are also impacted by hypoxia and SCZ genetics. CTIP2 is a marker of mature neurons primarily expressed in deep layers of cortical tissue and the CP of cerebral organoids (Daviaud et al. 2019). Two-way ANOVA at both developmental time points show significant main effects of disease, (D30: Interaction: $F_{(1,27)} = 0.3031$, $p = 0.5865$, Disease: $F_{(1,27)} = 6.304$, $p = 0.0183$, Treatment: $F_{(1,27)} = 0.1116$, $p = 0.7409$; D170: Interaction: $F_{(1,20)} = 0.2044$, $p = 0.6561$, Disease: $F_{(1,20)} = 9.452$, $p = 0.0060$, Treatment: $F_{(1,20)} = 0.8053$, $p = 0.3802$, **Figure 6A, B**).

TUJ1 is a marker of semi-mature neurons, where expression at earlier stages begins in the lowermost VZ and extends up through SVZ and CP with development (Daviaud et al.

2019). Immediately post-hypoxia, two-way ANOVA analysis reveals significant main effects of disease and treatment (Interaction: $F_{(1,27)} = 1.950$, $p = 0.1740$, Disease: $F_{(1,27)} = 16.36$, $p = 0.0004$, Treatment: $F_{(1,27)} = 6.805$, $p = 0.0146$, **Figure 6A**). However, when organoids reach full maturity, there is no significant main effect of treatment, disease, or interaction between factors (Interaction: $F_{(1,20)} = 4.026$, $p = 0.0578$, Disease: $F_{(1,20)} = 2.391$, $p = 0.1370$, Treatment: $F_{(1,20)} = 2.332$, $p = 0.4182$, **Figure 6B**).

Next, we turn to the glutamate hypothesis of SCZ, which suggests clinical symptoms, including cognitive impairment, are influenced by aberrant glutamate signalling (Räsänen et al. 2022). At a molecular level, in the prefrontal cortex of SCZ patients, there is a hypofunction of N-methyl-D-aspartate (NMDA) receptors that interacts with excessive glutamate release resulting in impaired signalling (Mei, Wu, and Zhou 2018). Increased susceptibility to developing SCZ is associated with single nucleotide polymorphisms of NMDA Receptor subunit genes, including NMDAR2A (GRIN2A, Trubetskoy et al. 2022). Additionally, in the human fetal cortex, GRIN2A mRNA and the corresponding protein, NMDAR2A, increase in expression between gw 15 to 24 (Bagasrawala et al. 2017), which is reflective of the developmental period our cerebral organoids recapitulate (Daviaud et al. 2019). We investigated NMDAR2A subunit expression through IF staining in D30 organoids. We observe a significant main effect of disease and treatment in a two-way ANOVA analysis (Interaction: $F_{(1,37)} = 0.1993$, $p = 0.6579$, Disease: $F_{(1,37)} = 4.991$, $p = 0.0316$, Treatment: $F_{(1,37)} = 7.182$, $p = 0.0109$, **Figure 7A, C**).

We also examined the expression of glutamatergic metabotropic receptors 2 and 3 (mGluR2/3) at the protein level in D30 organoids. The two-way ANOVA showed no significant main effects of treatment, disease, or interaction between factors (Interaction: $F_{(1,41)} = 0.2289$, $p = 0.6349$, Disease: $F_{(1,41)} = 0.1698$, $p = 0.6824$, Treatment: $F_{(1,41)} = 0.5488$, $p = 0.4630$, **Figure 5B**). At the transcriptomic level, RNA-Seq did not find differential expression of genes encoding mGluR2 (GRM2) or mGluR3 (GRM3) in SCZ or CTRL D30 organoids in response to hypoxia (GRM2, CTRL N vs H: $p = 0.2839$, SCZ N vs H: $p = 0.3656$; GRM3, CTRL N vs H: $p = 0.5176$, SCZ N vs H: $p = 0.9455$). At one month of development, glutamatergic neurons are still in the early stages of development,

whereby differences may become apparent after further migration and differentiation of glutamatergic neurons have occurred (Räsänen et al. 2022). To examine potential changes at later developmental stages, mRNA expression was measured for GRM2 and GRM3 at D170 (**Figure 6C**). Two-way AVOVAs exhibit significant main effects of disease for both GRM2 and GRM3 at D170 (GRM2: Interaction: $F_{(1,20)} = 0.8505$, $p = 0.3674$, Disease: $F_{(1,20)} = 9.939$, $p = 0.0050$, Treatment: $F_{(1,20)} = 1.529$, $p = 0.2306$; GRM3: Interaction: $F_{(1,20)} = 0.0385$, $p = 0.8465$, Disease: $F_{(1,20)} = 5.584$, $p = 0.0289$, Treatment: $F_{(1,20)} = 0.9729$, $p = 0.3364$). These results suggest innate differences in glutamate receptors at the transcriptomic and protein levels in SCZ organoids, where effects primarily become prominent in later stages of cortical differentiation. These results are supported by several SCZ iPSC studies that have found altered expression of glutamate receptor subunits and genes in iPSC-derived neurons from SCZ patients (Räsänen et al. 2022).

Altered dopamine transmission is also highly implicated in SCZ pathology (Brisch et al. 2014), so we investigated transcriptomic changes to dopamine receptor expression. RNA-Seq analysis revealed no differential expression of dopamine receptor D1 (DRD1) or dopamine receptor D2 (DRD1) in response to hypoxia or SCZ disease state (DRD1, CTRL N vs H: $p = 0.8908$, SCZ N vs H: $p = 0.9534$; DRD2, CTRL N vs H: $p = 0.4377$, SCZ N vs H: $p = 0.5513$). In qPCR, two-way ANOVAs on DRD1 mRNA expression show a significant main effect of disease in D170 organoids (Interaction: $F_{(1,20)} = 1.107$, $p = 0.3053$, Disease: $F_{(1,20)} = 5.411$, $p = 0.0306$, Treatment: $F_{(1,20)} = 1.807$, $p = 0.1939$, **Figure 6D**). In the qPCR analysis of DRD2 mRNA expression, a two-way ANOVA does not find any significant main effects or interaction between factors (Interaction: $F_{(1,20)} = 3.014$, $p = 0.0972$, Disease: $F_{(1,20)} = 0.0149$, $p = 0.9042$, Treatment: $F_{(1,20)} = 0.4477$, $p = 0.5131$, **Figure 6D**).

When the cytoskeleton is abnormally assembled during neuronal development, it can lead to the impairment of neurotransmission (Benitez-King et al. 2004); cytoskeleton dysfunction has been inferred in the pathology SCZ and other neuropsychiatric disorders (Marchisella, Coffey, and Hollos 2016). Using IF, we investigated alterations to

microtubule-associated protein 2 (MAP2), a critical regulator of neuron function and structure (Grubisha et al. 2021). Two-way ANOVA shows a significant main effect of disease (Interaction: $F_{(1,41)} = 2.232$, $p = 0.1428$, Disease: $F_{(1,41)} = 5.991$, $p = 0.0187$, Treatment: $F_{(1,41)} = 0.2323$, $p = 0.6324$, **Figure 7B, D**). Clinical studies do not report a decrease in MAP2 protein levels in adult SCZ patients but rather differential phosphorylation of MAP2 between SCZ and nonpsychiatric CTRLs (Grubisha et al. 2021; Shelton et al. 2015). However, an SCZ-iPSC cerebral organoid study analyzed the proteomes of SCZ organoids and reported down-regulation expression of MAP2 (Notaras, Lodhi, Fang, et al. 2021), which reflects our findings.
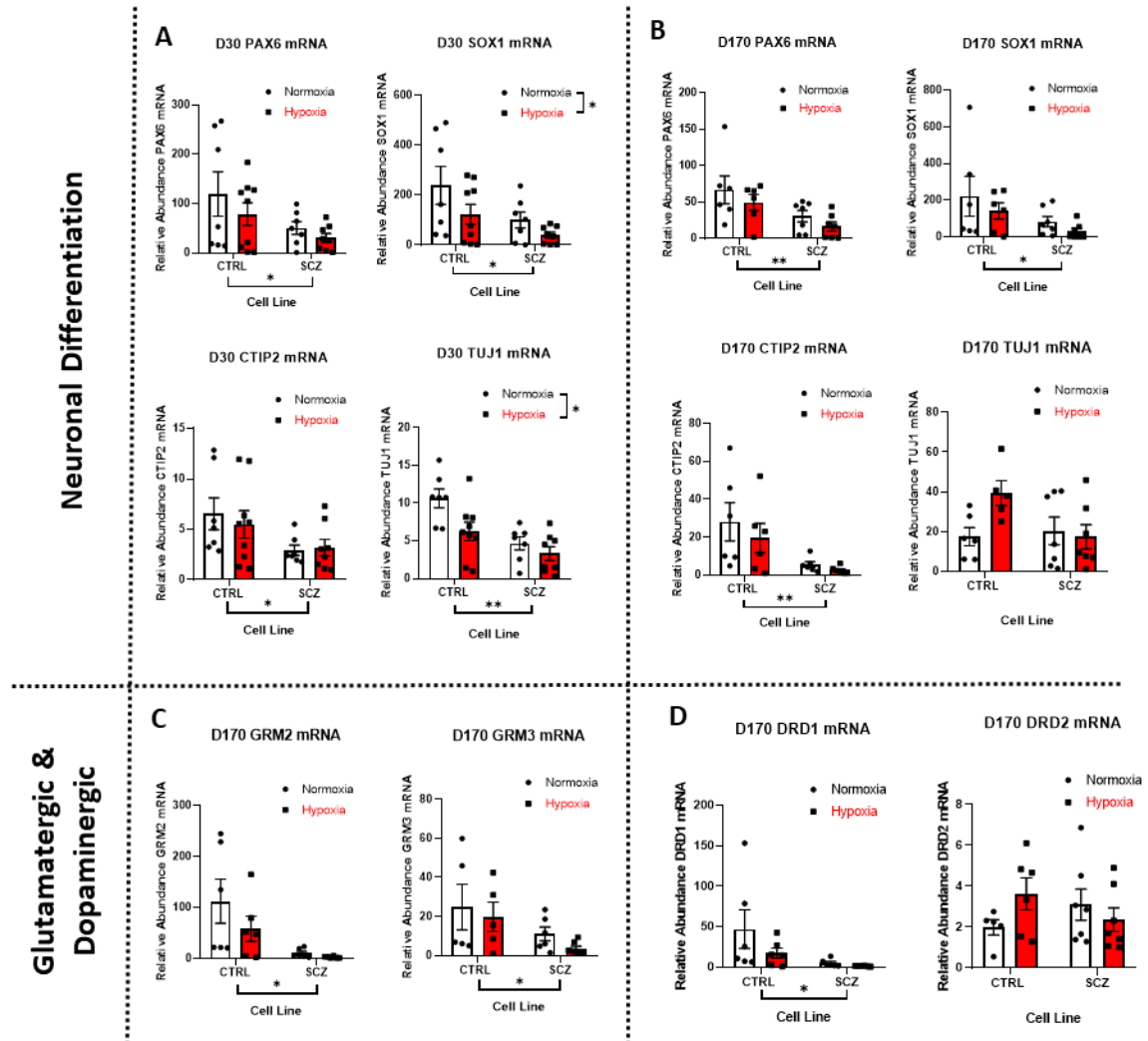
Figure 6 - SCZ organoids have changes in the expression of mRNA targets relating to neuronal differentiation, glutamatergic receptors, and dopaminergic receptors.

In qPCR, SCZ organoids show a decrease in immature radial glial cells, PAX6, and neural stem cell marker SOX1 across **(A)** immature (D30), and **(B)** mature (D170) time-points. Mature deep neuron marker CTIP2 expression is decreased at **(A)** D30 and **(B)** D170 in SCZ organoids. TUJ1, general neuronal marker, at **(A)** D30 shows main effects of treatment and innate differences between CTRL and SCZ organoids. At later stages **(B)**, there is no main effect of treatment or disease. **(C)** As the organoids mature, glutamate metabotropic receptors 2 and 3 (GRM2, GRM3) shows a main effect of disease for both mRNA targets. **(D)** Dopamine receptor D1 (DRD1) is decreased in SCZ organoids compared to CTRLs, and there are no differences between groups for dopamine receptor D2 (DRD2). Relative quantification of mRNA was performed using the $2^{-\Delta\Delta CT}$ method, where mRNA has been normalized to the geometric means of β-actin and GAPDH. Statistical analysis 2-way ANOVAs, main effects reported in legends and axes. D30: n =7-9, D170: n =5-7, *p<0.05, **p<0.01.
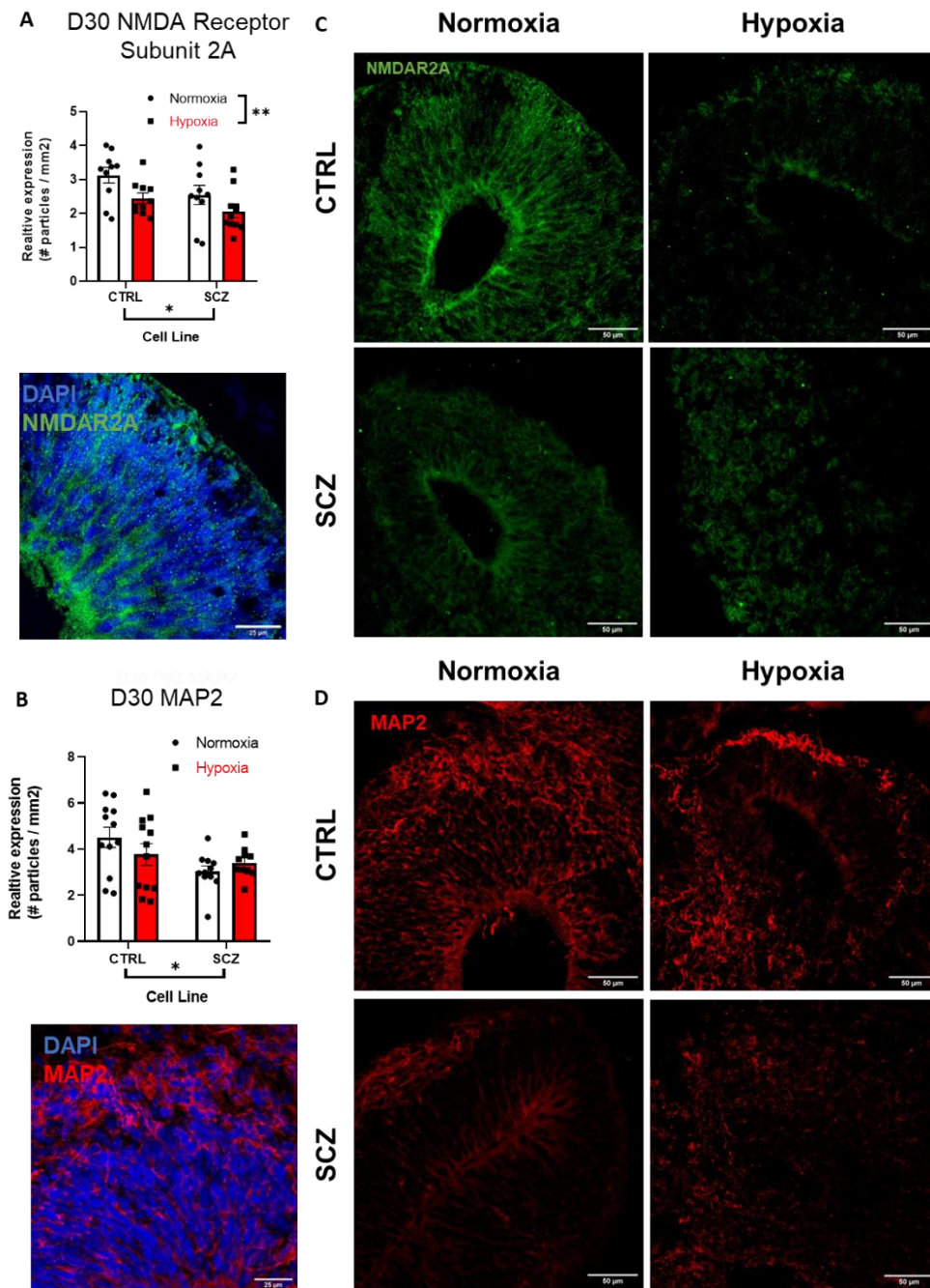
Figure 7 - SCZ organoids exhibit innate differences in neural progenitor and cytoskeletal development. Immunofluorescence quantification shows, (**A**) hypoxia leads to decreased expression of NMDA Receptor subunit 2A (NMDAR2A), and innate differences between CTRL and SCZ organoids. (**B**) Quantifications of MAP2 staining indicates SCZ organoids innately express lower levels compared to CTRL organoids. IF images for NMDAR2A (**C**) and MAP2 (**D**) for each experimental group. Images were acquired with a Leica SP8 confocal microscope at 40X magnification and processed and quantified using ImageJ Fiji. Scale bars in represent 20 µM (A, B) or 50 µM (C, D). Protein expression was normalized to ventricular size in mm^2. Statistical analysis 2-way ANOVAs, main effects reported in legends and axes. n =10-12,*p<0.05,**p<0.01.

3.3 Transcriptomic level changes in organoids via RNA-Sequencing

Total RNA-Seq data was collected from 1-month-old cerebral organoids from four SCZ and four CTRL patient cell lines. Approximately 50 million paired-end reads were obtained for each sample, then annotated and aligned to the latest ENSEMBL Homo Sapien GRCH38.p13 reference genome. Lowly expressed genes were filtered out using a counts per million (CPM) cut-off of 0.4 in at least 2 or more samples. Differential expression testing included p-value adjustment using Benjamini & Hochberg False Discovery Rate (FDR) correction to account for multiple testing. An FDR cut-off of < 0.05 and a log (base 2) fold change (log(2)FC) cut-off of +/- 2 were used to determine significance (**Figure 8A**).

To visualize the variability between samples, we generated a multidimensional scaling (MDS) plot, where the x-axis represents the dimension 1 (dim 1) variability that represents 53% of sample variability, and the y-axis shows dimension 2 (dim 2) that has 10% of sample variability (**Figure 8B**). In the SCZ samples, the greatest difference appears to be oxygen state as SCZ normoxic organoids group together and separately from the SCZ hypoxic organoids. CTRL organoids also group by oxygen state, but the samples do not group as closely on dim 1 as the SCZ samples do. Instead, CTRL samples appear to be separated by sex, where CTRL males' group separately from CTRL female samples. However, variability in response to sex is not found in the SCZ organoids, and sex effects have not been considered in other experimental conditions. Therefore, the RNA-Seq analysis only considered disease- and oxygen-state effects and pooled CTRL data regardless of sex.

To identify genes associated with the response to low oxygen, we identified genes differentially expressed between the hypoxia-exposed and normoxic organoids in both SCZ and CTRL organoids. In response to hypoxia, we identified 519 DE genes in CTRL organoids (452 upregulated, 67 downregulated, **Figure 9A**) and 593 DE genes in SCZ organoids (436 upregulated and 157 downregulated genes, **Figure 9B**, FDR ≤ 0.05, fold change ≥ 2.0) We generated a heat map of the DE genes found in the hypoxic response in

both CTRL and SCZ organoids, where SCZ cerebral organoids show similar gene expression patterns to CTRLs in response to hypoxia (**Figure 9E**).
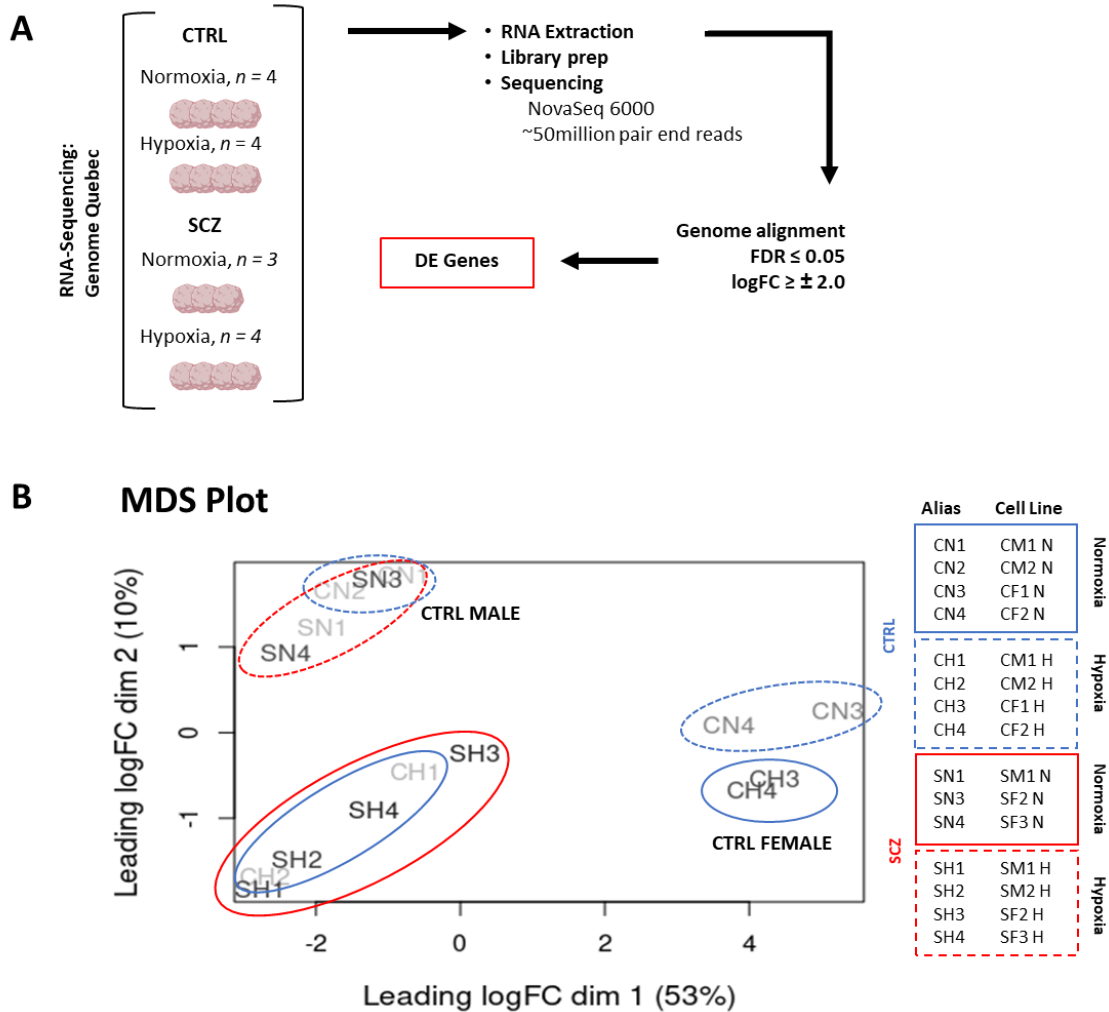
Figure 8 - Organoids exhibit variability between differentially expressed genes in normoxic and hypoxic conditions in both CTRL and SCZ organoids.
(A) Workflow schematic of RNA-Seq experimental setup. From each experimental group, 3 to 4 organoids were sent to Genome Quebec for RNA isolation and sequencing using the NovaSeq 6000 system, acquiring ~50 million pair-end reads for each sample. A Benjamini & Hochberg False Discovery Rate (FDR) correction was applied; an FDR cut-off of ≤ 0.05 and a log (base 2) fold change cut-off of ± 2 were used to determine significance. **(B)** Multidimensional scaling (MDS) plot to visualize the similarity and variance between samples. Solid lines represent untreated normoxia organoids; dotted lines highlight hypoxia-exposed organoids. SCZ samples are circled in red and CTRL organoids in blue. SCZ normoxia (red, solid line) and SCZ hypoxia (red, dotted line) organoids group together closely with the greatest variance relating to oxygen treatment state. CTRL organoids (blue lines) show the greatest variance by sex as C_1 and C_2 samples = male, C_3 and C_4 = female. Within sexes, samples also exhibit variance due to oxygen state. S=schizophrenia, C=control, N=normoxic, H=hypoxic, M=male, F=female.
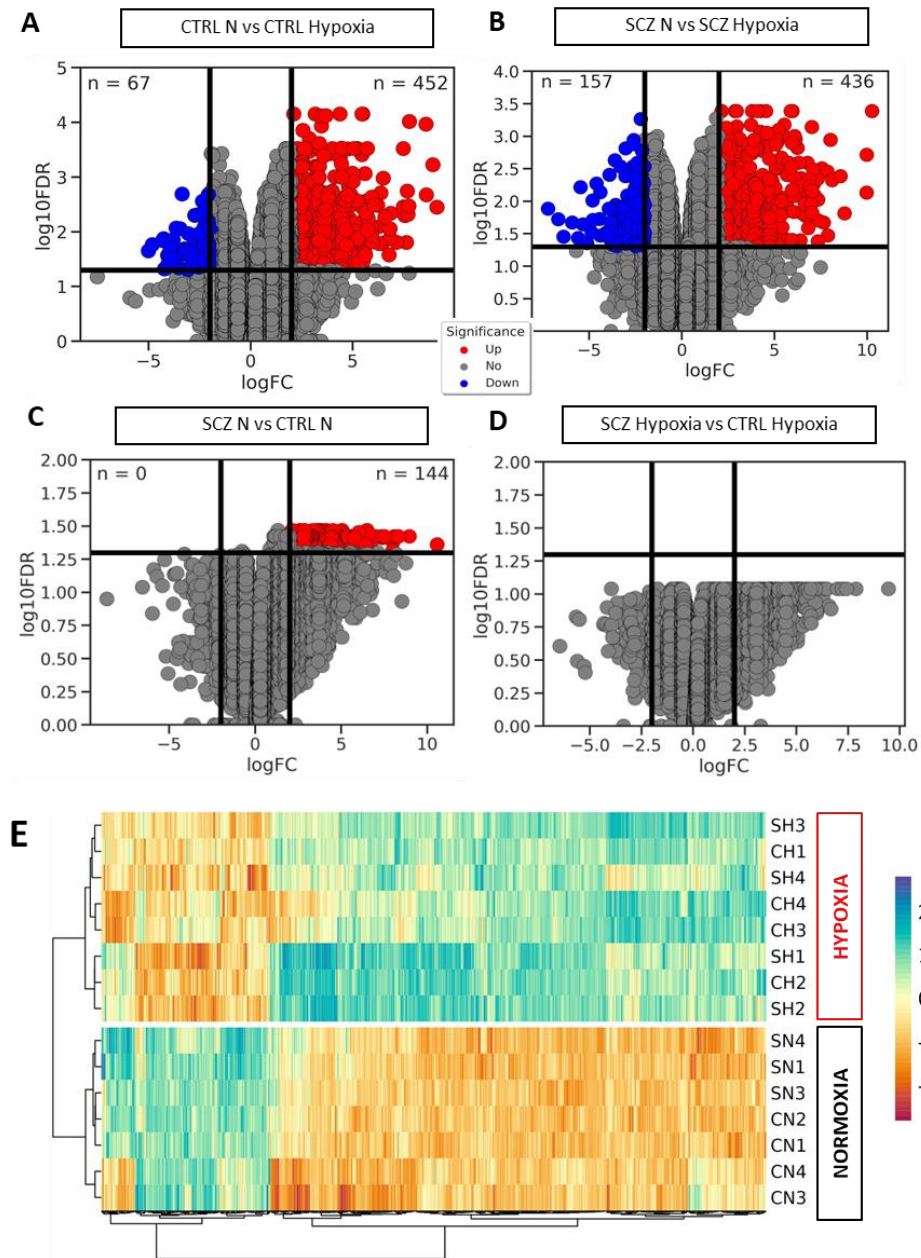
Figure 9 - Hypoxia leads to the differential expression of numerous genes in CTRL and SCZ organoids that exhibit similar transcriptomic changes regardless of disease state.

(A-D) Volcano plots represent the number of upregulated (red) and downregulated (blue) genes. CTRL hypoxia organoids exhibit $n = 452$ upregulated and $n = 67$ downregulated genes. SCZ hypoxia organoids exhibit $n = 436$ upregulated and $n = 157$ downregulated genes. In normoxic organoids, SCZ exhibits $n = 144$ upregulated genes compared to CTRL. No DE genes were found when comparing hypoxia-exposed SCZ and CTRL organoids. **(E)** Heat map of all DE genes across experimental groups indicates similar expression patterns in response to hypoxia in CTRL and SCZ organoids. Heat map data is clustered by oxygen state (normoxia and hypoxia), and data represents normalized log2(counts per million) values for each gene. The dendrograms on the left and bottom of the heat map show the hierarchical clustering of the transcripts for samples. $n = 3$-4

3.4   Functional enrichment analysis of RNA-Seq results

To gain further insight into which pathways are implicated in the DE gene lists obtained for SCZ and CTRL organoids, we ran an overrepresentation analysis across multiple databases, where an adjusted p-value threshold of < 0.05 was used to determine the significance of the functional enrichment analysis. In SCZ organoids, terms highlighted in the KEGG pathway analysis include terms relating to metabolism (fructose and mannose metabolism ($p = 4.0\text{e-}03$), oxidative phosphorylation ($p = 3.4\text{e-}04$), immune response (IL-17 signalling pathway, $p = 3.6\text{e-}05$; TNF signalling pathway, $p = 2.5\text{e-}03$) and hypoxia response (HIF-1 signalling pathway, p = 1.8e-05) **Figure 10A**). For a visual representation of the genes in SCZ hypoxia DE gene list implicated in each of these KEGG pathways, see Appendix 5.2.1.

Interestingly, most DE genes in the KEGG HIF-1 signalling pathway are directly or indirectly related to mitochondrial function and metabolism (**Figure 10B**). For example, PDK1 (pyruvate dehydrogenase kinase 1) inactivates the pyruvate dehydrogenase (PDH) enzyme, which produces the starting compound of the TCA cycle acetyl-CoA. When PDK1 expression is increased, as is the case in SCZ hypoxia organoids ($p = 0.00142$, $\log(2)\text{FC} = 2.29$), TCA cycle metabolism is inhibited (J. Kim et al. 2006). Genes involved in shifting cellular energy responses to anaerobic metabolism are upregulated in SCZ hypoxia organoids compared to untreated SCZ organoids, such as hexokinase (HK*, $p = 0.00503$, $\log(2)\text{FC} = 3.76$), aldolase, fructose-bisphosphate A (ALDOA, $p = 0.00168$, $\log(2)\text{FC} = 2.47$), solute carrier family 2 member 1 (GLUT1, $p = 0.00871$, $\log(2)\text{FC} = 2.99$), lactate dehydrogenase A (LDHA, $p = 0.00135$, $\log(2)\text{FC} = 2.66$), and 6-phosphofructo-2-kinase/fructose-2,6-biphosphatase 3 (PFK2, $p = 0.00369$, $\log(2)\text{FC} = 3.07$). The dual implication of mitochondrial dysfunction in SCZ organoids also being highly related to HIF-1 signalling responses highlights connections between a hallmark of SCZ pathophysiology and the influence of hypoxia on said pathways.

Gene ontology (GO) analysis was completed on DE gene lists for hypoxia-exposed SCZ organoids and rank-ordered hits according to significance (*p*-value, **Figure 11A, B**). In the GO: Biological Process (GO: BP) and GO: Molecular Function (GO: MF) analysis,

many terms are related to DNA structure and function and protein folding responses. DNA-related terms overrepresented in the SCZ hypoxia GO analysis include nucleosome assembly (p = 7.61e-31), nucleosome organization (p = 2.14e-28), chromatin remodelling (p = 4.28e-15), and DNA binding (p = 6.17e-12). Genes in the DE list commonly associated with these terms include various histones, all of which are upregulated in SCZ hypoxia organoids. Research has shown that hypoxia can cause alterations in chromatin structure, specifically affecting histone methylation, acetylation, and DNA methylation (Batie, del Peso, and Rocha 2018).

Hypoxia has been linked to protein folding in cancer as this process is oxygen-dependent and tumour microenvironments are commonly hypoxic in nature (Chipurupalli et al. 2019). The unfolded protein response (UPR) pathway is induced during periods of cellular stress and aims to restore protein homeostasis (Wang and Kaufman 2016). An organoid study using a similar hypoxia-exposure protocol used an allosteric regulator to block the UPR response, which rescued many of the neuronal development deficits observed in hypoxia-exposed organoids (Paşca et al. 2019). In our GO:BP and GO:MF analysis, terms such as response to unfolded protein (p = 3.72e-06), protein folding (p = 4.76e-05), unfolded protein binding (p = 2.24e-05), and heat shock protein binding (p = 0.00391) are overrepresented in the DE genes for hypoxia-exposed SCZ organoids (**Figure 11A, B**). REACTOME analysis of the same DE gene set reveals an overrepresentation of the cellular response to heat stress term (p = 1.93e-10). When cells are exposed to stressors, such as hypoxia, it initiates a set of protective mechanisms known as the "heat shock response" designed to enable cells to repair protein damage caused by said stressors (Baler, Dahl, and Voellmy 1993). In SCZ hypoxia-exposed organoids, DE genes represented in this pathway include heat shock protein family A (Hsp70) member 6 (HSPA6, p = 0.00193, log(2)FC = 9.98), heat shock protein family A (Hsp70) member 8 (HSPA8, p = 0.00133, log(2)FC = 2.64), and death effector domain containing 2 (DEDD2, p = 0.00517, log(2)FC = 2.15).
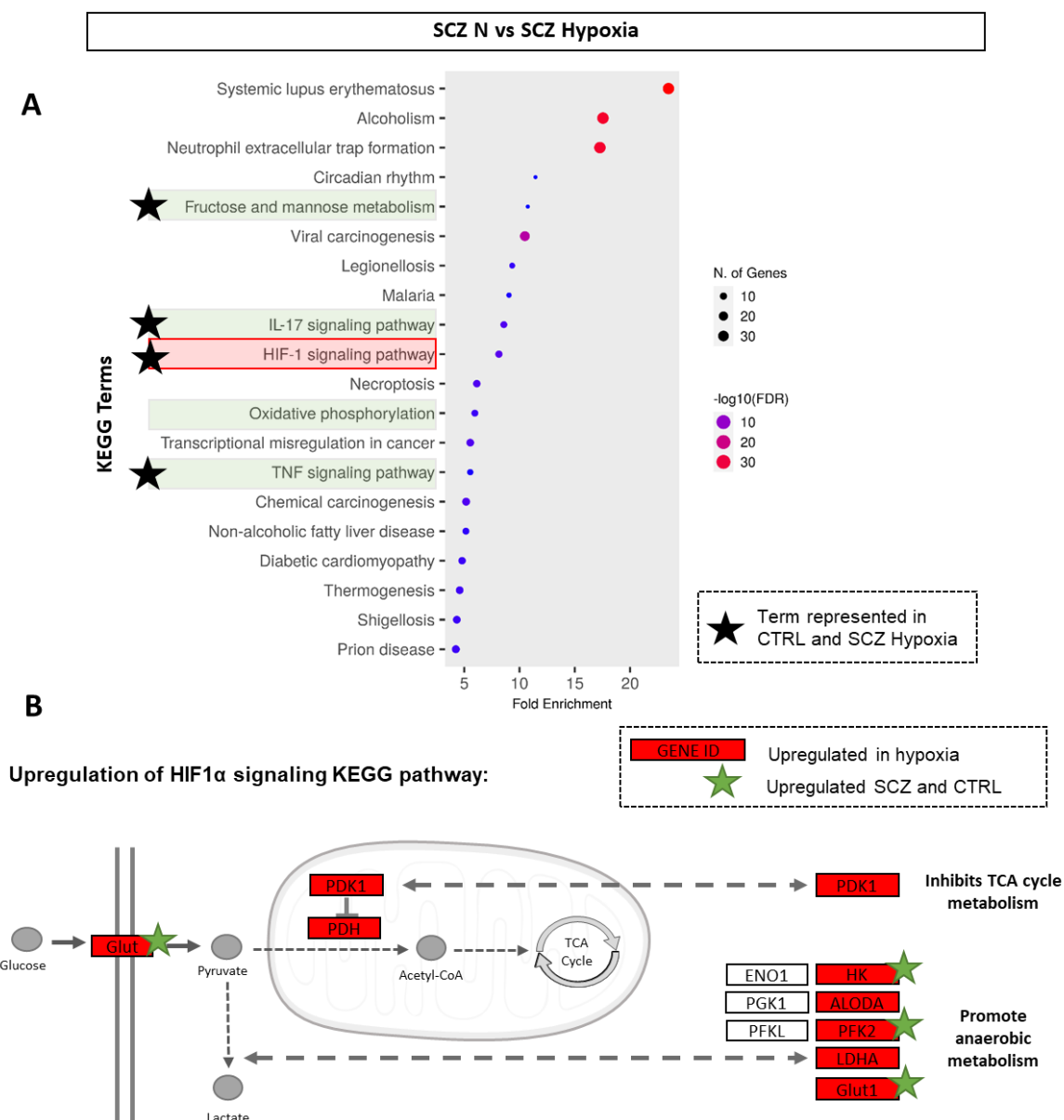
Figure 10 - In response to hypoxia, SCZ organoids exhibit differential expression of genes relating to metabolism and mitochondrial function, HIF-1α signalling, and inflammation/immune response.
(**A**) Dot plot of the top 20 KEGG Terms overrepresented in the DE gene list in SCZ hypoxia organoids, ranked by fold enrichment. Terms of biological interest are highlighted in green and red. Of these terms, those with a black star also appear in the top 20 list for CTRL hypoxia-exposed organoids. For visual representations of which genes are differentially expressed for each term, see Appendix 5.2.1 (**B**) Schematic of HIF-1α signalling KEGG pathway, representing mitochondrial-associated genes detected in the overrepresentation analysis of DE genes. Red-coloured genes are upregulated in hypoxia-exposed SCZ organoids, and green stars represent upregulation in SCZ and CTRL organoids in response to hypoxia.
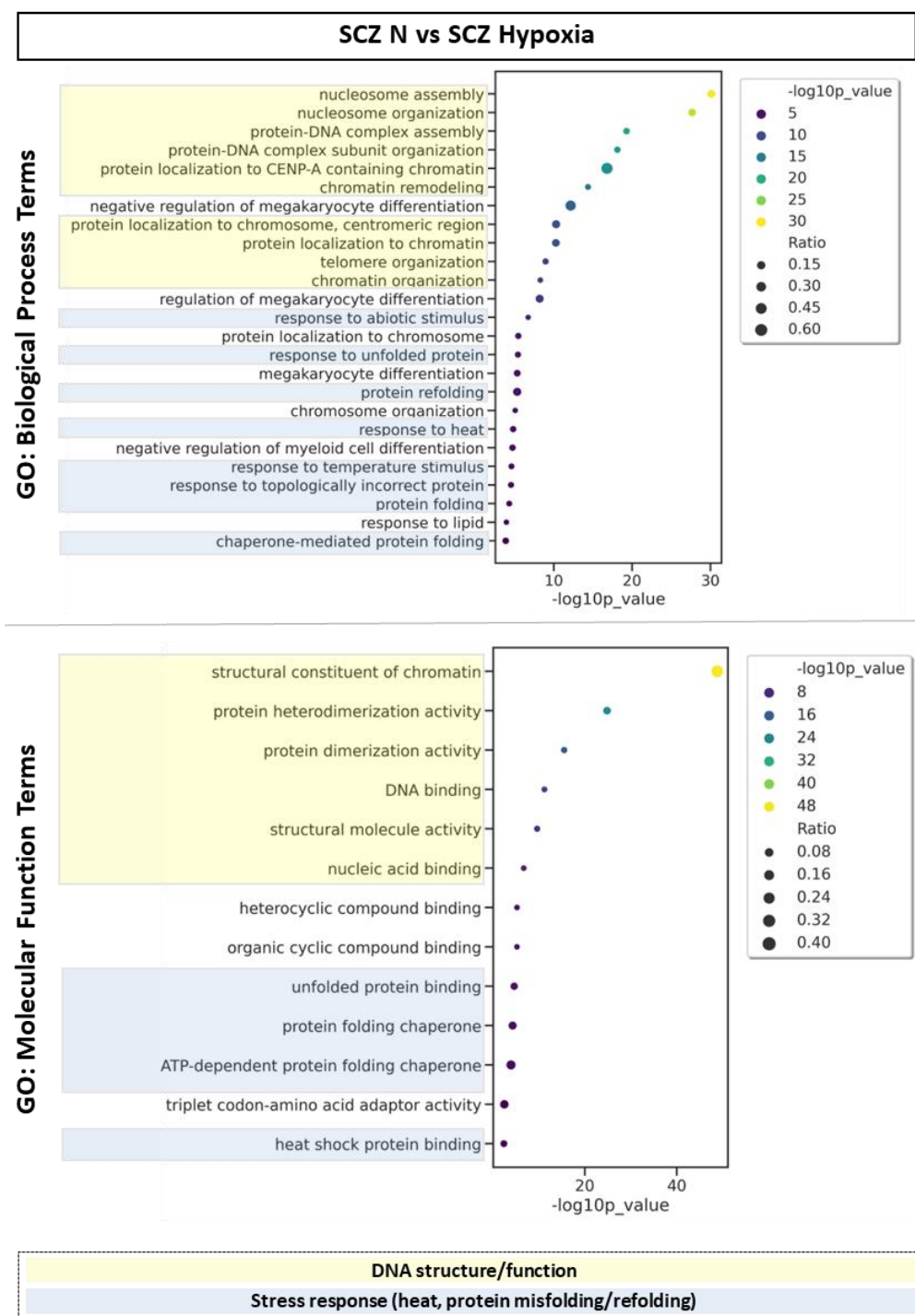
Figure 11 - Hypoxia is associated with changes to DNA structure and function and cellular stress responses in SCZ organoids.
Gene Ontology (GO) overrepresentation analysis of hypoxia-exposed SCZ organoids for **(A)** Biological Process terms and **(B)** Molecular Function terms. Terms highlighted in yellow relate to DNA structure and functionality, and terms highlighted in blue relate to cellular stress responses, including heat response and protein unfolding, misfolding, and refolding processes.

3.5   Phenotype inquiries and validation of RNA-Seq results

To determine specific genes associated with various phenotypes of interest to this project, we employed VarElect Next Generation Sequencing Phenotyper (varelect.genecards.org, Stelzer, Plaschkes, et al. 2016). DE genes resulting from hypoxia exposure in SCZ organoids were input, and search queries included the terms "hypoxia", "schizophrenia", and "mitochondrial dysfunction". Within each phenotype, the top 20 genes were considered. Genes were ranked by "score" which VarElect defines as: "an indication of the strength of the connection between the gene and the queried phenotype". **Table 5** summarizes a few select genes detected in the VarElect analysis associated with at least one of the phenotypes of interest. To validate the RNA-Seq findings, the expression changes of Table 5 genes were confirmed using qPCR (**Figure 12**).

Genes associated with the "hypoxia" phenotype found in the SCZ hypoxia DE gene list include vascular endothelial growth factor (VEGFA) and PDK1. VEGFA is a direct transcriptional downstream target of hypoxia response factors HIF-1α and HIF-1β (Krock, Skuli, and Simon 2011); expression is expected to increase in response to low oxygen. This upregulation trend was observed in SCZ hypoxia and CTRL hypoxia organoids in the RNA-Seq (SCZ: $p = 0.0008$, log(2)FC = 2.89, CTRL: $p = 0.0004$, log(2)FC = 2.31). Two-way ANOVA analysis of VEGFA mRNA expression shows a significant main effect of treatment and disease and an interaction between factors (Interaction: $F_{(1,26)} = 7.542$, $p = 0.0108$, Disease: $F_{(1,26)} = 6.858$, $p = 0.0145$, Treatment: $F_{(1,26)} = 91.31$, $p < 0.0001$). *Post hoc* multiple comparisons show increased VEGFA mRNA expression in response to hypoxia compared to untreated counterparts for both SCZ ($p < 0.0001$) and CTRLs ($p < 0.0001$, **Figure 12B**). There are no significant differences between SCZ normoxia and CTRL normoxia organoids ($p = 0.9309$). Another downstream target of the hypoxia response is PDK1. Activation of PDK1 by HIF-1α/β leads to the inhibition of PDH, preventing pyruvate from entering the TCA cycle and instead causing a shift to anaerobic metabolism via lactate production (J. Kim et al. 2006). In response to hypoxia, RNA-Seq observes upregulated of PDK1 in SCZ ($p = 0.00142$, log(2)FC = 2.29) and CTRL organoids ($p = 0.00192$, log(2)FC = 1.90). In qPCR, two-way ANOVA analysis shows a significant main effect of treatment but not

disease, and an interaction between factors (Interaction: $F_{(1,27)} = 4.440$, $p = 0.00445$, Disease: $F_{(1,27)} = 0.0912$, $p = 0.7650$, Treatment: $F_{(1,27)} = 58.81$, $p < 0.0001$). *Post hoc* multiple comparisons reveal an increase in PDK1 mRNA in hypoxia organoids compared to untreated counterparts in SCZ ($p = 0.0005$) and CTRL organoids ($p < 0.001$, **Figure 12C**).

Genes encoding various heat-shock proteins involved in cellular stress responses were found to be associated with the "schizophrenia" phenotype (**Table 5**). We validated the hypoxia-induced upregulation of heat shock protein family A (Hsp70) member 1A and 1B (HSPA1A/B) via qPCR. Two-way ANOVA found significant main effects of treatment (Interaction: $F_{(1,27)} = 3.090$, $p = 0.0901$, Disease: $F_{(1,27)} = 2.834$, $p = 0.1038$, Treatment: $F_{(1,27)} = 113.5$, $p < 0.0001$, **Figure 12A**). These results reflect the upregulation in response to hypoxia in the RNA-Seq analysis of SCZ ($p = 0.00041$, $\log(2)FC = 5.97$) and CTRLs ($p = 7.05e-05$, $\log(2)FC = 9.43$).

Fos Proto-Oncogene, AP-1 Transcription Factor Subunit (FOS) encodes transcription factors that complex with proteins of the Jun Proto-Oncogene family to form a major regulator of gene transcription, activator protein 1 (AP-1), which is highly involved in inflammatory responses and cytokine production (Zenz et al. 2008). These associations of FOS to immune responses implicated it in SCZ pathology (Huang et al. 2019). In response to hypoxia, SCZ and CTRL organoids have an upregulation of FOS in RNA-Seq (SCZ: $p = 0.001$, $\log(2)FC = 5.52$, CTRL: $p = 0.003$, $\log(2)FC = 5.07$). The same trend is found in qPCR, as the two-way ANOVA shows a main effect of treatment (Interaction: $F_{(1,26)} = 3.413$, $p = 0.0761$, Disease: $F_{(1,26)} = 3.454$, $p = 0.0744$, Treatment: $F_{(1,26)} = 19.97$, $p = 0.0001$, **Figure 12D**).

Mitochondrial dysfunction is a major component of SCZ pathology and hypoxic response pathways which is reflected in our VarElect analysis that implicated mitochondrially encoded NADH dehydrogenase 1 (MT-ND1) and mitochondrially encoded NADH dehydrogenase 5 (MT-ND5) in the "schizophrenia" and "mitochondrial dysfunction" phenotype queries (**Table 5**). In the RNA-Seq analysis, both of these genes were downregulated in hypoxia-exposed SCZ organoids (MT-ND1: $p = 0.00293$, $\log(2)FC = -$

2.63, MT-ND5: $p = 0.00305$, log(2)FC = -2.18). In hypoxia-exposed CTRL organoids, these genes met the statistical cut-off (MT-ND1: $p = 0.009306$, MT-ND5: $p = 0.00824$), but did not get classified as DE genes as they did not meet the fold-change cut-off of +/- 2.0 (MT-ND1: log(2)FC = -1.73, MT-ND5: log(2)FC = -1.53). In the qPCR validation of both genes, two-way ANOVAs revealed significant main effects of treatment for both MT-ND1 (Interaction: $F_{(1,27)} = 0.2056$, $p = 0.6539$, Disease: $F_{(1,27)} = 0.0531$, $p = 0.8196$, Treatment: $F_{(1,27)} = 21.53$, $p < 0.0001$) and MT-ND5 (Interaction: $F_{(1,27)} = 0.0634$, $p = 0.8028$, Disease: $F_{(1,27)} = 0.0588$, $p = 0.8103$, Treatment: $F_{(1,27)} = 35.61$, $p < 0.0001$, **Figure 12E, F**).

Table 5 - VarElect Phenotype Query Results for Hypoxia-exposed SCZ Organoids

Symbol	Phenotype	Gene Name	Expression
VEGFA	Hypoxia Schizophrenia	Vascular endothelial growth factor A	Upregulated
PDK1	Hypoxia	Pyruvate dehydrogenase kinase 1	Upregulated
HSPA1A	Schizophrenia	Heat shock protein family A member 1A	Upregulated
HSPA1B	Schizophrenia	Heat shock protein family A member 1B	Upregulated
FOS	Schizophrenia	Fos proto-oncogene, AP-1 transcription factor subunit	Downregulated
MT-ND1	Schizophrenia Mitochondrial dysfunction	Mitochondrially encoded NADH dehydrogenase 1	Downregulated
MT-ND5	Mitochondrial dysfunction	Mitochondrially encoded NADH dehydrogenase 5	Downregulated
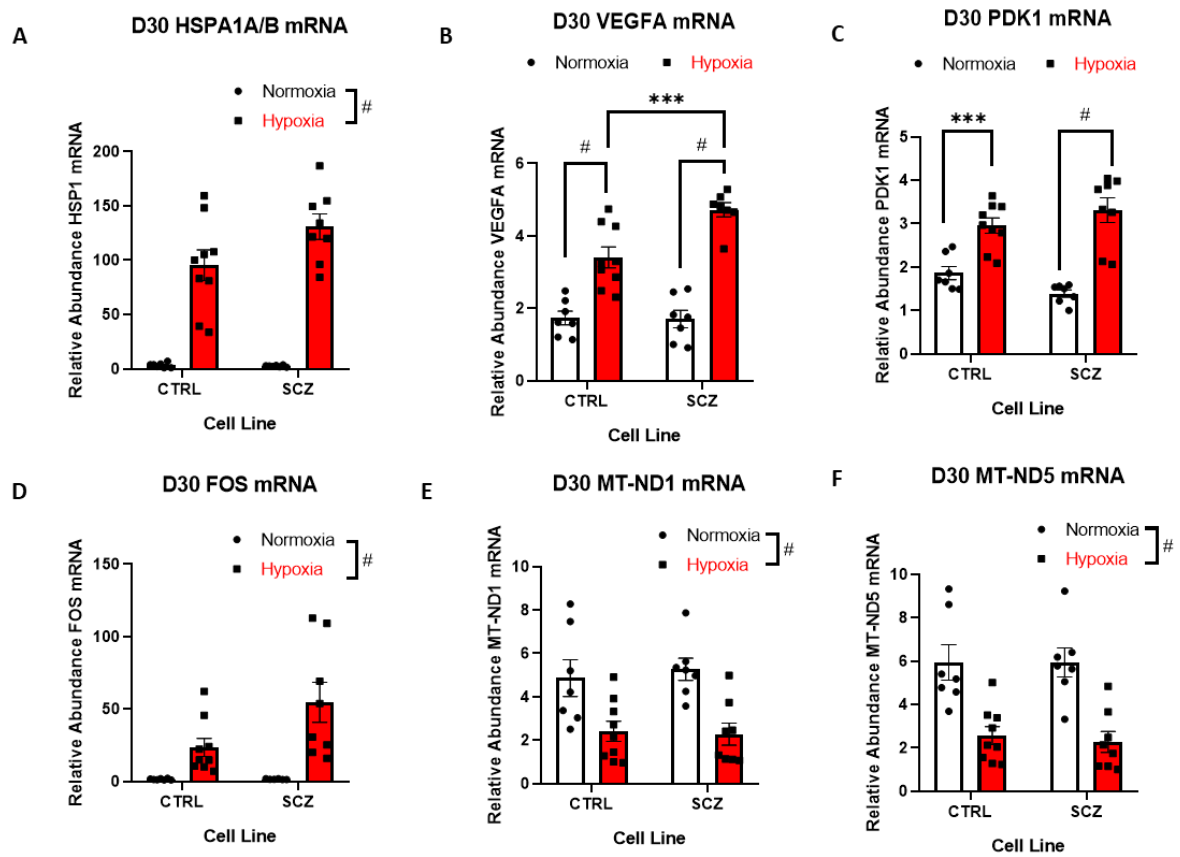
Figure 12 - qPCR results confirm directional changes in the expression of genes identified in RNA-Seq analysis. In qPCR, in response to hypoxia there is increased abundance of **(A)** Heat shock protein family A members 1A and 1B (HSP1 A/B), **(B)** vascular endothelial growth factor A (VEGFA), **(C)** Pyruvate dehydrogenase kinase 1 (PDK1), and Fos proto-oncogene (FOS). Hypoxia results in a decrease in the expression of mitochondrially encoded NADH:Ubiquinone oxidoreductase core **(E)** Subunit 1 (MT-ND1) and **(F)** Subunit 5 (MT-ND5). To generate these targets, DE genes in SCZ hypoxia vs normoxia comparison were input into VarElect and assayed for the following phenotypes: 'hypoxia', 'schizophrenia' and 'mitochondrial dysfunction'. Of the top 20 phenotype's gene hits, 2 to 3 genes were selected for validation through qPCR. The RNA-Seq results of these genes are listed in Table 6. Relative quantification of mRNA was performed using the $2^{-\Delta\Delta CT}$ method, where mRNA was normalized to the geometric means of β-actin and GAPDH. Statistical analysis 2-way ANOVAs, main effects reported in legends and axes. If interaction terms were significant, Fisher's LSD *post hoc* test was performed. *n* =7-9, * p<0.05, ** p<0.01, *** p< 0.001, # p<0.0001.

3.6 Hypoxia induces changes to mitochondrial-associated proteins and genes short- and long-term.

To further investigate the mitochondrial-specific DE genes in response to hypoxia, we utilized the Human MitoCarta 3.0 database. We found 16 DE genes implicated in human mitochondrial pathways in SCZ hypoxia organoids and 8 DE genes in CTRL hypoxia organoids (**Table 6**). Of these genes, hypoxia-exposed SCZ organoids exhibited widespread downregulation of genes that encode protein complexes in the mitochondrial ETC. Specifically, there was downregulation of genes encoding ATP synthase (complex V) subunits 6 and 8 ($p = 0.0011$, $p < 0.0001$, respectively), cytochrome c oxidase (complex IV) subunits 1, 2, and 3 ($p < 0.0001$, $p < 0.0001$, $p < 0.0001$, respectively), and NADH dehydrogenase (complex I) subunits 1, 5, and 6 ($p < 0.0001$, $p < 0.0001$, $p < 0.0001$, respectively). In hypoxia-exposed CTRL organoids, the only ETC gene downregulated is ATP synthase subunit 8 ($p = 0.0004$). These results highlight a SCZ-specific response to hypoxia whereby the SCZ organoids at the transcriptomic level appear more sensitive to the insult than hypoxia-exposed CTRL organoids.

To determine the protein-level impacts of hypoxia and SCZ genetics, we employed Western blot to assess protein levels of ETC proteins and enzymes involved in the TCA cycle. Immediately post-hypoxia, there is a trending increase in ATP synthase (complex V) expression in CTRL hypoxia organoids compared to CTRL normoxia ($U = 34$, $p = 0.0512$, **Figure 13**A). A significant increase in ATP synthase in response to hypoxia is observed in the SCZ organoids ($t_{(18)} = 2.885$, $p = 0.0098$, **Figure 13**B). When comparing the baseline expression of ATP synthase in untreated SCZ organoids to untreated CTRLs, there is no significant difference in expression ($t_{(20)} = 0.8212$, $p = 0.4212$, Appendix 5.2). After a period of recovery and maturity, D170 organoids do not show differences in ATP expression in response to hypoxia in either SCZ or CTRL organoids (SCZ: $t_{(13)} = 0.8613$, $p = 0.4047$, CTRL: $t_{(13)} = 0.7119$, $p = 0.489$, Appendix 5.2). Cytochrome c reductase (complex III) in the ETC chain increases in response to hypoxia in CTRL organoids ($U = 28$, $p = 0.0336$, **Figure 13**C). However, there is no change in expression in SCZ hypoxia-exposed organoids ($t_{(19)} = 1.589$, $p = 0.1286$, **Figure 13**D). Citrate synthase, the rate-limiting TCA cycle enzyme, expression immediately post-hypoxia is unchanged in

response to hypoxia in both CTRL and SCZ organoids (CTRL: $t_{(20)} = 1.481$, $p = 0.1541$, SCZ: $t_{(19)} = 1.425$, $p = 0.1703$,). However, at mature stages, the hypoxia-exposed SCZ organoids compared to untreated SCZ show increased citrate synthase expression ($t_{(15)} = 2.421$, $p = 0.0286$, **Figure 13**F). This trend is not observed in the CTRL organoids as there is no change in expression between normoxia and hypoxia organoids ($t_{(13)} = 0.4525$, $p = 0.6583$, **Figure 13**E).

Table 6 - Differential Expression of Mitochondrial-associated Genes in Response to Hypoxia

Condition	Gene Name	log2(fold_change)	*P* value	Expression
CTRL Hypoxia	UCP1	4.891	0.0041	Upregulated
	DHRS2	2.219	0.0035	Upregulated
	DNAJC28	-2.267	0.0001	Downregulated
SCZ Hypoxia	ADCY10	2.391	0.0025	Upregulated
	PDK1	2.292	<0.0001	Upregulated
	NOCT	2.022	0.0002	Upregulated
	*MT-ATP6	-2.006	0.0011	Downregulated
	*MT-CO3	-2.153	0.0003	Downregulated
	*MT-ND5	-2.188	<0.0001	Downregulated
	HPDL	-2.426	0.0005	Downregulated
	*MT-CO2	-2.457	<0.0001	Downregulated
	*MT-CO1	-2.589	<0.0001	Downregulated
	*MT-ND1	-2.631	<0.0001	Downregulated
	*MT-ND6	-2.756	<0.0001	Downregulated
BOTH	MTFP1	3.129	<0.0001	Upregulated
	BNIP3	3.109	<0.0001	Upregulated
	CSKMT	-2.203	0.0008	Upregulated
	*MT-ATP8	-3.031	<0.0001	Downregulated
	DDX28	2.376	0.0050	Downregulated

* Genes associated with mitochondrial ETC protein complexes
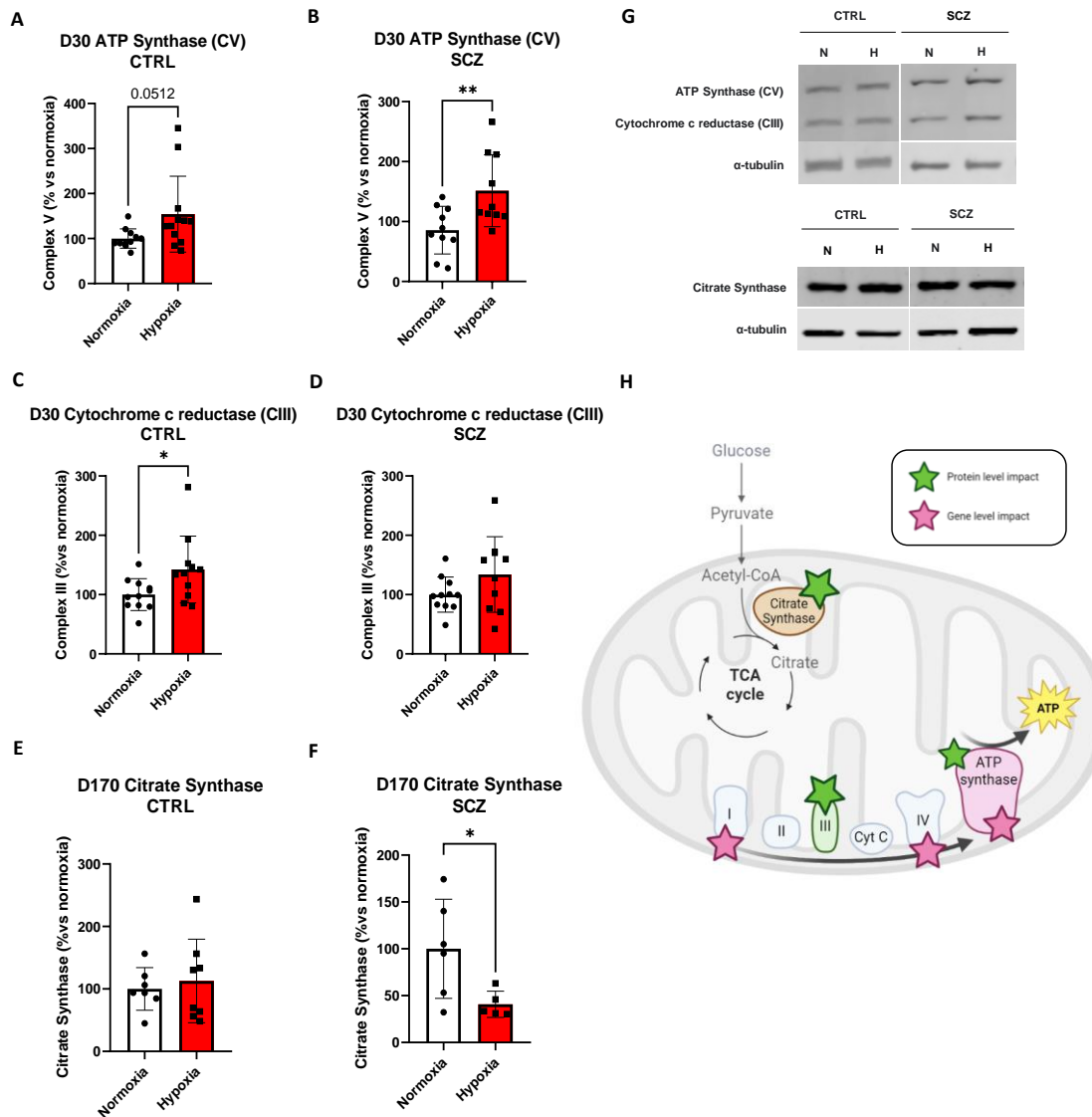
Figure 13 - In response to hypoxia, organoids exhibit changes in the expression of proteins essential to mitochondrial ATP production.
In western blot analysis of D30 organoids **(A, B)** ATP synthase (Complex V) of the electron transport chain (ETC) expression is trending towards an increase in hypoxia CTRL organoids **(A)** and shows a significant increase in the hypoxia-exposed SCZ organoids **(B)**. Cytochrome c reductase (Complex III), hypoxia-exposed CTRL organoids **(C)** exhibit significant protein expression increase, with no changes in the SCZ organoids **(D)**. Citrate synthase, the first conversion enzyme of the tricarboxylic acid cycle (TCA) cycle, is sensitive to hypoxia only in SCZ organoids **(F)**, but change is observed in CTRL organoids **(E)**. **(G)** Representative western blots for ATP synthase, cytochrome c reductase, and citrate synthase. **(H)** Schematic of mitochondrial ETC and TCA cycle proteins impacted by hypoxia in the organoid model. 'Protein level impacts' represent western blot data, and 'gene level impacts' indicate upregulation or downregulation in RNA-seq data. Comparisons were made using Unpaired two-sided t tests or Mann-Whitney U test if normality was not achieved. D30 CTRL n =11-12, D30 SCZ n =10-11; D170 CTRL n =7-8, SCZ n =5-6. * p<0.05, ** p<0.01. Protein expression has been normalized to housekeeping protein α-tubulin.

3.7   Innate differences between SCZ and CTRL organoid gene expression

Thus far, our RNA-Seq results show evident changes in SCZ and CTRL organoids in response to hypoxia, with similar trends appearing in both groups regardless of disease state. However, when comparing untreated SCZ organoids to untreated CTRLs, the DE gene lists reveal innate differences in gene expression solely due to SCZ genetic input. SCZ organoids compared to CTRLs reveal 144 DE genes, all upregulated (**Figure 9C**, FDR $\leq$ 0.05, fold change $\geq$ 2.0). GO analysis of Biological Processes and Molecular Functions finds multiple terms relating to immune responses, metabolism and reactive oxygen species generation, and lipid binding, production, and transfer (**Figure 14**). These terms are of specific interest due to their relevance in the existing SCZ literature that reports irregular immune responses, mitochondria, and lipids.

Immune response terms include regulation of the immune effector process (p = 5.30e-05), regulation of leukocyte differentiation (p = 6.50e-07), and neutrophil-mediated immunity (p = 0.00619). The innate immune system in which leukocytes and neutrophils (a type of leukocyte) have been studied in SCZ pathology where one found neutrophil levels increased in the blood of SCZ patients, while others have linked increases in neutrophil production to overproduction of ROS in SCZ (Ermakov et al. 2022; Jackson and Miller 2020; Sirota, Gavrieli, and Wolach 2003). Toll-like receptors (TLR) are broadly expressed in the CNS and have roles in neurogenesis and neuroplasticity. They are also an important component of the innate immune system (Balaji et al. 2020). GO:MF analysis highlighted the overrepresentation of the term "toll-like receptor binding (p = 1.13e-04). Within this term, the gene CD36 is upregulated in SCZ organoids (p = 0.03399, log(2)FC = 2.61). This gene is critical to specific TLR signalling pathways involved in inflammation and tissue damage responses (Abe et al. 2010).

Terms linked to lipid production and binding include high-density lipoprotein (HDL) particle binding (p = 0.00584), low-density lipoprotein (LDL) particle binding (p = 0.032), and cholesterol transfer activity (p = 0.050). HDLs comprise lipid rafts crucial to cell signalling and play roles in neurodegenerative diseases (Cheng et al. 2023). HDLs and LDLs are also involved in neuroinflammatory processes (D. Yang et al. 2022). This

connection is also highlighted in which genes were upregulated within the lipid-associated GO terms. For example, within the GO:MF term "response to lipids," which is overrepresented in the SCZ organoids ($p = 0.00771$), genes such as CD86 ($p = 0.03786$, $\log(2)FC = 4.84$) which is expressed in B-cells, and TREM2 ($p = 0.03786$, $\log(2)FC = 4.87$), which is expressed on microglia, the immune cells of the CNS are upregulated in SCZ organoids. While there were commonalities in the hypoxia response in CTRL and SCZ organoids, the differences specifically implicating mitochondrial dysfunction and immune system responses may be driven by these innate differences observed in the RNA-Seq results.
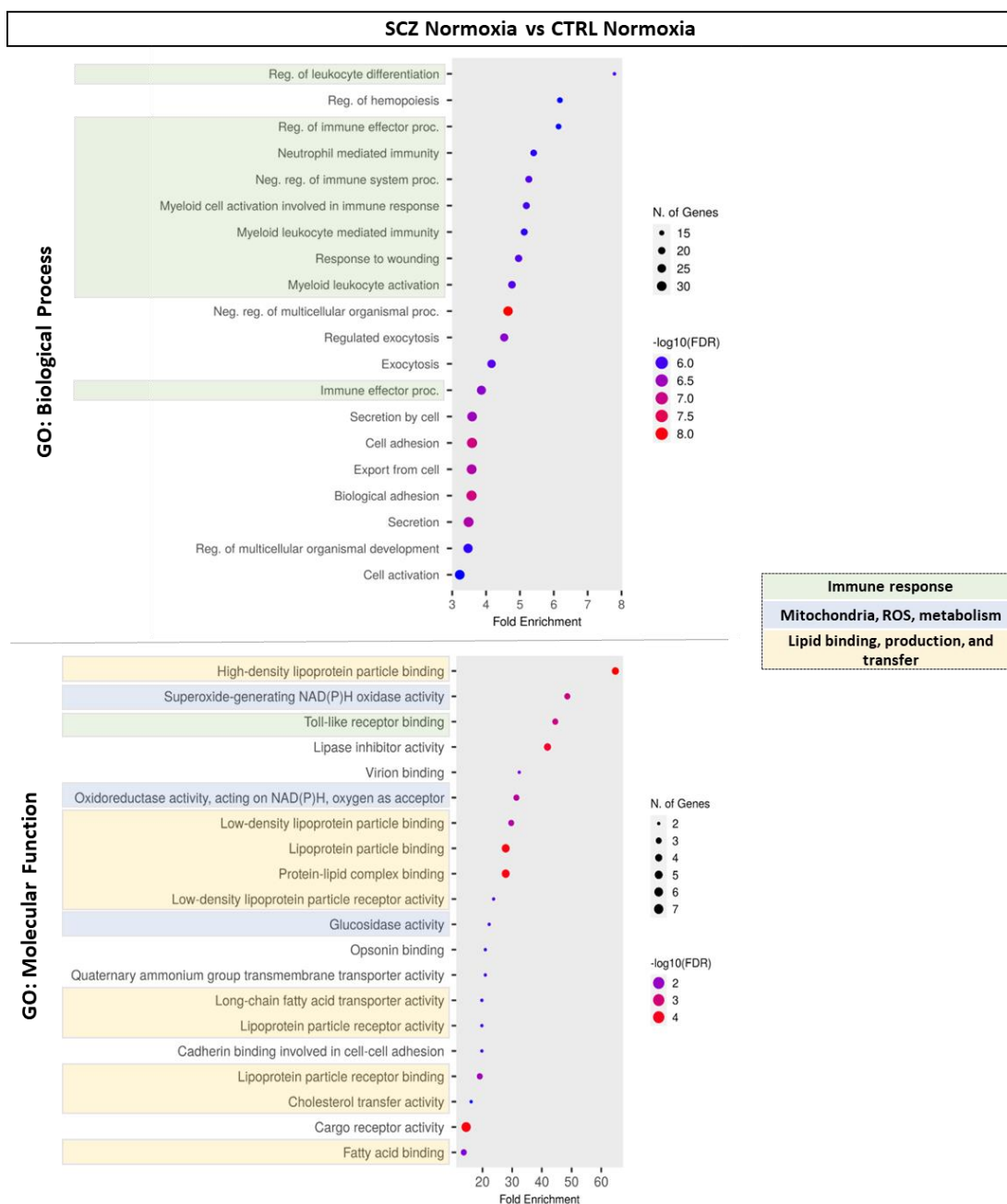
Figure 14 - Untreated SCZ organoids show differential expression of pathways relating to immune system responses, metabolism, and lipid binding compared to CTRL organoids.
To determine the baseline disease effect of SCZ organoids, Gene Ontology (GO) overrepresentation analysis for **(A)** Biological Process terms and **(B)** Molecular Function terms.
Terms highlighted in green relate to immune system responses. Blue relates to mitochondrial processes, reactive oxygen species production, and cellular metabolism. Yellow boxes indicate terms relating to lipid production and binding. These results highlight commonly associated pathways associated with SCZ pathophysiology in the SCZ organoid model.

4 Discussion

This project aimed to develop and characterize an *in vitro* cerebral organoid model of prenatal hypoxia in SCZ populations to study the gene-environment interactions in SCZ brain development. We investigated differences between SCZ and CTRL organoids at baseline and the impact of hypoxia on both types of organoids to incorporate the GEI aspect. We confirmed the expected molecular responses to the hypoxic insult in our organoids, as seen by increased HIF-1α protein stabilization and upregulation of HIF-1α genetic targets such as VEGFA and PDK1. Further characterization of the organoids revealed that SCZ organoids exhibited reductions in proteins and genes required for normal brain development compared to healthy controls. Investigation into the effects of hypoxia on mitochondria and the gene and protein level revealed mitochondrial dysfunction in SCZ organoids, reflective of clinical SCZ pathology. While discussing the findings obtained from patient-derived 3D cerebral organoids within the context of disease, it is crucial to emphasize that organoid systems are still experimental models and cannot perfectly substitute for actual brain experimentation. However, the data obtained from these systems is a valuable 3D macroenvironment closely resembling early brain development. Hence, we interpret our results considering these limitations. This project reveals innate differences in brain development markers in SCZ and the impact of hypoxia on development via mitochondrial dysfunction and cellular stress responses.

4.1 Irregularities in neurodevelopment in SCZ organoids

Characterization of our CTRL and SCZ organoids at baseline reflects previous studies regarding the proteins expressed and the spatial distribution of said proteins. By day 30 of development, we see the expression of synaptophysin, which is crucial for neurotransmitter release from synapses, metabotropic glutamate receptors 2 and 3, which indicates glutamatergic neuron identity, and CTIP2, expressed in mature deep-layer cortical neurons. All these proteins are spatially distributed on the outermost layers of ventricular-like regions. This is expected as this region represents the cortical plate equivalent of fetal brain tissue. Another critical protein expressed in our organoids is the proliferation marker Ki67, primarily concentrated in the lowermost VZ of the ventricular-

like regions at the early stages of development. Stachowiak et al. (2017) analyzed the distribution of Ki67+ cells and found that in SCZ organoids, there were increased distances between cells, and therefore disorganization of proliferating neural progenitors. This study also reported an increase in Ki67 expression in SCZ organoids, a result we did not observe in our study. However, their organoids were assayed at 14 days post-differentiation, and our D30 analysis may have missed the period where differentiation rates are significantly higher.

Abnormalities in neurogenesis and development in SCZ organoids are reported across multiple studies where vulnerable cell types range from neural stem cells and progenitors to mature neurons. Our results further reflect the literature as we observed reductions in neuronal marker MAP2 expression in SCZ organoids compared to CTRLs. Cytoskeletal dysregulation, specifically relating to microtubules and MAP2, has recently been deemed a hallmark of SCZ pathology (Marchisella, Coffey, and Hollos 2016). In psychiatric patients, including SCZ, loss of dendrite complexity and synaptic density can be attributed to anomalies in cell architecture, a key role of MAP2. In clinical studies, MAP2 protein levels appear to be unchanged in the brains of SCZ patients; however, the immunoreactivity of MAP2 with downstream targets is impaired (Grubisha et al. 2021). We did not observe transcriptomic reductions in MAP2 expression in RNA-Seq, however, our protein analyses via IF revealed reductions in MAP2. These results reflect another iPSC-organoid study of SCZ patients that also reports MAP2 reductions through proteomic analysis (Notaras, Lodhi, Fang, et al. 2021; Notaras et al. 2022). While the SCZ organoids do not show the same method of cytoskeletal dysregulation as adult clinical SCZ studies, it accurately captures dysregulation as a whole, highlighting the power behind this *in vitro* model.

Transcriptomic and protein alterations to target receptors of glutamate neurotransmission were also altered in SCZ organoids at immature and mature developmental stages. These results directly relate to the "glutamate hypothesis of SCZ" that associates hypofunction of NMDA receptors and excessive glutamate release in the PFC with cognitive impairment (Mei, Wu, and Zhou 2018). There also may be an association between MAP2

reactivity and glutamate transmission as phosphorylation of MAP2 can be mediated by glutamatergic receptors; phosphorylation of MAP2 leads to conformational changes associated with microtubule stabilization (Itoh et al. 1997; Quinlan and Halpain 1996). Collectively, the results of this study are indicative of neuronal deficits in SCZ neuronal development reflect the clinical pathophysiology of SCZ and previous iPSC studies of SCZ.

Thus far, we have focused on changes to neurodevelopmental markers in SCZ organoids cultured under normoxic conditions. We were also interested in potential differences between normoxic and hypoxia-exposed SCZ organoids. Across most proteins of interest, including NPCs and mature neuronal markers, reductions were observed in SCZ organoids regardless of treatment. If the hypoxic insult was immediately and directly influencing the expression of these neuronal markers, we would expect to see further dysregulation between normoxic and hypoxic SCZ organoids. For the majority of markers, there is no difference in mRNA (PAX6, SOX1, CTIP2, TUJ1, GRM2, GRM3, DRD1) or protein (MAP2, NMDAR2A) expression between normoxia and hypoxia SCZ organoids. In most analyses, main effects of treatment indicate an effect of hypoxia, however insignificant interaction terms do not allow for further investigation into differences within and between groups. Instead, it appears the effect of hypoxia on neurodevelopmental markers is similar regardless of genetic background. Therefore, the effect of hypoxia influencing SCZ risk and development may be on other systems, such as further dysregulation of mitochondrial function and efficiency or genomic-level changes through DNA damage. We investigated this possibility using RNA-Seq analysis of hypoxia-exposed SCZ organoids.

4.2   Mitochondrial deficits in SCZ organoids in response to hypoxia

In response to hypoxia, we consistently observed disruptions of mitochondrial proteins and genes required for normal energy metabolism and oxidative stress responses. We specifically focused on genes and proteins associated with the TCA cycle and the ETC of mitochondria due to their relevance in SCZ pathology and hypoxia responses. Without sufficient oxygen supplies, mitochondria are sensitive to impairments of the electron

transport chain for ATP production. While there are mitochondrial-associated impacts in CTRL organoids for some proteins and genes, the scale of mitochondrial impact is quite widespread in SCZ organoids. In SCZ organoids, ATP synthase expression increases in response to hypoxia immediately post-insult, but there is a downregulation of ATP synthase subunit genes, specifically MT-ATP6 and MT-ATP8. In hypoxic conditions, the availability of oxygen is limited, leading to electron accumulation and a decrease in the efficiency of ATP production (H.-S. Li et al. 2019). In SCZ, dysregulation in mitochondrial genes and pathways associated with ATP production has been observed (Roberts 2021). Gene expression studies have revealed widespread downregulation of genes related to oxidative phosphorylation, the tricarboxylic acid (TCA) cycle, and glycolysis in the prefrontal cortex of post-mortem schizophrenia brains (Roberts 2021). Specifically, genes encoding key enzymes involved in ATP production, such as complex V (ATP synthase) and complex I (NADH dehydrogenase) subunits, have shown decreased expression in individuals with schizophrenia (Maurer, Zierz, and Möller 2001). In our SCZ hypoxia organoids, genes encoding subunits of ATP synthase, NADH dehydrogenase, and cytochrome c oxidase were downregulated. Overall, disruptions to oxidative phosphorylation pathways in SCZ pathology and hypoxia responses are well documented in the literature and reflected in our SCZ hypoxia organoid model.

The overproduction of ROS as a by-product of disrupted OXPHOS in mitochondria is also associated with cellular stress and hypoxic conditions. The imbalance between oxygen access and metabolic demand increased ROS production (Wheaton and Chandel 2011; Guo et al. 2013). Excessive ROS can cause oxidative damage to mitochondrial components, including DNA, proteins, and lipids, further contributing to mitochondrial dysfunction (Guo et al. 2013). In both CTRL and SCZ organoids in response to hypoxia, there is upregulation of genes associated with changes to DNA structure and function. This includes heat shock proteins and histone deacetylases (HDAC) enzymes that can regulate gene transcription in response to cellular stress responses (Baler, Dahl, and Voellmy 1993; Seto and Yoshida 2014). While hypoxia induced similar responses in CTRL and SCZ organoids at the transcriptomic level, innate differences between disease states could influence the degree of mitochondrial dysfunction and DNA damage. For

example, SCZ organoids under normoxic conditions were found to differentially express genes involved in reactive oxygen species generation and metabolism. Pairing these innate deficits with the hypoxic insult may contribute to the larger number of mitochondrially-associated genes implicated in hypoxia response in SCZ organoids compared to CTRLs.

4.3   Innate transcriptomic differences between SCZ and controls

As discussed, many of the immediate changes to specific proteins and gene expression in response to hypoxia in broad terms are very similar in CTRL and SCZ organoids. We have observed inherent differences in neuronal development in our IF image analysis and qPCR investigation into genes involved in neurogenesis and neuronal maturation. Further RNA-Seq analysis comparing differentially expressed genes between CTRL and SCZ organoids cultured under normoxic conditions revealed the upregulation of many cellular pathways involved in SCZ pathophysiology.

4.3.1 *Immune system responses in SCZ organoids*

GO analysis of SCZ organoid transcriptomics revealed an overrepresentation of many terms involved in innate and adaptive immune responses. It is important to note that while other groups have observed microglia innately present in cerebral organoids (Ormel et al. 2018), this study did not assay for the presence of microglia or other immune cell types. Thus, in the RNA-Seq analysis, overrepresentation of terms that implicate the immune system may reflect differential expression of genes not exclusively expressed in microglia. For example, genes classified as encoding cytokines and chemokines are overrepresented in SCZ organoids compared to CTRLs, genes that are not uniquely expressed only in immune cell types. Consequently, we discuss these results in reference to their relevance to implications of the immune system in clinical SCZ populations understanding the limitations of the current cerebral organoid model.

Several immune system abnormalities have been observed in individuals with SCZ, including chronic low-grade inflammation, abnormal immune cell activity and function, and genetic variants identified in GWAS show a strong genetic association between the

human leukocyte antigen (HLA) locus and SCZ (Ermakov et al. 2022; Mokhtari and Lachman 2016). Part of the innate immune system, leukocytes are divided into subgroups, including the myeloid stem cells. Myeloid stem cells can be subdivided into various immune cells, including basophils, neutrophils, eosinophils, and monocytes (Herz et al. 2017). Various meta-analyses implicating different immune cell types in SCZ pathology find that neutrophil and monocyte levels are significantly increased in SCZ patients (Karpiński et al. 2018; Ermakov et al. 2022; Tarantino et al. 2021). The conclusions for eosinophils and basophils are less concrete as some studies report increases in relative numbers of these cells, while others observed no quantitative changes. We found the upregulation of myeloid cell-mediated immunity and activity as a common thread across various databases in our RNA-Seq analysis of SCZ organoids compared to CTRLs. Another topic of interest includes TLRs, as their involvement in the innate immune system is also associated with SCZ. However, although the direction and degree of change of different types of TLRs are not well-defined in SCZ (Ermakov et al. 2022). We found an overrepresentation of TLR-mediated immunity genes, specifically CD36, a coreceptor to other TLR proteins that promotes neuroinflammation (Abe et al. 2010). Overall, our SCZ-iPSCs-derived organoid model reflects clinical SCZ immunity disturbances at the transcriptomic level.

4.3.2 *Lipid alterations in SCZ pathology and organoids*

Lipids play an important role in brain growth and proper functioning throughout life; aberrant lipid compositions are associated with neuropsychiatric disorders, including SCZ (Martinat et al. 2021). Our RNA-Seq analysis of SCZ organoids revealed innate differences in lipid-related pathways compared to CTRLs. For example, we saw upregulation of genes involved in high- and low-density lipid binding, lipoprotein receptor activity, fatty acid binding, and cholesterol transfer. Lipidomic analysis of the DLPFC grey matter of SCZ patients found that approximately 10% of lipids identified were altered in the SCZ lipidome (Yu et al. 2020). Rodents exposed to poly-unsaturated fatty acid deficiency prenatally exhibit SCZ-like behaviours; the authors suggested this was due to epigenetic regulation of nuclear receptor genes (Maekawa et al. 2017). There also appears to be a genetic contribution to lipid alterations in SCZ, as there are reports of

alterations in genes involved in the transport and metabolism of fatty acids (A. Watanabe et al. 2007; Martinat et al. 2021). Hypoxia can also influence lipid synthesis and metabolism as the oxidation of fatty acids into energy supplies through mitochondria is reliant on oxygen supplies being available in mitochondria. Shifts in metabolism may also apply to various lipids in response to hypoxia, like the shifts in carbohydrate/glucose metabolism away from oxidative phosphorylation.

Additionally, a decrease in the precursors required for fatty acid conversion results from hypoxic conditions due to inhibition of the TCA cycle that usually supplies said precursors. While our transcriptomic analysis of hypoxia-exposed SCZ organoids did not directly identify lipid alterations at the gene level, the innate differences between SCZ and CTRLs may contribute to some of the hypoxia responses observed in SCZ organoids absent from CTRLs. An RNA-Seq study on the DLPFC grey matter of SCZ patients reported enrichment in mRNAs involved in the lipid metabolism pathways (Maas et al. 2020). Lipid metabolism is reliant on normal mitochondrial functioning to complete processes such as fatty acid production and integration of cholesterol into HDL particles (X. Yang et al. 2017), and it has been suggested that aberrant lipid homeostasis due to disruption of these processes is associated with SCZ etiology (Maas et al. 2020). A combination of hypoxic disruption to metabolism in mitochondria and baseline differences in lipid composition could contribute to disruptions in neurodevelopmental processes observed in our SCZ hypoxia organoids.

4.4   Gene-environment interaction?

At the core of this project was the aim of exploring the interaction of hypoxia with SCZ genetic contributions to neurodevelopmental processes. This GEI is the basis of the two-hit hypothesis of SCZ whereby the expression of risk-gene mutations primes the CNS into a vulnerable state that hypoxia acts upon to further disrupt brain development and subsequent SCZ clinical symptomology (Bayer, Falkai, and Maier 1999). In this study, the effect of hypoxia on various neuronal markers at the mRNA and protein levels was very similar between CTRL and SCZ organoids. Instead of hypoxia further disrupting expression of these markers, i.e., more up- or down-regulated compared to normoxic

conditions, we report that across multiple markers, SCZ organoids exhibit innate disruptions in various genes and proteins such as PAX6, SOX1, CTIP2, TUJ1, DRD1, GRM2, GRM3, NMDA receptor subunit 2A, and MAP2. Differences in response to hypoxia are observed between certain markers. For example, TUJ1 mRNA and NDMA receptor 2A levels decrease in response to hypoxia in CTRLs; however, expression is already innately lower in normoxic SCZ organoids, and the hypoxia is not further lowering expression. In these cases, hypoxia may not be compounding with SCZ genetics to cause further disruptions. Rather it reveals that neurodevelopmental disruptions in SCZ can come from genetics or environmental influence alone, and these factors do not always interact.

Our RNA-Seq results follow a similar trend; while pathways affected by hypoxia overlap in CTRL and SCZ organoids, there are still differences in which genes are affected and the degree to which pathways are impacted in response to hypoxia. For example, changes to mitochondrial protein and transcriptomics were found in CTRLs, but the degree of change indicated by the number of mitochondrial-associated genes was greater in the SCZ organoids. Overall, we observe innate differences in brain development in the organoid model of SCZ genetics and the ability of hypoxia to disrupt neurodevelopment and energy homeostasis through mitochondrial dysfunction regardless of genetic background. Rather than observing GEI between SCZ genetics and hypoxia across all developmental processes studied, we find GEI is more associated with the degree of alteration and targeting of specific cell types.

4.5 Limitations and Future Directions

4.5.1 *Alterations to differentiation and growth protocol*

While cerebral organoids are a powerful model for studying GEI across various neuropsychiatric disorders, they come with limitations. One limitation is the lack of vascularization and active blood supply in organoids. This limits how we model hypoxic insults and organoid growth as a whole. Because organoids rely on diffusion of nutrients and oxygen from media into tissue for growth, as they grow in size, the innermost areas are at risk of becoming necrotic (Choe et al. 2021). One group characterized the core vs

outer layers of organoids for cell death and hypoxic markers after 70 days of development and found increased expression of HIF-1α and cleaved caspase 3 in the core (Choe et al. 2021). This project used whole organoids during protein/RNA extraction for western blot, qPCR, and RNA-Seq. Long-term culturing of organoids is associated with increased risk of cell death, and necrotic cores could be masking effects only found in the outermost mature neuronal sections. One solution proposed by Choe et al. (2021) is to manually cut organoids into two or four pieces depending on their original size and then return them to normal culturing conditions. They found that after a 7-day recovery period, circularity between cut and uncut organoids was the same and expression of HIF-1α and cleaved caspase 3 was lower in cut organoids. These results support the theory of better nutrient and oxygen diffusion through organoids for better maintenance in long-term cultures. However, further manipulation of organoids increases the risk of culture contamination and potentially disrupts connections between neurons which could have unknown impacts on neuronal development and limit what conclusions could be drawn.

Another future addition to our organoid hypoxia model would include the vascularization of organoids. This would create a better platform for mimicking clinical environments experienced during fetal hypoxia. As previously discussed, pure hypoxic conditions are uncommon in clinical settings (Thompson et al. 2015). Instead, restricted blood flow to the brain comes with reduced access to oxygen and glucose. To mimic these conditions, one organoid study lowered the glucose levels in the growth media during the hypoxic insult to model ischemia (Iwasa et al. 2021). One of the most effective methods of mimicking hypoxia and ischemic insults would be to co-culture cerebral organoids with *in vitro* vascular cells leading to organoid vascularization that could achieve blood circulation when implanted into a mouse model. This model also overcomes the issue of nutrient diffusion into organoid cores during long-term organoid cultures.

Another limitation of this project is the lack of resident immune cells of the CNS, such as microglia, in the organoids. This becomes especially important when dysregulation of immune responses is linked so strongly to SCZ pathophysiology. More recently, protocols developed methods to incorporate microglia into cerebral organoids through a

co-culturing method. Abud et al. (2017) cultured iPSC-derived microglia-like cells (iMGLs) with cerebral organoids and determined by day 3, iMGLs were successfully integrated into the organoids. When neuronal injury was induced, microglia adopted morphology similar to "activated" microglia in injured brain tissue (Abud et al. 2017). Microglia are also important in the context of hypoxic injury. In response to low oxygen, activated microglial release inflammatory cytokines and reactive oxygen species that ultimately lead to neuronal death and degradation of axons (Kaur, Rathnasamy, and Ling 2013). Incorporating these cell types into our model would provide further insights into the influences of hypoxia and SCZ genetics alone and in tandem on immune responses.

4.5.2 *Inherent limitations of the differentiation protocol*

Genetic variability between cell lines could be a potential limitation of this study. The influence of genetics on SCZ risk is well known, but there is no set list for the specific set of genes sufficient and necessary for clinical presentation. One of the first and most cited SCZ organoid papers used only three iPSC cell lines (Stachowiak et al. 2017). Although we were able to derive organoids from six SCZ iPSC cell lines and despite this increase, the heterogeneity of these patients' genetic influence may contribute to some of the variability we observe in our results. However, we also observed significant variability in results within CTRL organoids, hinting at a core limitation of this model. Cerebral organoids are extremely complex and contain thousands of cell types mimicking brain formation, but the exact cytoarchitecture depends on the specific culture protocol used (Brémond Martin et al. 2021). This project derived organoids using a commercially available differentiation kit in hopes of increasing consistency across projects and batches. However, our organoids are developed from an undirected/self-patterned protocol. The result is larger cortical and more complex regions compared to regionally directed differentiation protocols (i.e. dorsal or ventral forebrain organoids), but also greater variability in cell types between organoids (Kelava and Lancaster 2016; Brémond Martin et al. 2021). In the future, repeating this study with directed differentiated organoids may help to decrease variability between samples. Regardless of generation protocol, an inherent limitation is batch-to-batch variability, termed "batch syndrome", and variability within batches (Kelava and Lancaster 2016; Poli, Magliaro, and Ahluwalia

2019). A well-established contributor of both forms of variability relates to 3D matrixes (i.e., Matrigel). In the differentiation step where EBs are embedded into Matrigel droplets, slight differences in the thickness of Matrigel can lead to significant differences in oxygen and nutrient gradients within the organoid, ultimately causing differences in cell differentiation (Poli, Magliaro, and Ahluwalia 2019). As this is an unavoidable and critical component of the differentiation protocol, increasing n size within experiments and validating results across multiple independent batches is the best way to combat this limitation.

4.5.3 *Techniques to investigate functional changes in hypoxia*

This study focused on protein and gene expression changes in pathways central to hypoxia responses and SCZ pathology. An important missing component that could be expanded on in future studies is the functional characterization of the impacts of hypoxia on mitochondrial energetics and potential changes to the electrophysiological profiles of organoids.

Future studies could use the Aligent Seahorse XF Cell Mito Stress Test to characterize mitochondria function in SCZ organoids in normoxic and hypoxic conditions. In this assay, various chemical modulators of ETC complexes are applied to organoid slices and subsequent oxygen consumption records are taken. After applying each modulator, changes in oxygen consumption rate provide information relating to organoids' basal respiration, ATP-linked respiration, extracellular acidification rate, and maximal respiration. A previous study by Kathuria et al. (2020) found iPSC-derived cerebral organoids from SCZ populations found decreases in basal respiration, ATP production, proton leaks, and non-mitochondrial oxygen consumption. In response to reduced access to oxygen immediately following the hypoxic injury, we would expect these decreases to be exaggerated in the SCZ organoids at greater rates compared to CTRLs. It is unclear if these changes would persist after recovery from injury. Therefore, examining whether these alterations to mitochondrial dynamics are only an immediate cellular response or have long-term consequences would be necessary.

Recordings of neuronal populations' activity within organoids have been successfully completed using various techniques, including MEA plates, patch-clamp electrophysiology, optical electrophysiology, and calcium imaging (Passaro and Stice 2021). Applying these techniques to our SCZ organoid model of hypoxia to investigate how hypoxic insults can influence neurons' electrical properties would provide further insights into the exact mechanisms underlying this GEI. Disorganized neuronal discharge due to an imbalance in excitatory and inhibitory signals in the PFC of SCZ patients is well-documented (Krajcovic et al. 2019). Hypoxic environments have also been shown to disrupt normal neuronal firing patterns across various animal models of hypoxia (Y.-S. Yang et al. 2018; Dergacheva et al. 2014; Calabresi et al. 1995; Krnjević 2008). In hippocampal and corticostrial slices of rats exposed to hypoxic periods longer than ~10 minutes results in prolonged depolarization of neurons, which causes reduced electrical activity and synaptic response (Calabresi et al. 1995; Krnjević 2008). With extended depolarization, a large influx of ions leads to high internal calcium levels and accumulation of free radicals as energy demands exceed the limits of mitochondrial function without sufficient oxygen (Krnjević 2008). Examining how neuronal firing patterns are altered in an organoid-based hypoxia model that incorporates SCZ genetic bases would be an interesting addition to this project in the future.

4.6   Conclusions

Prenatal hypoxia during fetal development is a significant environmental risk factor linked to SCZ vulnerability. However, hypoxia's impacts on human brain development at the cellular level remain unclear. In addition, how hypoxia may increase SCZ vulnerability for individuals already at genetic risk for SCZ is not well understood. Cerebral organoids are a complex *in vitro* 3D model that recapitulates many aspects of a developing human brain. To generate a platform to investigate the pathophysiology of SCZ and hypoxia in tandem, we developed iPSC-derived cerebral organoids from six CTR and six SCZ patient cell lines. Hypoxia-exposed organoids exhibited the expected molecular response via increases in hypoxia-indicators HIF-1α and VEGFA expression, and an increase in cell death under stress. Characterization of organoid proteins demonstrates that the organoids express expected neuronal molecular markers (MAP2,

mGluR2/3, CTIP2, VGLUT1, NMDA receptor 2A, etc.) at various stages of development. Hypoxia changes the expression of proteins relating to the mitochondrial electron transport chain (cytochrome c reductase, ATP synthase) within SCZ and CTRL organoids immediately following the insult. Mitochondrial dysfunction is common in post-mortem analyses of SCZ patient samples with differences in mitochondria morphology, cell respiration, and oxidative stress responses; this is reflected within the organoid model. Changes to the expression of various neuronal-related genes have been shown in previous SCZ organoid models. Using qPCR, we have observed clear differences in the expression of various neuronal markers (PAX6, EOMES, TBR1, CTIP2, TUJ1, SOX1) with higher mRNA levels in the CTRL versus SCZ organoids. Transcriptomic analysis of organoids via RNA-Seq reveals hypoxia's impact on cellular stress responses relating to protein folding and DNA damage. Hypoxia also impacts the expression of proteins required for proper metabolism within cells in both control and SCZ organoids. Our findings highlight critical differences in the expression of several key neuronal populations between healthy and SCZ populations and highlight hypoxia's further impacts on neurodevelopmental pathophysiology related to SCZ risk.

References

Abe, Takato, Munehisa Shimamura, Katherine Jackman, Hitomi Kurinami, Josef Anrather, Ping Zhou, and Costantino Iadecola. 2010. 'Key Role of CD36 in Toll-Like Receptor 2 Signaling in Cerebral Ischemia'. *Stroke; a Journal of Cerebral Circulation* 41 (5): 898–904. https://doi.org/10.1161/STROKEAHA.109.572552.

Abud, Edsel M., Ricardo N. Ramirez, Eric S. Martinez, Luke M. Healy, Cecilia H.H. Nguyen, Sean A. Newman, Andriy V. Yeromin, et al. 2017. 'iPSC-Derived Human Microglia-like Cells to Study Neurological Diseases'. *Neuron* 94 (2): 278-293.e9. https://doi.org/10.1016/j.neuron.2017.03.042.

Andreazza, Ana C., Li Shao, Jun-Feng Wang, and L. Trevor Young. 2010. 'Mitochondrial Complex I Activity and Oxidative Damage to Mitochondrial Proteins in the Prefrontal Cortex of Patients with Bipolar Disorder'. *Archives of General Psychiatry* 67 (4): 360–68. https://doi.org/10.1001/archgenpsychiatry.2010.22.

Badr Zahr, Lina Kurdahi, and Isabell Purdy. 2006. 'Brain Injury in the Infant: The Old, the New, and the Uncertain'. *The Journal of Perinatal & Neonatal Nursing* 20 (2): 163–75; quiz 176–77. https://doi.org/10.1097/00005237-200604000-00011.

Bagasrawala, Inseyah, Fani Memi, Nevena V. Radonjić, and Nada Zecevic. 2017. 'N-Methyl d-Aspartate Receptor Expression Patterns in the Human Fetal Cerebral Cortex'. *Cerebral Cortex (New York, NY)* 27 (11): 5041–53. https://doi.org/10.1093/cercor/bhw289.

Balaji, Renu, Manjula Subbanna, Venkataram Shivakumar, Fazal Abdul, Ganesan Venkatasubramanian, and Monojit Debnath. 2020. 'Pattern of Expression of Toll like Receptor (TLR)-3 and -4 Genes in Drug-Naïve and Antipsychotic Treated Patients Diagnosed with Schizophrenia'. *Psychiatry Research* 285 (March): 112727. https://doi.org/10.1016/j.psychres.2019.112727.

Baler, R., G. Dahl, and R. Voellmy. 1993. 'Activation of Human Heat Shock Genes Is Accompanied by Oligomerization, Modification, and Rapid Translocation of Heat Shock Transcription Factor HSF1'. *Molecular and Cellular Biology* 13 (4): 2486–96. https://doi.org/10.1128/mcb.13.4.2486-2496.1993.

Batie, Michael, Luis del Peso, and Sonia Rocha. 2018. 'Hypoxia and Chromatin: A Focus on Transcriptional Repression Mechanisms'. *Biomedicines* 6 (2): 47. https://doi.org/10.3390/biomedicines6020047.

Bayer, T. A., P. Falkai, and W. Maier. 1999. 'Genetic and Non-Genetic Vulnerability Factors in Schizophrenia: The Basis of the "Two Hit Hypothesis"'. *Journal of Psychiatric Research* 33 (6): 543–48. https://doi.org/10.1016/s0022-3956(99)00039-4.

Benitez-King, G., G. Ramírez-Rodríguez, L. Ortíz, and I. Meza. 2004. 'The Neuronal Cytoskeleton as a Potential Therapeutical Target in Neurodegenerative Diseases and Schizophrenia'. *Current Drug Targets. CNS and Neurological Disorders* 3 (6): 515–33. https://doi.org/10.2174/1568007043336761.

Berra, Edurne, Danièle Roux, Darren E. Richard, and Jacques Pouysségur. 2001. 'Hypoxia-Inducible Factor-1α (HIF-1α) Escapes O2-Driven Proteasomal Degradation Irrespective of Its Subcellular Localization: Nucleus or Cytoplasm'. *EMBO Reports* 2 (7): 615–20. https://doi.org/10.1093/embo-reports/kve130.

Białoń, Magdalena, and Agnieszka Wąsik. 2022. 'Advantages and Limitations of Animal Schizophrenia Models'. *International Journal of Molecular Sciences* 23 (11): 5968. https://doi.org/10.3390/ijms23115968.

Brémond Martin, Clara, Camille Simon Chane, Cédric Clouchoux, and Aymeric Histace. 2021. 'Recent Trends and Perspectives in Cerebral Organoids Imaging and Analysis'. *Frontiers in Neuroscience* 15. https://www.frontiersin.org/articles/10.3389/fnins.2021.629067.

Brisch, Ralf, Arthur Saniotis, Rainer Wolf, Hendrik Bielau, Hans-Gert Bernstein, Johann Steiner, Bernhard Bogerts, et al. 2014. 'The Role of Dopamine in Schizophrenia from a Neurobiological and Evolutionary Perspective: Old Fashioned, but Still in Vogue'. *Frontiers in Psychiatry* 5 (May): 47. https://doi.org/10.3389/fpsyt.2014.00047.

Brown, Alan S. 2012. 'Epidemiologic Studies of Exposure to Prenatal Infection and Risk of Schizophrenia and Autism'. *Developmental Neurobiology* 72 (10): 1272–76. https://doi.org/10.1002/dneu.22024.

Bubber, P., V. Hartounian, G. E. Gibson, and J. P. Blass. 2011. 'Abnormalities in the Tricarboxylic Acid (TCA) Cycle in the Brains of Schizophrenia Patients'. *European Neuropsychopharmacology* 21 (3): 254–60. https://doi.org/10.1016/j.euroneuro.2010.10.007.

Cakir, Bilal, Yangfei Xiang, Yoshiaki Tanaka, Mehmet H. Kural, Maxime Parent, Young-Jin Kang, Kayley Chapeton, et al. 2019. 'Engineering of Human Brain Organoids with a Functional Vascular-like System'. *Nature Methods* 16 (11): 1169–75. https://doi.org/10.1038/s41592-019-0586-5.

Calabresi, Paolo, Antonio Pisani, Nicola B. Mercuri, and Giorgio Bernardi. 1995. 'Hypoxia-Induced Electrical Changes in Striatal Neurons'. *Journal of Cerebral Blood Flow & Metabolism* 15 (6): 1141–45. https://doi.org/10.1038/jcbfm.1995.142.

Cannon, Mary, Peter B. Jones, and Robin M. Murray. 2002. 'Obstetric Complications and Schizophrenia: Historical and Meta-Analytic Review'. *American Journal of Psychiatry* 159 (7): 1080–92. https://doi.org/10.1176/appi.ajp.159.7.1080.

Cannon, Tyrone D., Theo G. M. van Erp, Isabelle M. Rosso, Matti Huttunen, Jouko Lönnqvist, Tiia Pirkola, Oili Salonen, Leena Valanne, Veli-Pekka Poutanen, and Carl-Gustav Standertskjöld-Nordenstam. 2002. 'Fetal Hypoxia and Structural Brain Abnormalities in Schizophrenic Patients, Their Siblings, and Controls'. *Archives of General Psychiatry* 59 (1): 35–41. https://doi.org/10.1001/archpsyc.59.1.35.

Cerychova, Radka, and Gabriela Pavlinkova. 2018. 'HIF-1, Metabolism, and Diabetes in the Embryonic and Adult Heart'. *Frontiers in Endocrinology* 9: 460. https://doi.org/10.3389/fendo.2018.00460.

Cheng, Ning, Huan Ma, Ke Zhang, Caiyi Zhang, and Deqin Geng. 2023. 'The Predictive Value of Monocyte/High-Density Lipoprotein Ratio (MHR) and Positive Symptom Scores for Aggression in Patients with Schizophrenia'. *Medicina (Kaunas, Lithuania)* 59 (3): 503. https://doi.org/10.3390/medicina59030503.

Chipurupalli, Sandhya, Elango Kannan, Vinay Tergaonkar, Richard D'Andrea, and Nirmal Robinson. 2019. 'Hypoxia Induced ER Stress Response as an Adaptive Mechanism in Cancer'. *International Journal of Molecular Sciences* 20 (3): 749. https://doi.org/10.3390/ijms20030749.

Choe, Mu Seog, So Jin Kim, Seung Taek Oh, Chang Min Bae, Won-Young Choi, Kyung Min Baek, Joong Sun Kim, and Min Young Lee. 2021. 'A Simple Method to Improve the Quality and Yield of Human Pluripotent Stem Cell-Derived Cerebral Organoids'. *Heliyon* 7 (6): e07350. https://doi.org/10.1016/j.heliyon.2021.e07350.

Cortés-Albornoz, María Camila, Danna Paola García-Guáqueta, Alberto Velez-van-Meerbeke, and Claudia Talero-Gutiérrez. 2021. 'Maternal Nutrition and Neurodevelopment: A Scoping Review'. *Nutrients* 13 (10): 3530. https://doi.org/10.3390/nu13103530.

Daviaud, Nicolas, Clément Chevalier, Roland H. Friedel, and Hongyan Zou. 2019. 'Distinct Vulnerability and Resilience of Human Neuroprogenitor Subtypes in Cerebral Organoid Model of Prenatal Hypoxic Injury'. *Frontiers in Cellular Neuroscience* 13: 336. https://doi.org/10.3389/fncel.2019.00336.

Dergacheva, Olga, Jhansi Dyavanapalli, Ramón A. Piñol, and David Mendelowitz. 2014. 'Chronic Intermittent Hypoxia and Hypercapnia Inhibits the Hypothalamic Paraventricular Nucleus Neurotransmission to Parasympathetic Cardiac Neurons in the Brainstem'. *Hypertension* 64 (3): 597–603. https://doi.org/10.1161/HYPERTENSIONAHA.114.03603.

Deverman, Benjamin E., and Paul H. Patterson. 2009. 'Cytokines and CNS Development'. *Neuron* 64 (1): 61–78. https://doi.org/10.1016/j.neuron.2009.09.002.

Dirnagl, U., C. Iadecola, and M. A. Moskowitz. 1999. 'Pathobiology of Ischaemic Stroke: An Integrated View'. *Trends in Neurosciences* 22 (9): 391–97. https://doi.org/10.1016/s0166-2236(99)01401-0.

Dixon, Thomas Anthony, and Alysson R. Muotri. 2023. 'Advancing Preclinical Models of Psychiatric Disorders with Human Brain Organoid Cultures'. *Molecular Psychiatry* 28 (1): 83–95. https://doi.org/10.1038/s41380-022-01708-2.

El-Fishawy, Paul. 2013. 'Common Disease-Common Variant Hypothesis'. In *Encyclopedia of Autism Spectrum Disorders*, edited by Fred R. Volkmar, 719–20. New York, NY: Springer. https://doi.org/10.1007/978-1-4419-1698-3_1998.

Elgueta, Daniela, Paola Murgas, Erick Riquelme, Guang Yang, and Gonzalo I. Cancino. 2022. 'Consequences of Viral Infection and Cytokine Production During Pregnancy on Brain Development in Offspring'. *Frontiers in Immunology* 13. https://www.frontiersin.org/articles/10.3389/fimmu.2022.816619.

Ermakov, Evgeny A., Mark M. Melamud, Valentina N. Buneva, and Svetlana A. Ivanova. 2022. 'Immune System Abnormalities in Schizophrenia: An Integrative View and Translational Perspectives'. *Frontiers in Psychiatry* 13 (April): 880568. https://doi.org/10.3389/fpsyt.2022.880568.

Fineberg, Anna M., Lauren M. Ellman, Stephen Buka, Robert Yolken, and Tyrone D. Cannon. 2013. 'Decreased Birth Weight in Psychosis: Influence of Prenatal Exposure to Serologically Determined Influenza and Hypoxia'. *Schizophrenia Bulletin* 39 (5): 1037–44. https://doi.org/10.1093/schbul/sbs084.

Fitzgerald, Eamon, Kahyee Hor, and Amanda J. Drake. 2020. 'Maternal Influences on Fetal Brain Development: The Role of Nutrition, Infection and Stress, and the Potential for Intergenerational Consequences'. *Early Human Development* 150 (November): 105190. https://doi.org/10.1016/j.earlhumdev.2020.105190.

Fulzele, Sadanand, and Anilkumar Pillai. 2009. 'Decreased VEGF mRNA Expression in the Dorsolateral Prefrontal Cortex of Schizophrenia Subjects'. *Schizophrenia Research* 115 (2–3): 372–73. https://doi.org/10.1016/j.schres.2009.06.005.

Gallagher, Denis, Andreea A. Norman, Cameron L. Woodard, Guang Yang, Andrée Gauthier-Fisher, Masashi Fujitani, John P. Vessey, et al. 2013. 'Transient Maternal IL-6 Mediates Long-Lasting Changes in Neural Stem Cell Pools by Deregulating an Endogenous Self-Renewal Pathway'. *Cell Stem Cell* 13 (5): 564–76. https://doi.org/10.1016/j.stem.2013.10.002.

Ge, Steven Xijin, Dongmin Jung, and Runan Yao. 2020. 'ShinyGO: A Graphical Gene-Set Enrichment Tool for Animals and Plants'. *Bioinformatics* 36 (8): 2628–29. https://doi.org/10.1093/bioinformatics/btz931.

Gillespie, Marc, Bijay Jassal, Ralf Stephan, Marija Milacic, Karen Rothfels, Andrea Senff-Ribeiro, Johannes Griss, et al. 2022. 'The Reactome Pathway Knowledgebase 2022'. *Nucleic Acids Research* 50 (D1): D687–92. https://doi.org/10.1093/nar/gkab1028.

Giussani, Dino A. 2016. 'The Fetal Brain Sparing Response to Hypoxia: Physiological Mechanisms'. *The Journal of Physiology* 594 (5): 1215–30. https://doi.org/10.1113/JP271099.

Glass, Hannah C., and Donna M. Ferriero. 2007. 'Treatment of Hypoxic-Ischemic Encephalopathy in Newborns'. *Current Treatment Options in Neurology* 9 (6): 414–23. https://doi.org/10.1007/s11940-007-0043-0.

Goldman-Rakic, P. S., and L. D. Selemon. 1997. 'Functional and Anatomical Aspects of Prefrontal Pathology in Schizophrenia'. *Schizophrenia Bulletin* 23 (3): 437–58. https://doi.org/10.1093/schbul/23.3.437.

Grubisha, M. J., X. Sun, M. L. MacDonald, M. Garver, Z. Sun, K. A. Paris, D. S. Patel, et al. 2021. 'MAP2 Is Differentially Phosphorylated in Schizophrenia, Altering Its Function'. *Molecular Psychiatry* 26 (9): 5371–88. https://doi.org/10.1038/s41380-021-01034-z.

Guerrin, Cyprien G.J., Janine Doorduin, Iris E. Sommer, and Erik F.J. De Vries. 2021. 'The Dual Hit Hypothesis of Schizophrenia: Evidence from Animal Models'. *Neuroscience & Biobehavioral Reviews* 131 (December): 1150–68. https://doi.org/10.1016/j.neubiorev.2021.10.025.

Gumusoglu, Serena B., Rebecca S. Fine, Samuel J. Murray, Jada L. Bittle, and Hanna E. Stevens. 2017. 'The Role of IL-6 in Neurodevelopment after Prenatal Stress'. *Brain, Behavior, and Immunity* 65 (October): 274–83. https://doi.org/10.1016/j.bbi.2017.05.015.

Guo, Chunyan, Li Sun, Xueping Chen, and Danshen Zhang. 2013. 'Oxidative Stress, Mitochondrial Damage and Neurodegenerative Diseases'. *Neural Regeneration Research* 8 (21): 2003–14. https://doi.org/10.3969/j.issn.1673-5374.2013.21.009.

Hany, Manassa, Baryiah Rehman, Yusra Azhar, and Jennifer Chapman. 2023. 'Schizophrenia'. In *StatPearls [Internet]*. StatPearls Publishing. https://www.ncbi.nlm.nih.gov/books/NBK539864/.

Henkel, Nicholas D., Xiajoun Wu, Sinead M. O'Donovan, Emily A. Devine, Jessica M. Jiron, Laura M. Rowland, Zoltan Sarnyai, et al. 2022. 'Schizophrenia: A Disorder of Broken Brain Bioenergetics'. *Molecular Psychiatry* 27 (5): 2393–2404. https://doi.org/10.1038/s41380-022-01494-x.

Henriksen, Mads G., Julie Nordgaard, and Lennart B. Jansson. 2017. 'Genetics of Schizophrenia: Overview of Methods, Findings and Limitations'. *Frontiers in*

Human Neuroscience 11.
https://www.frontiersin.org/articles/10.3389/fnhum.2017.00322.

Herz, Jasmin, Anthony J. Filiano, Ashtyn T. Wiltbank, Nir Yogev, and Jonathan Kipnis. 2017. 'Myeloid Cells in the Central Nervous System'. *Immunity* 46 (6): 943–56. https://doi.org/10.1016/j.immuni.2017.06.007.

Holper, L., D. Ben-Shachar, and J. J. Mann. 2019. 'Multivariate Meta-Analyses of Mitochondrial Complex I and IV in Major Depressive Disorder, Bipolar Disorder, Schizophrenia, Alzheimer Disease, and Parkinson Disease'. *Neuropsychopharmacology: Official Publication of the American College of Neuropsychopharmacology* 44 (5): 837–49. https://doi.org/10.1038/s41386-018-0090-0.

Huang, Jing, Fangkun Liu, Bolun Wang, Hui Tang, Ziwei Teng, Lehua Li, Yan Qiu, Haishan Wu, and Jindong Chen. 2019. 'Central and Peripheral Changes in FOS Expression in Schizophrenia Based on Genome-Wide Gene Expression'. *Frontiers in Genetics* 10 (March): 232. https://doi.org/10.3389/fgene.2019.00232.

Itoh, T. J., S. Hisanaga, T. Hosoi, T. Kishimoto, and H. Hotani. 1997. 'Phosphorylation States of Microtubule-Associated Protein 2 (MAP2) Determine the Regulatory Role of MAP2 in Microtubule Dynamics'. *Biochemistry* 36 (41): 12574–82. https://doi.org/10.1021/bi962606z.

Iwasa, Naoki, Takeshi K. Matsui, Naohiko Iguchi, Kaoru Kinugawa, Naritaka Morikawa, Yoshihiko M. Sakaguchi, Tomo Shiota, et al. 2021. 'Gene Expression Profiles of Human Cerebral Organoids Identify PPAR Pathway and PKM2 as Key Markers for Oxygen-Glucose Deprivation and Reoxygenation'. *Frontiers in Cellular Neuroscience* 15 (June): 605030. https://doi.org/10.3389/fncel.2021.605030.

Jackson, Alricka J., and Brian J. Miller. 2020. 'Meta-Analysis of Total and Differential White Blood Cell Counts in Schizophrenia'. *Acta Psychiatrica Scandinavica* 142 (1): 18–26. https://doi.org/10.1111/acps.13140.

Kanehisa, Minoru, Miho Furumichi, Yoko Sato, Mari Ishiguro-Watanabe, and Mao Tanabe. 2021. 'KEGG: Integrating Viruses and Cellular Organisms'. *Nucleic Acids Research* 49 (D1): D545–51. https://doi.org/10.1093/nar/gkaa970.

Karayiorgou, Maria, and Joseph A. Gogos. 2004. 'The Molecular Genetics of the 22q11-Associated Schizophrenia'. *Brain Research. Molecular Brain Research* 132 (2): 95–104. https://doi.org/10.1016/j.molbrainres.2004.09.029.

Karayiorgou, Maria, Tony J. Simon, and Joseph A. Gogos. 2010. '22q11.2 Microdeletions: Linking DNA Structural Variation to Brain Dysfunction and Schizophrenia'. *Nature Reviews. Neuroscience* 11 (6): 402–16. https://doi.org/10.1038/nrn2841.

Karpiński, Paweł, Jerzy Samochowiec, Dorota Frydecka, Maria M. Sąsiadek, and Błażej Misiak. 2018. 'Further Evidence for Depletion of Peripheral Blood Natural Killer Cells in Patients with Schizophrenia: A Computational Deconvolution Study'. *Schizophrenia Research* 201 (November): 243–48. https://doi.org/10.1016/j.schres.2018.04.026.

Kathuria, Annie, Kara Lopez-Lengowski, Smita S. Jagtap, Donna McPhie, Roy H. Perlis, Bruce M. Cohen, and Rakesh Karmacharya. 2020. 'Transcriptomic Landscape and Functional Characterization of Induced Pluripotent Stem Cell-Derived Cerebral Organoids in Schizophrenia'. *JAMA Psychiatry* 77 (7): 745–54. https://doi.org/10.1001/jamapsychiatry.2020.0196.

Kathuria, Annie, Kara Lopez-Lengowski, Donna McPhie, Bruce M. Cohen, and Rakesh Karmacharya. 2023. 'Disease-Specific Differences in Gene Expression, Mitochondrial Function and Mitochondria-Endoplasmic Reticulum Interactions in iPSC-Derived Cerebral Organoids and Cortical Neurons in Schizophrenia and Bipolar Disorder'. *Discover Mental Health* 3 (1): 8. https://doi.org/10.1007/s44192-023-00031-8.

Kaur, Charanjit, Gurugirijha Rathnasamy, and Eng-Ang Ling. 2013. 'Roles of Activated Microglia in Hypoxia Induced Neuroinflammation in the Developing Brain and the Retina'. *Journal of Neuroimmune Pharmacology: The Official Journal of the Society on NeuroImmune Pharmacology* 8 (1): 66–78. https://doi.org/10.1007/s11481-012-9347-2.

Kelava, Iva, and Madeline A. Lancaster. 2016. 'Dishing out Mini-Brains: Current Progress and Future Prospects in Brain Organoid Research'. *Developmental Biology* 420 (2): 199–209. https://doi.org/10.1016/j.ydbio.2016.06.037.

Kim, Jung-whan, Irina Tchernyshyov, Gregg L. Semenza, and Chi V. Dang. 2006. 'HIF-1-Mediated Expression of Pyruvate Dehydrogenase Kinase: A Metabolic Switch Required for Cellular Adaptation to Hypoxia'. *Cell Metabolism* 3 (3): 177–85. https://doi.org/10.1016/j.cmet.2006.02.002.

Kim, Min Soo, Da-Hyun Kim, Hyun Kyoung Kang, Myung Geun Kook, Soon Won Choi, and Kyung-Sun Kang. 2021. 'Modeling of Hypoxic Brain Injury through 3D Human Neural Organoids'. *Cells* 10 (2): 234. https://doi.org/10.3390/cells10020234.

Krajcovic, Branislav, Iveta Fajnerova, Jiri Horacek, Eduard Kelemen, Stepan Kubik, Jan Svoboda, and Ales Stuchlik. 2019. 'Neural and Neuronal Discoordination in Schizophrenia: From Ensembles through Networks to Symptoms'. *Acta Physiologica* 226 (4): e13282. https://doi.org/10.1111/apha.13282.

Krnjević, Krešimir. 2008. 'Electrophysiology of Cerebral Ischemia'. *Neuropharmacology* 55 (3): 319–33. https://doi.org/10.1016/j.neuropharm.2008.01.002.

Krock, Bryan L., Nicolas Skuli, and M. Celeste Simon. 2011. 'Hypoxia-Induced Angiogenesis'. *Genes & Cancer* 2 (12): 1117–33. https://doi.org/10.1177/1947601911423654.

Kwak, Minhye, Sanghee Lim, Eunchai Kang, Orion Furmanski, Hongjun Song, Yun Kyoung Ryu, and C. David Mintz. 2015. 'Effects of Neonatal Hypoxic-Ischemic Injury and Hypothermic Neuroprotection on Neural Progenitor Cells in the Mouse Hippocampus'. *Developmental Neuroscience* 37 (4–5): 428–39. https://doi.org/10.1159/000430862.

Lancaster, Madeline A, and Juergen A Knoblich. 2014. 'Generation of Cerebral Organoids from Human Pluripotent Stem Cells'. *Nature Protocols* 9 (10): 2329–40. https://doi.org/10.1038/nprot.2014.158.

Lancaster, Madeline A., Magdalena Renner, Carol-Anne Martin, Daniel Wenzel, Louise S. Bicknell, Matthew E. Hurles, Tessa Homfray, Josef M. Penninger, Andrew P. Jackson, and Juergen A. Knoblich. 2013. 'Cerebral Organoids Model Human Brain Development and Microcephaly'. *Nature* 501 (7467): 373–79. https://doi.org/10.1038/nature12517.

Lee, Sheng-An, and Kuo-Chuan Huang. 2016. 'Epigenetic Profiling of Human Brain Differential DNA Methylation Networks in Schizophrenia'. *BMC Medical Genomics* 9 (Suppl 3): 68. https://doi.org/10.1186/s12920-016-0229-y.

Levison, Steven W., Raymond P. Rothstein, Michael J. Romanko, Matthew J. Snyder, Roland L. Meyers, and Susan J. Vannucci. 2001. 'Hypoxia/Ischemia Depletes the Rat Perinatal Subventricular Zone of Oligodendrocyte Progenitors and Neural Stem Cells'. *Developmental Neuroscience* 23 (3): 234–47. https://doi.org/10.1159/000046149.

Li, Hong-Sheng, Yan-Ni Zhou, Lu Li, Sheng-Fu Li, Dan Long, Xue-Lu Chen, Jia-Bi Zhang, Li Feng, and You-Ping Li. 2019. 'HIF-1α Protects against Oxidative Stress by Directly Targeting Mitochondria'. *Redox Biology* 25 (July): 101109. https://doi.org/10.1016/j.redox.2019.101109.

Li, Xin, Wanyan Zhou, and Zhenghui Yi. 2022. 'A Glimpse of Gender Differences in Schizophrenia'. *General Psychiatry* 35 (4): e100823. https://doi.org/10.1136/gpsych-2022-100823.

Li, Zhitao, Xinyu Sun, Jia He, Dongyan Kong, Jinyi Wang, and Lili Wang. 2023. 'Identification of a Hypoxia-Related Signature as Candidate Detector for Schizophrenia Based on Genome-Wide Gene Expression'. *Human Heredity* 88 (1): 18–28. https://doi.org/10.1159/000529902.

Lizano, Paulo, Olivia Lutz, George Ling, Jaya Padmanabhan, Neeraj Tandon, John Sweeney, Carol Tamminga, et al. 2018. 'VEGFA GENE Variation Influences Hallucinations and Frontotemporal Morphology in Psychotic Disorders: A B-

SNIP Study'. *Translational Psychiatry* 8 (October): 215. https://doi.org/10.1038/s41398-018-0271-y.

Lu, Yi, Jennie G Pouget, Ole A Andreassen, Srdjan Djurovic, Tõnu Esko, Christina M Hultman, Andres Metspalu, Lili Milani, Thomas Werge, and Patrick F Sullivan. 2018. 'Genetic Risk Scores and Family History as Predictors of Schizophrenia in Nordic Registers'. *Psychological Medicine* 48 (7): 1201–8. https://doi.org/10.1017/S0033291717002665.

Luo, Chongyuan, Madeline A. Lancaster, Rosa Castanon, Joseph R. Nery, Juergen A. Knoblich, and Joseph R. Ecker. 2016. 'Cerebral Organoids Recapitulate Epigenomic Signatures of the Human Fetal Brain'. *Cell Reports* 17 (12): 3369–84. https://doi.org/10.1016/j.celrep.2016.12.001.

Luo, Weijun, and Cory Brouwer. 2013. 'Pathview: An R/Bioconductor Package for Pathway-Based Data Integration and Visualization'. *Bioinformatics* 29 (14): 1830–31. https://doi.org/10.1093/bioinformatics/btt285.

Luvsannyam, Enkhmaa, Molly S. Jain, Maria Kezia Lourdes Pormento, Hira Siddiqui, Angela Ria A. Balagtas, Bernard O. Emuze, and Teresa Poprawski. 2022. 'Neurobiology of Schizophrenia: A Comprehensive Review'. *Cureus* 14 (4): e23959. https://doi.org/10.7759/cureus.23959.

Maas, Dorien A., Marijn B. Martens, Nikos Priovoulos, Wieteke A. Zuure, Judith R. Homberg, Brahim Nait-Oumesmar, and Gerard J. M. Martens. 2020. 'Key Role for Lipids in Cognitive Symptoms of Schizophrenia'. *Translational Psychiatry* 10 (1): 1–12. https://doi.org/10.1038/s41398-020-01084-x.

Maekawa, M., A. Watanabe, Y. Iwayama, T. Kimura, K. Hamazaki, S. Balan, H. Ohba, et al. 2017. 'Polyunsaturated Fatty Acid Deficiency during Neurodevelopment in Mice Models the Prodromal State of Schizophrenia through Epigenetic Changes in Nuclear Receptor Genes'. *Translational Psychiatry* 7 (9): e1229. https://doi.org/10.1038/tp.2017.182.

Malik, Sabrina, Govindaiah Vinukonda, Linnea R. Vose, Daniel Diamond, Bala B. R. Bhimavarapu, Furong Hu, Muhammad T. Zia, Robert Hevner, Nada Zecevic, and Praveen Ballabh. 2013. 'Neurogenesis Continues in the Third Trimester of Pregnancy and Is Suppressed by Premature Birth'. *The Journal of Neuroscience: The Official Journal of the Society for Neuroscience* 33 (2): 411–23. https://doi.org/10.1523/JNEUROSCI.4445-12.2013.

Mansour, Abed AlFatah, J. Tiago Gonçalves, Cooper W. Bloyd, Hao Li, Sarah Fernandes, Daphne Quang, Stephen Johnston, Sarah L. Parylak, Xin Jin, and Fred H. Gage. 2018. 'An in Vivo Model of Functional and Vascularized Human Brain Organoids'. *Nature Biotechnology* 36 (5): 432–41. https://doi.org/10.1038/nbt.4127.

Marchisella, Francesca, Eleanor T. Coffey, and Patrik Hollos. 2016. 'Microtubule and Microtubule Associated Protein Anomalies in Psychiatric Disease'. *Cytoskeleton* 73 (10): 596–611. https://doi.org/10.1002/cm.21300.

Martinat, Maud, Moïra Rossitto, Mathieu Di Miceli, and Sophie Layé. 2021. 'Perinatal Dietary Polyunsaturated Fatty Acids in Brain Development, Role in Neurodevelopmental Disorders'. *Nutrients* 13 (4): 1185. https://doi.org/10.3390/nu13041185.

Martínez, Antígona, Pablo A. Gaspar, Steven A. Hillyard, Stephan Bickel, Peter Lakatos, Elisa C. Dias, and Daniel C. Javitt. 2015. 'Neural Oscillatory Deficits in Schizophrenia Predict Behavioral and Neurocognitive Impairments'. *Frontiers in Human Neuroscience* 9. https://www.frontiersin.org/articles/10.3389/fnhum.2015.00371.

Martínez-Reyes, Inmaculada, and Navdeep S. Chandel. 2020. 'Mitochondrial TCA Cycle Metabolites Control Physiology and Disease'. *Nature Communications* 11 (1): 102. https://doi.org/10.1038/s41467-019-13668-3.

Matsui, Takeshi K., Masaya Matsubayashi, Yoshihiko M. Sakaguchi, Ryusei K. Hayashi, Canbin Zheng, Kazuma Sugie, Masatoshi Hasegawa, Takahiko Nakagawa, and Eiichiro Mori. 2018. 'Six-Month Cultured Cerebral Organoids from Human ES Cells Contain Matured Neural Cells'. *Neuroscience Letters* 670 (March): 75–82. https://doi.org/10.1016/j.neulet.2018.01.040.

Matsui, Takeshi K., Yuichiro Tsuru, Koichi Hasegawa, and Ken-ichiro Kuwako. 2021. 'Vascularization of Human Brain Organoids'. *STEM CELLS* 39 (8): 1017–24. https://doi.org/10.1002/stem.3368.

Maurer, I., S. Zierz, and H. Möller. 2001. 'Evidence for a Mitochondrial Oxidative Phosphorylation Defect in Brains from Patients with Schizophrenia'. *Schizophrenia Research* 48 (1): 125–36. https://doi.org/10.1016/s0920-9964(00)00075-x.

Maynard, T. M., L. Sikich, J. A. Lieberman, and A.-S. LaMantia. 2001. 'Neural Development, Cell-Cell Signaling, and the "Two-Hit" Hypothesis of Schizophrenia'. *Schizophrenia Bulletin* 27 (3): 457–76. https://doi.org/10.1093/oxfordjournals.schbul.a006887.

McClellan, Jon M., Ezra Susser, and Mary-Claire King. 2007. 'Schizophrenia: A Common Disease Caused by Multiple Rare Alleles'. *British Journal of Psychiatry* 190 (3): 194–99. https://doi.org/10.1192/bjp.bp.106.025585.

Mei, Yu-Ying, Dong Chuan Wu, and Ning Zhou. 2018. 'Astrocytic Regulation of Glutamate Transmission in Schizophrenia'. *Frontiers in Psychiatry* 9. https://www.frontiersin.org/articles/10.3389/fpsyt.2018.00544.

Meisenzahl, Eva M., Doerthe Seifert, Ronald Bottlender, Stefan Teipel, Thomas Zetzsche, Markus Jäger, Nikolaos Koutsouleris, et al. 2010. 'Differences in Hippocampal Volume between Major Depression and Schizophrenia: A Comparative Neuroimaging Study'. *European Archives of Psychiatry and Clinical Neuroscience* 260 (2): 127–37. https://doi.org/10.1007/s00406-009-0023-3.

Meyer, G. 2001. 'Human Neocortical Development: The Importance of Embryonic and Early Fetal Events'. *The Neuroscientist: A Review Journal Bringing Neurobiology, Neurology and Psychiatry* 7 (4): 303–14. https://doi.org/10.1177/107385840100700407.

Middleton, Frank A., Karoly Mirnics, Joseph N. Pierri, David A. Lewis, and Pat Levitt. 2002. 'Gene Expression Profiling Reveals Alterations of Specific Metabolic Pathways in Schizophrenia'. *The Journal of Neuroscience* 22 (7): 2718–29. https://doi.org/10.1523/JNEUROSCI.22-07-02718.2002.

Mitra, Sayantanava, Shamsul Haque Nizamie, Nishant Goyal, and Sai Krishna Tikka. 2017. 'Electroencephalogram Alpha-to-Theta Ratio over Left Fronto-Temporal Region Correlates with Negative Symptoms in Schizophrenia'. *Asian Journal of Psychiatry* 26 (April): 70–76. https://doi.org/10.1016/j.ajp.2017.01.013.

Mokhtari, Ryan, and Herbert M Lachman. 2016. 'The Major Histocompatibility Complex (MHC) in Schizophrenia: A Review'. *Journal of Clinical & Cellular Immunology* 7 (6): 479. https://doi.org/10.4172/2155-9899.1000479.

Nascimento, Juliana Minardi, Verônica M. Saia-Cereda, Giuliana S. Zuccoli, Guilherme Reis-de-Oliveira, Victor Corasolla Carregari, Bradley J. Smith, Stevens K. Rehen, and Daniel Martins-de-Souza. 2022. 'Proteomic Signatures of Schizophrenia-Sourced iPSC-Derived Neural Cells and Brain Organoids Are Similar to Patients' Postmortem Brains'. *Cell & Bioscience* 12 (1): 189. https://doi.org/10.1186/s13578-022-00928-x.

Notaras, Michael, Aiman Lodhi, Friederike Dündar, Paul Collier, Nicole M. Sayles, Hagen Tilgner, David Greening, and Dilek Colak. 2021. 'Schizophrenia Is Defined by Cell-Specific Neuropathology and Multiple Neurodevelopmental Mechanisms in Patient-Derived Cerebral Organoids'. *Molecular Psychiatry*, November. https://doi.org/10.1038/s41380-021-01316-6.

Notaras, Michael, Aiman Lodhi, Haoyun Fang, David Greening, and Dilek Colak. 2021. 'The Proteomic Architecture of Schizophrenia iPSC-Derived Cerebral Organoids Reveals Alterations in GWAS and Neuronal Development Factors'. *Translational Psychiatry* 11 (October): 541. https://doi.org/10.1038/s41398-021-01664-5.

Nour, Matthew M., and Oliver D. Howes. 2015. 'Interpreting the Neurodevelopmental Hypothesis of Schizophrenia in the Context of Normal Brain Development and

Ageing'. *Proceedings of the National Academy of Sciences* 112 (21): E2745–E2745. https://doi.org/10.1073/pnas.1502170112.

Orlando, Ilaria M. C., Véronique N. Lafleur, Federica Storti, Patrick Spielmann, Lisa Crowther, Sara Santambrogio, Johannes Schödel, David Hoogewijs, David R. Mole, and Roland H. Wenger. 2020. 'Distal and Proximal Hypoxia Response Elements Cooperate to Regulate Organ-Specific Erythropoietin Gene Expression'. *Haematologica* 105 (12): 2774–84. https://doi.org/10.3324/haematol.2019.236406.

Ormel, Paul R., Renata Vieira de Sá, Emma J. van Bodegraven, Henk Karst, Oliver Harschnitz, Marjolein A. M. Sneeboer, Lill Eva Johansen, et al. 2018. 'Microglia Innately Develop within Cerebral Organoids'. *Nature Communications* 9 (1): 4167. https://doi.org/10.1038/s41467-018-06684-2.

Owen, Michael J., Michael C. O'Donovan, Anita Thapar, and Nicholas Craddock. 2011. 'Neurodevelopmental Hypothesis of Schizophrenia'. *The British Journal of Psychiatry* 198 (3): 173–75. https://doi.org/10.1192/bjp.bp.110.084384.

Paşca, Anca M., Jin-Young Park, Hyun-Woo Shin, Qihao Qi, Omer Revah, Rebecca Krasnoff, Ruth O'Hara, A. Jeremy Willsey, Theo D. Palmer, and Sergiu P. Paşca. 2019. 'Human 3D Cellular Model of Hypoxic Brain Injury of Prematurity'. *Nature Medicine* 25 (5): 784–91. https://doi.org/10.1038/s41591-019-0436-0.

Paşca, Anca M., Steven A. Sloan, Laura E. Clarke, Yuan Tian, Christopher D. Makinson, Nina Huber, Chul Hoon Kim, et al. 2015. 'Functional Cortical Neurons and Astrocytes from Human Pluripotent Stem Cells in 3D Culture'. *Nature Methods* 12 (7): 671–78. https://doi.org/10.1038/nmeth.3415.

Passaro, Austin P., and Steven L. Stice. 2021. 'Electrophysiological Analysis of Brain Organoids: Current Approaches and Advancements'. *Frontiers in Neuroscience* 14: 1405. https://doi.org/10.3389/fnins.2020.622137.

Perrottelli, Andrea, Giulia Maria Giordano, Francesco Brando, Luigi Giuliani, and Armida Mucci. 2021. 'EEG-Based Measures in At-Risk Mental State and Early Stages of Schizophrenia: A Systematic Review'. *Frontiers in Psychiatry* 12 (May): 653642. https://doi.org/10.3389/fpsyt.2021.653642.

Pham, Missy T., Kari M. Pollock, Melanie D. Rose, Whitney A. Cary, Heather R. Stewart, Ping Zhou, Jan A. Nolta, and Ben Waldau. 2018. 'Generation of Human Vascularized Brain Organoids'. *Neuroreport* 29 (7): 588–93. https://doi.org/10.1097/WNR.0000000000001014.

Poli, Daniele, Chiara Magliaro, and Arti Ahluwalia. 2019. 'Experimental and Computational Methods for the Study of Cerebral Organoids: A Review'. *Frontiers in Neuroscience* 13. https://www.frontiersin.org/articles/10.3389/fnins.2019.00162.

Prabakaran, S., J. E. Swatton, M. M. Ryan, S. J. Huffaker, J. T.-J. Huang, J. L. Griffin, M. Wayland, et al. 2004. 'Mitochondrial Dysfunction in Schizophrenia: Evidence for Compromised Brain Metabolism and Oxidative Stress'. *Molecular Psychiatry* 9 (7): 684–97, 643. https://doi.org/10.1038/sj.mp.4001511.

Purcell, Shaun M., Naomi R. Wray, Jennifer L. Stone, Peter M. Visscher, Michael C. O'Donovan, Patrick F. Sullivan, Pamela Sklar, et al. 2009. 'Common Polygenic Variation Contributes to Risk of Schizophrenia and Bipolar Disorder'. *Nature* 460 (7256): 748–52. https://doi.org/10.1038/nature08185.

Qian, Xuyu, Yijing Su, Christopher D. Adam, Andre U. Deutschmann, Sarshan R. Pather, Ethan M. Goldberg, Kenong Su, et al. 2020. 'Sliced Human Cortical Organoids for Modeling Distinct Cortical Layer Formation'. *Cell Stem Cell* 26 (5): 766-781.e9. https://doi.org/10.1016/j.stem.2020.02.002.

Qin, Xianzheng, Jiang Chen, and Tian Zhou. 2020. '22q11.2 Deletion Syndrome and Schizophrenia'. *Acta Biochimica et Biophysica Sinica* 52 (11): 1181–90. https://doi.org/10.1093/abbs/gmaa113.

Quinlan, E. M., and S. Halpain. 1996. 'Postsynaptic Mechanisms for Bidirectional Control of MAP2 Phosphorylation by Glutamate Receptors'. *Neuron* 16 (2): 357–68. https://doi.org/10.1016/s0896-6273(00)80053-7.

Rappaport, Noa, Noam Nativ, Gil Stelzer, Michal Twik, Yaron Guan-Golan, Tsippi Iny Stein, Iris Bahir, et al. 2013. 'MalaCards: An Integrated Compendium for Diseases and Their Annotation'. *Database: The Journal of Biological Databases and Curation* 2013 (April): bat018. https://doi.org/10.1093/database/bat018.

Räsänen, Noora, Jari Tiihonen, Marja Koskuvi, Šárka Lehtonen, and Jari Koistinaho. 2022. 'The iPSC Perspective on Schizophrenia'. *Trends in Neurosciences* 45 (1): 8–26. https://doi.org/10.1016/j.tins.2021.11.002.

Rees, Elliott, Michael C O'Donovan, and Michael J Owen. 2015. 'Genetics of Schizophrenia'. *Current Opinion in Behavioral Sciences*, Behavioral genetics, 2 (April): 8–14. https://doi.org/10.1016/j.cobeha.2014.07.001.

Réthelyi, János M., Judit Benkovits, and István Bitter. 2013. 'Genes and Environments in Schizophrenia: The Different Pieces of a Manifold Puzzle'. *Neuroscience & Biobehavioral Reviews* 37 (10): 2424–37. https://doi.org/10.1016/j.neubiorev.2013.04.010.

Roberts, Rosalinda C. 2021. 'Mitochondrial Dysfunction in Schizophrenia: With a Focus on Postmortem Studies'. *Mitochondrion* 56 (January): 91–101. https://doi.org/10.1016/j.mito.2020.11.009.

Rosso, I. M., T. D. Cannon, T. Huttunen, M. O. Huttunen, J. Lönnqvist, and T. L. Gasperoni. 2000. 'Obstetric Risk Factors for Early-Onset Schizophrenia in a

Finnish Birth Cohort'. *The American Journal of Psychiatry* 157 (5): 801–7. https://doi.org/10.1176/appi.ajp.157.5.801.

Sawada, Tomoyo, Thomas E. Chater, Yohei Sasagawa, Mika Yoshimura, Noriko Fujimori-Tonou, Kaori Tanaka, Kynon J. M. Benjamin, et al. 2020. 'Developmental Excitation-Inhibition Imbalance Underlying Psychoses Revealed by Single-Cell Analyses of Discordant Twins-Derived Cerebral Organoids'. *Molecular Psychiatry* 25 (11): 2695–2711. https://doi.org/10.1038/s41380-020-0844-z.

Schindelin, Johannes, Ignacio Arganda-Carreras, Erwin Frise, Verena Kaynig, Mark Longair, Tobias Pietzsch, Stephan Preibisch, et al. 2012. 'Fiji: An Open-Source Platform for Biological-Image Analysis'. *Nature Methods* 9 (7): 676–82. https://doi.org/10.1038/nmeth.2019.

Schmidt-Kastner, Rainald, Sinan Guloksuz, Thomas Kietzmann, Jim van Os, and Bart P. F. Rutten. 2020. 'Analysis of GWAS-Derived Schizophrenia Genes for Links to Ischemia-Hypoxia Response of the Brain'. *Frontiers in Psychiatry* 11 (May): 393. https://doi.org/10.3389/fpsyt.2020.00393.

Schmitt, Andrea, Berend Malchow, Alkomiet Hasan, and Peter Falkai. 2014. 'The Impact of Environmental Factors in Severe Psychiatric Disorders'. *Frontiers in Neuroscience* 8: 19. https://doi.org/10.3389/fnins.2014.00019.

Selemon, L. D., and N. Zecevic. 2015. 'Schizophrenia: A Tale of Two Critical Periods for Prefrontal Cortical Development'. *Translational Psychiatry* 5 (8): e623–e623. https://doi.org/10.1038/tp.2015.115.

Semenza, Gregg L. 2007. 'Hypoxia-Inducible Factor 1 (HIF-1) Pathway'. *Science's STKE* 2007 (407): cm8–cm8. https://doi.org/10.1126/stke.4072007cm8.

Seto, Edward, and Minoru Yoshida. 2014. 'Erasers of Histone Acetylation: The Histone Deacetylase Enzymes'. *Cold Spring Harbor Perspectives in Biology* 6 (4): a018713. https://doi.org/10.1101/cshperspect.a018713.

Shelton, Micah A., Jason T. Newman, Hong Gu, Allan R. Sampson, Kenneth N. Fish, Matthew L. MacDonald, Caitlin E. Moyer, et al. 2015. 'Loss of Microtubule-Associated Protein 2 Immunoreactivity Linked to Dendritic Spine Loss in Schizophrenia'. *Biological Psychiatry* 78 (6): 374–85. https://doi.org/10.1016/j.biopsych.2014.12.029.

Shi, Limin, Nora Tu, and Paul H. Patterson. 2005. 'Maternal Influenza Infection Is Likely to Alter Fetal Brain Development Indirectly: The Virus Is Not Detected in the Fetus'. *International Journal of Developmental Neuroscience: The Official Journal of the International Society for Developmental Neuroscience* 23 (2–3): 299–305. https://doi.org/10.1016/j.ijdevneu.2004.05.005.

Shi, Yingchao, Le Sun, Mengdi Wang, Jianwei Liu, Suijuan Zhong, Rui Li, Peng Li, et al. 2020. 'Vascularized Human Cortical Organoids (vOrganoids) Model Cortical Development in Vivo'. *PLoS Biology* 18 (5): e3000705. https://doi.org/10.1371/journal.pbio.3000705.

Shin, Jeong Eun, Haejin Lee, Kwangsoo Jung, Miri Kim, Kyujin Hwang, Jungho Han, Joohee Lim, Il Sun Kim, Kwang Il Lim, and Kook In Park. 2020. 'Cellular Response of Ventricular-Subventricular Neural Progenitor/Stem Cells to Neonatal Hypoxic-Ischemic Brain Injury and Their Enhanced Neurogenesis'. *Yonsei Medical Journal* 61 (6): 492–505. https://doi.org/10.3349/ymj.2020.61.6.492.

Shou, Yikai, Feng Liang, Shunliang Xu, and Xuekun Li. 2020. 'The Application of Brain Organoids: From Neuronal Development to Neurological Diseases'. *Frontiers in Cell and Developmental Biology* 8 (October): 579659. https://doi.org/10.3389/fcell.2020.579659.

Sirota, Pinkhas, Ronit Gavrieli, and Baruch Wolach. 2003. 'Overproduction of Neutrophil Radical Oxygen Species Correlates with Negative Symptoms in Schizophrenic Patients: Parallel Studies on Neutrophil Chemotaxis, Superoxide Production and Bactericidal Activity'. *Psychiatry Research* 121 (2): 123–32. https://doi.org/10.1016/s0165-1781(03)00222-1.

Slemc, Lucija, and Tanja Kunej. 2016. 'Transcription Factor HIF1A: Downstream Targets, Associated Pathways, Polymorphic Hypoxia Response Element (HRE) Sites, and Initiative for Standardization of Reporting in Scientific Literature'. *Tumor Biology* 37 (11): 14851–61. https://doi.org/10.1007/s13277-016-5331-4.

Srikanth, Priya, Valentina N. Lagomarsino, Christina R. Muratore, Steven C. Ryu, Amy He, Walter M. Taylor, Constance Zhou, Marlise Arellano, and Tracy L. Young-Pearse. 2018. 'Shared Effects of DISC1 Disruption and Elevated WNT Signaling in Human Cerebral Organoids'. *Translational Psychiatry* 8 (1): 1–14. https://doi.org/10.1038/s41398-018-0122-x.

Stachowiak, E K, C A Benson, S T Narla, A Dimitri, L E Bayona Chuye, S Dhiman, K Harikrishnan, et al. 2017. 'Cerebral Organoids Reveal Early Cortical Maldevelopment in Schizophrenia— Computational Anatomy and Genomics, Role of FGFR'. *Translational Psychiatry*, 24.

Stelzer, Gil, Inbar Plaschkes, Danit Oz-Levi, Anna Alkelai, Tsviya Olender, Shahar Zimmerman, Michal Twik, et al. 2016. 'VarElect: The Phenotype-Based Variation Prioritizer of the GeneCards Suite'. *BMC Genomics* 17 (2): 444. https://doi.org/10.1186/s12864-016-2722-2.

Stelzer, Gil, Naomi Rosen, Inbar Plaschkes, Shahar Zimmerman, Michal Twik, Simon Fishilevich, Tsippi Iny Stein, et al. 2016. 'The GeneCards Suite: From Gene Data

Mining to Disease Genome Sequence Analyses'. *Current Protocols in Bioinformatics* 54 (1): 1.30.1-1.30.33. https://doi.org/10.1002/cpbi.5.

STEMCELL Technologies Inc. 2019. 'Maintenance of Human Pluripotent Stem Cells in mTeSR^{TM} Plus'.

Stolp, Helen, Ain Neuhaus, Rohan Sundramoorthi, and Zoltán Molnár. 2012. 'The Long and the Short of It: Gene and Environment Interactions During Early Cortical Development and Consequences for Long-Term Neurological Disease'. *Frontiers in Psychiatry* 3 (June): 50. https://doi.org/10.3389/fpsyt.2012.00050.

Strat, Yann, Nicolas Ramoz, and Philip Gorwood. 2009. 'The Role of Genes Involved in Neuroplasticity and Neurogenesis in the Observation of a Gene-Environment Interaction (GxE) in Schizophrenia'. *Current Molecular Medicine* 9 (4): 506–18. https://doi.org/10.2174/156652409788167104.

Tang, Ke, Yuandong Yu, Liyan Zhu, Pingwei Xu, Jie Chen, Jingwei Ma, Huafeng Zhang, et al. 2019. 'Hypoxia-Reprogrammed Tricarboxylic Acid Cycle Promotes the Growth of Human Breast Tumorigenic Cells'. *Oncogene* 38 (44): 6970–84. https://doi.org/10.1038/s41388-019-0932-1.

Tarantino, Nadine, Marion Leboyer, Arthur Bouleau, Nora Hamdani, Jean Romain Richard, Wahid Boukouaci, Wu Ching-Lien, et al. 2021. 'Natural Killer Cells in First-Episode Psychosis: An Innate Immune Signature?' *Molecular Psychiatry* 26 (9): 5297–5306. https://doi.org/10.1038/s41380-020-01008-7.

Thompson, Loren P., Sarah Crimmins, Bhanu P. Telugu, and Shifa Turan. 2015. 'Intrauterine Hypoxia: Clinical Consequences and Therapeutic Perspectives'. *Research and Reports in Neonatology* 5 (September): 79–89. https://doi.org/10.2147/RRN.S57990.

Trubetskoy, Vassily, Antonio F. Pardiñas, Ting Qi, Georgia Panagiotaropoulou, Swapnil Awasthi, Tim B. Bigdeli, Julien Bryois, et al. 2022. 'Mapping Genomic Loci Implicates Genes and Synaptic Biology in Schizophrenia'. *Nature* 604 (7906): 502–8. https://doi.org/10.1038/s41586-022-04434-5.

Tzameli, Iphigenia. 2012. 'The Evolving Role of Mitochondria in Metabolism'. *Trends in Endocrinology & Metabolism* 23 (9): 417–19. https://doi.org/10.1016/j.tem.2012.07.008.

Uher, R. 2009. 'The Role of Genetic Variation in the Causation of Mental Illness: An Evolution-Informed Framework'. *Molecular Psychiatry* 14 (12): 1072–82. https://doi.org/10.1038/mp.2009.85.

Uhlén, Mathias, Linn Fagerberg, Björn M. Hallström, Cecilia Lindskog, Per Oksvold, Adil Mardinoglu, Åsa Sivertsson, et al. 2015. 'Tissue-Based Map of the Human

Proteome'. *Science* 347 (6220): 1260419.
https://doi.org/10.1126/science.1260419.

Wang, Miao, and Randal J. Kaufman. 2016. 'Protein Misfolding in the Endoplasmic
Reticulum as a Conduit to Human Disease'. *Nature* 529 (7586): 326–35.
https://doi.org/10.1038/nature17041.

Watanabe, Akiko, Tomoko Toyota, Yuji Owada, Takeshi Hayashi, Yoshimi Iwayama,
Miho Matsumata, Yuichi Ishitsuka, et al. 2007. 'Fabp7 Maps to a Quantitative
Trait Locus for a Schizophrenia Endophenotype'. *PLoS Biology* 5 (11): e297.
https://doi.org/10.1371/journal.pbio.0050297.

Watanabe, Momoko, Jillian R. Haney, Neda Vishlaghi, Felix Turcios, Jessie E. Buth,
Wen Gu, Amanda J. Collier, et al. 2019. 'TGFβ Superfamily Signaling Regulates
the State of Human Stem Cell Pluripotency and Competency to Create
Telencephalic Organoids'. https://doi.org/10.1101/2019.12.13.875773.

Wheaton, William W., and Navdeep S. Chandel. 2011. 'Hypoxia. 2. Hypoxia Regulates
Cellular Metabolism'. *American Journal of Physiology - Cell Physiology* 300 (3):
C385–93. https://doi.org/10.1152/ajpcell.00485.2010.

Yang, Danying, Xifeng Wang, Lieliang Zhang, Yang Fang, Qingcui Zheng, Xing Liu,
Wen Yu, Shoulin Chen, Jun Ying, and Fuzhou Hua. 2022. 'Lipid Metabolism and
Storage in Neuroglia: Role in Brain Development and Neurodegenerative
Diseases'. *Cell & Bioscience* 12 (July): 106. https://doi.org/10.1186/s13578-022-
00828-0.

Yang, X., L. Sun, A. Zhao, X. Hu, Y. Qing, J. Jiang, C. Yang, et al. 2017. 'Serum Fatty
Acid Patterns in Patients with Schizophrenia: A Targeted Metabonomics Study'.
Translational Psychiatry 7 (7): e1176–e1176. https://doi.org/10.1038/tp.2017.152.

Yang, Yoon-Sil, Sook Jin Son, Joon Ho Choi, and Jong-Cheol Rah. 2018. 'Synaptic
Transmission and Excitability during Hypoxia with Inflammation and
Reoxygenation in Hippocampal CA1 Neurons'. *Neuropharmacology* 138
(August): 20–31. https://doi.org/10.1016/j.neuropharm.2018.05.011.

Yogarajah, Mahinda, Mar Matarin, Christian Vollmar, Pamela J. Thompson, John S.
Duncan, Mark Symms, Anthony T. Moore, et al. 2016. 'PAX6, Brain Structure
and Function in Human Adults: Advanced MRI in Aniridia'. *Annals of Clinical
and Translational Neurology* 3 (5): 314–30. https://doi.org/10.1002/acn3.297.

Yoon, Se-Jin, Lubayna S. Elahi, Anca M. Pașca, Rebecca M. Marton, Aaron Gordon,
Omer Revah, Yuki Miura, et al. 2019. 'Reliability of Human Cortical Organoid
Generation'. *Nature Methods* 16 (1): 75–78. https://doi.org/10.1038/s41592-018-
0255-0.

Yu, Qianhui, Zhisong He, Dmitry Zubkov, Shuyun Huang, Ilia Kurochkin, Xiaode Yang, Tobias Halene, et al. 2020. 'Lipidome Alterations in Human Prefrontal Cortex during Development, Aging, and Cognitive Disorders'. *Molecular Psychiatry* 25 (11): 2952–69. https://doi.org/10.1038/s41380-018-0200-8.

Zecevic, N., A. Milosevic, S. Rakic, and M. Marín-Padilla. 1999. 'Early Development and Composition of the Human Primordial Plexiform Layer: An Immunohistochemical Study'. *The Journal of Comparative Neurology* 412 (2): 241–54.

Zenz, Rainer, Robert Eferl, Clemens Scheinecker, Kurt Redlich, Josef Smolen, Helia B. Schonthaler, Lukas Kenner, Erwin Tschachler, and Erwin F. Wagner. 2008. 'Activator Protein 1 (Fos/Jun) Functions in Inflammatory Bone and Skin Disease'. *Arthritis Research & Therapy* 10 (1): 201. https://doi.org/10.1186/ar2338.

Zornberg, G. L., S. L. Buka, and M. T. Tsuang. 2000. 'Hypoxic-Ischemia-Related Fetal/Neonatal Complications and Risk of Schizophrenia and Other Nonaffective Psychoses: A 19-Year Longitudinal Study'. *The American Journal of Psychiatry* 157 (2): 196–202. https://doi.org/10.1176/appi.ajp.157.2.196.

Zourray, Clara, Manju A. Kurian, Serena Barral, and Gabriele Lignani. 2022. 'Electrophysiological Properties of Human Cortical Organoids: Current State of the Art and Future Directions'. *Frontiers in Molecular Neuroscience* 15. https://www.frontiersin.org/articles/10.3389/fnmol.2022.839366.

5   Appendices

5.1   Reagent Preparation Recipes

5.1.1 *7.5% Gelatin Solution for Embedding*

To prepare 100 mL of gelatin solution: To 100 mL of D-PBS, add 10.0 g of sucrose. Add 7.5 µg of gelatin to the sucrose solution and mix thoroughly. Store at 4ºC and rewarm to room temperature in a water bath to use.

5.1.2 *Preparations of STEMdiff Cerebral Organoid Media*

Medium	Kit Component	Volume
EB Formation Medium	STEMdiff™ Cerebral Organoid Basal Medium 1	40 mL
	STEMdiff™ Cerebral Organoid Supplement A	10 mL
Induction Medium	STEMdiff™ Cerebral Organoid Basal Medium 1	49.5 mL
	STEMdiff™ Cerebral Organoid Supplement B	0.5 mL
Expansion Medium	STEMdiff™ Cerebral Organoid Basal Medium 2	24.25 mL
	STEMdiff™ Cerebral Organoid Supplement C	0.25 mL
	STEMdiff™ Cerebral Organoid Supplement D	0.5 mL
Maturation Medium	STEMdiff™ Cerebral Organoid Basal Medium 2	98 mL
	STEMdiff™ Cerebral Organoid Supplement E	2 mL
	Cultrex Reduced Growth Factor Basement Membrane Extract, Type 2, Select*	0.5 mL

* Added to maturation medium at D40+ of organoid growth at a dilution of 1:200

5.2   Supplemental RNA-Seq Data

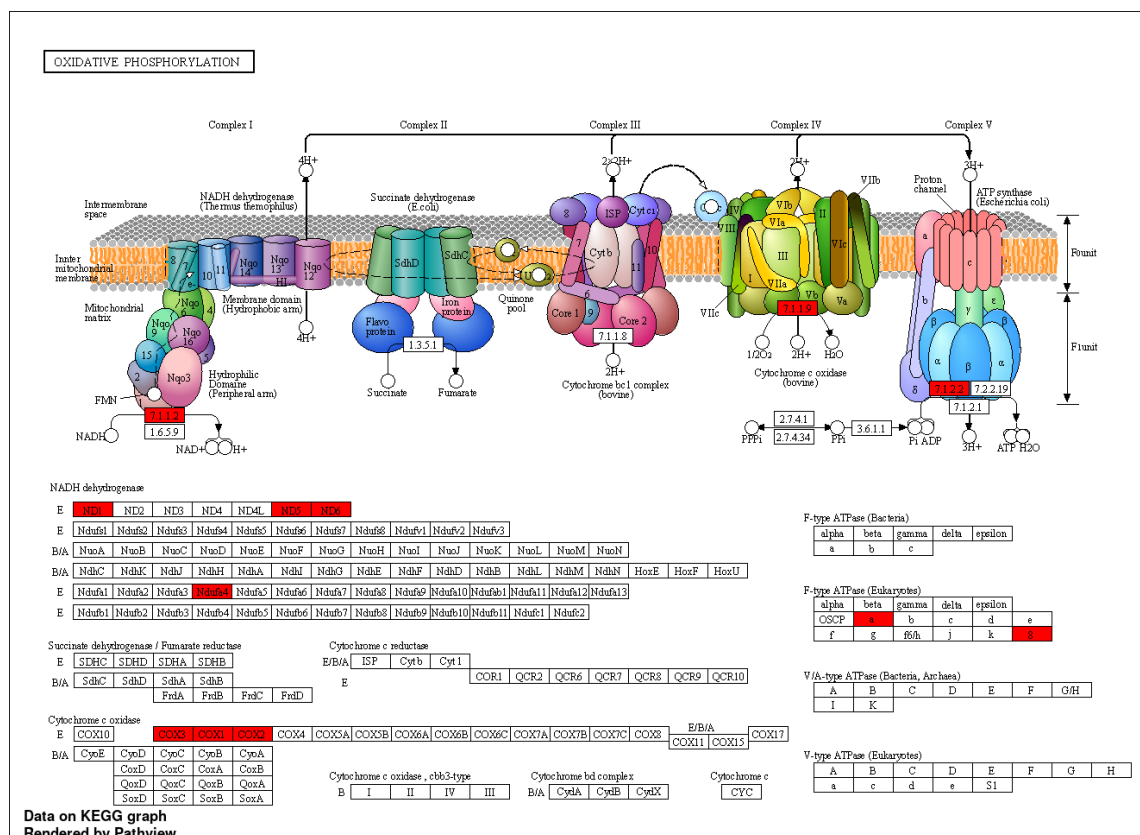### 5.2.1 *Visual representation of KEGG Terms in DE gene lists*

Figure 15 - Genes differentially expressed in the 'Oxidative Phosphorylation' KEGG Pathway in SCZ hypoxia-exposed organoids.
Genes highlighted in red were differentially expression (up- or downregulated) in the DE gene list acquired for SCZ hypoxia vs SCZ normoxia organoids (FDR ≤ 0.05). Figure generated using ShinyGO 0.77 Bioinformatics platform with R package Pathview integration.

Figure 16 - Genes differentially expressed in the 'TNF Signalling' KEGG Pathway in SCZ hypoxia-exposed organoids. Genes highlighted in red were differentially expression (up- or downregulated) in the DE gene list acquired for SCZ hypoxia vs SCZ normoxia organoids (FDR ≤ 0.05). Figure generated using ShinyGO 0.77 Bioinformatics platform with R package Pathview integration.
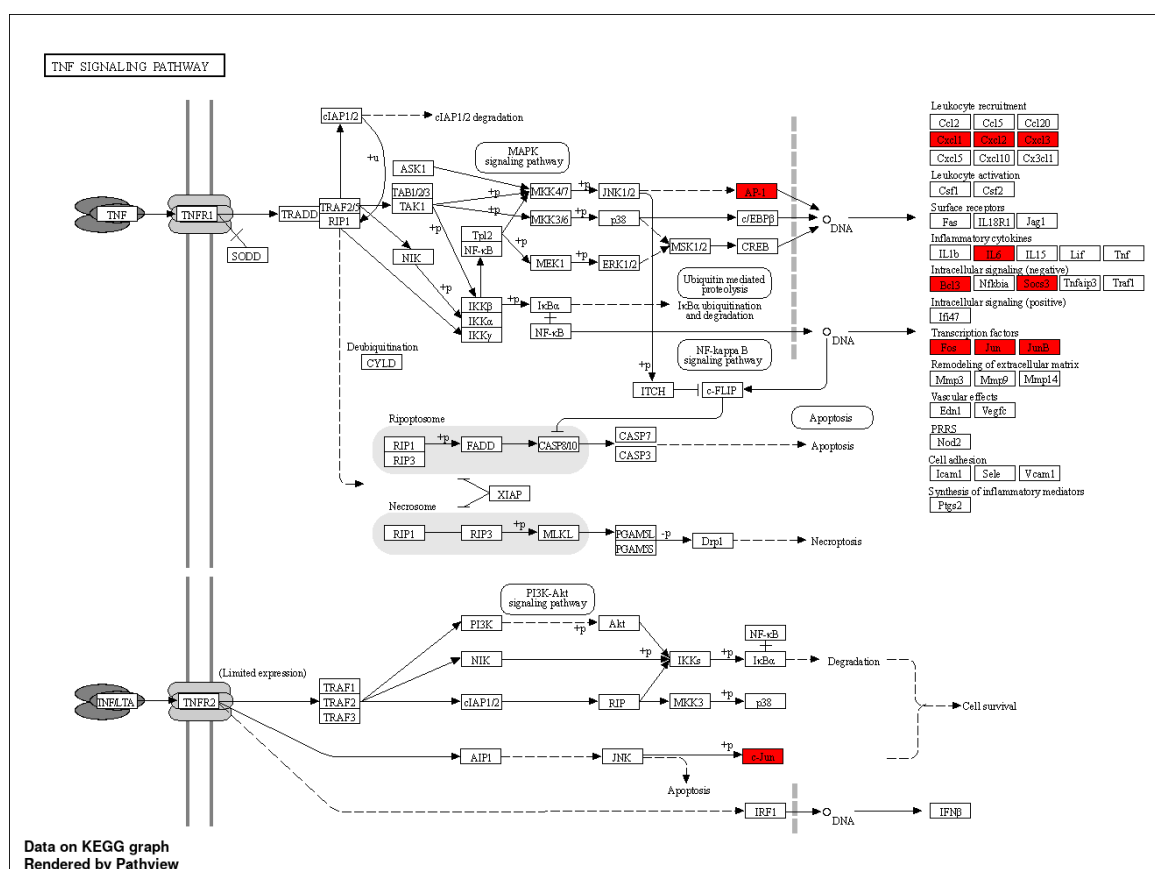
Figure 17 – Visual representation of the 'IL-17 Signalling' KEGG Pathway in SCZ hypoxia-exposed organoids. Genes highlighted in red were differentially expression (up- or downregulated) in the DE gene list acquired for SCZ hypoxia vs SCZ normoxia organoids (FDR ≤ 0.05). Figure generated using ShinyGO 0.77 Bioinformatics platform with R package Pathview integration.

Figure 18 - Genes differentially expressed in the 'HIF-1 Signalling" KEGG Pathway in SCZ hypoxia-exposed organoids.

Genes highlighted in red were differentially expression (up- or downregulated) in the DE gene list acquired for SCZ hypoxia vs SCZ normoxia organoids (FDR ≤ 0.05). Figure generated using ShinyGO 0.77 Bioinformatics platform with R package Pathview integration.

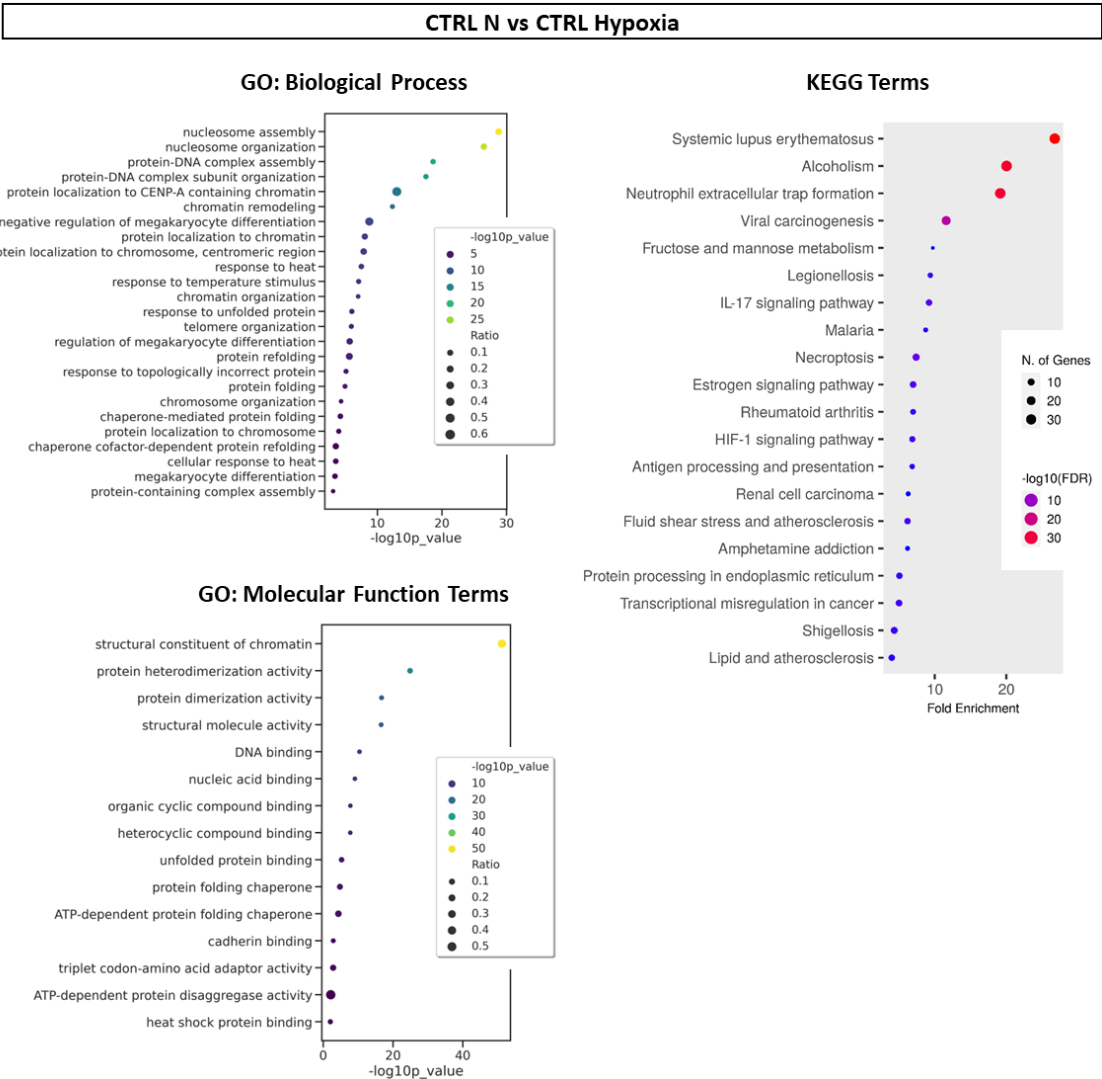### 5.2.2 *RNA-Seq Gene Enrichment Analysis of CTRL Hypoxia organoids*

Figure 19 - In response to hypoxia, CTRL organoids exhibit DE of similar genes detected in the SCZ organoids. Dot plot of (**A**) GO: Biological Process Terms and (**B**) Go: Molecular Function Terms overrepresented in the DE gene list in CTRL hypoxia organoids, ranked by fold enrichment. (**C**) Dot plot of the top 20 KEGG Terms overrepresented in the DE gene list in SCZ hypoxia organoids, ranked by fold enrichment.
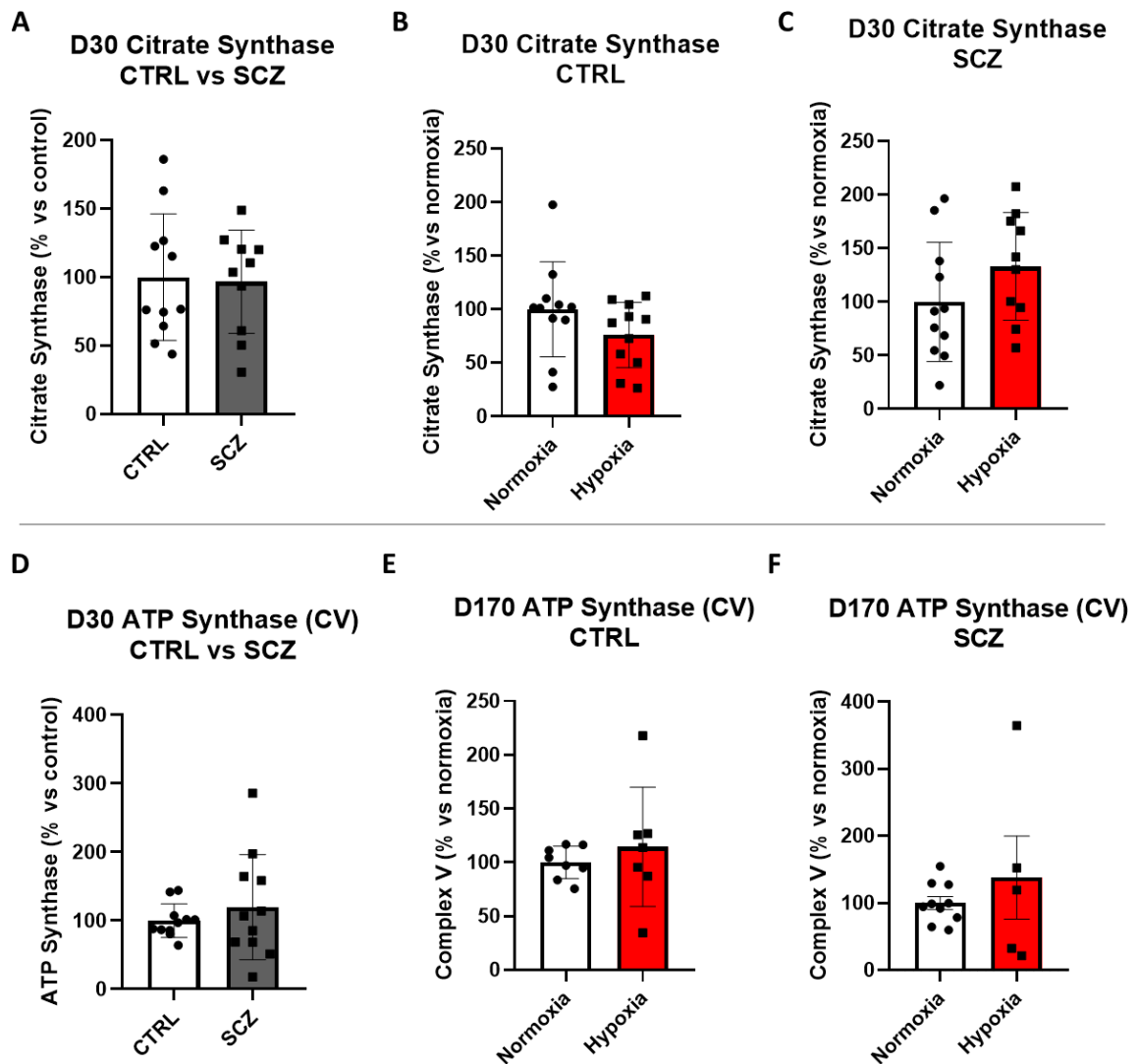
5.3   Supplemental Western Blot Data

Figure 20 – Null results for differences in expression of ATP Synthase (Complex V) and Citrate synthase at D30 and D170.
(A) No baseline differences of expression of citrate synthase between D30 SCZ and CTRL organoids. **(B, C)** In response to hypoxia, there is no change in citrate synthase expression in CTRL or SCZ organoids compared to their untreated counterparts. **(D)** There are no innate differences in ATP synthase expression at 1 month of development between CTRL and SCZ organoids. **(E, F)** ATP synthase expression is not impacted long-term by hypoxia exposure as there are not significant differences in expression in CTRL or SCZ organoids.

Curriculum Vitae

Name:	Dana Gummerson
Post-secondary Education and Degrees:	The University of Western Ontario London, Ontario, Canada 2021-2023 M.Sc. Neuroscience Lakehead University Thunder Bay, Ontario, Canada 2017-2021 B.Sc Biology (Honours)
Honours and Awards:	Canada Graduate Scholarship – Master's 2022 Natural Sciences and Engineering Research Council of Canada University of Western Ontario Poster Award Winner 2023 London Health Research Day London, Ontario, Canada Poster Award Winner 2023 Schizophrenia International Research Society Conference Toronto, Ontario, Canada NSERC Undergraduate Student Research Awards 2018, 2019 Lakehead University James Hillier Scientific Research Scholarship 2017-2021 James Hillier Foundation, Brantford Canada Lakehead University Presidential Scholarship 2017-2021 Lakehead University

Publications:

Oral Presentations

    Gummerson D., Dayer G., Zehbe I. Confirming differential interactome results for two human papillomavirus sub-lineage E6 proteins using reverse co-immunoprecipitation. Undergraduate Thesis Oral Presentation, Lakehead University, Thunder Bay, Ontario, Canada, April 2021

    Gummerson, D., Dayer, G., Zehbe, I. Evaluating the interaction of RBX1 with two HPV16 sub-lineage E6 oncoproteins. Research and Innovation Week, Lakehead University, Thunder Bay, Ontario, Canada, March 2021

    Gummerson D., Rodriguez-Ruiz M., Proud E., Rushlow W., Laviolette S.R. Modelling Prenatal Hypoxia in a Cerebral Organoid Model of Schizophrenia. Joint Mental Health Research and Innovation Day, University of Western Ontario, London, Ontario, Canada, October 2022.

Poster Presentations

    Gummerson D., Rodriguez-Ruiz M., Proud E., Vanin S., Lee K., Hardy D.B, Rushlow W., Laviolette S.R Modelling prenatal hypoxia as a risk factor for schizophrenia vulnerability in patient-derived cerebral organoids. Schizophrenia International Research Society 2023 (SIRS) - Toronto, Ontario, Canada

Peer-reviewed Publications

    Sarikahya M, Cousineau S., De Felice M., Lee K., Wong K., DeVuono M.V., Jung T., Rodríguez-Ruiz M., Ng J, **Gummerson D.**, Proud E., Hardy D.B, Yeung K., Rushlow W.R, Laviolette S.R. Prenatal THC Exposure Induces Sex-Dependent Neuropsychiatric Endophenotypes in Offspring and Long-Term Disruptions in Fatty-Acid Signaling Pathways Directly in the Mesolimbic Circuitry. *eNeuro* **9**, ENEURO.0253-22.2022 (2022)

    Sarikahya M, Cousineau S., De Felice M., Szkudlarek H., Wong K., Lee K., Rodríguez-Ruiz M., **Gummerson D.**, Proud E., Ng J., Hudson R., Jung T., Hardy D.B, Yeung K., Schmid S., Rushlow W.R, Laviolette S.R. Prenatal THC exposure induces long-term, sex-dependent cognitive dysfunction associated with lipidomic and neuronal pathology in the prefrontal cortex-hippocampal network Mol Psychiatry (2023). https://doi.org/10.1038/s41380-023-02190-0